Study on epithelial homeostasis mechanism at the initial stage of carcinogenesis

(発がんの超初期段階における上皮組織恒常性 維持機構に関する研究)

Division of Molecular Oncology,
Graduate School of Chemical Sciences and Engineering,
Hokkaido University

Kojiro Ishibashi

2019

Table of Contents

Abbreviations

ATP	adenosine triphosphate
BSA	bovine serum albumin
DCA	dichloro acetate
DMSO	dimethyl sulfoxide
DMEM	Dulbecco's modified Eagle's medium
EGFP	enhanced green fluorescent protein
EPLIN	Epithelial Protein Lost in Neoplasm
FCS	fetal calf serum
FRET	fluorescence resonance energy transfer
JNK	c-Jun N-terminal kinase
LDH	lactate dehydrogenase
MDCK	Mardin-Darby canine kidney
NOS	nitric oxide synthase
PBS	phosphate buffered saline
PCR	polymerase chin reaction
PDH	pyruvate dehydrogenase
PDK	pyruvate dehydrogenase kinase
PI3K	phosphoinositide 3-kinase
PKA	protein kinase A
PKC	protein kinase C
Ras	rat sarcoma
ROS	reactive oxygen species
RT-qPCR	real-time quantitative PCR
SDS-PAGE	sodium dodecyl labeling with amino acids in cell culture
Src	Rous sarcoma oncogene
TBS	Tris buffered saline
TCA	tricarboxylic acid
Tet	tetracycline
TMRM	tetramethylrhodamine methyl ester
TRPC	transient receptor potential channel

Chapter 1:

GENERAL INTRODUCTION

1. General Introduction

1.1. The Idea Behind This Study

In human, more than 80% of cancer arises from epithelia, and almost carcinomas are result is that multiple mutations occur in oncogenes and/or tumor suppressor genes. In most cancers, transformation begins in a single cell in an epithelial cell sheet. However, it is not known what happens at the interface between normal and transformed cells once the initial transformation has occurred. To address this question, previously Yasuyuki Fujita group has established a mammalian cell culture system. Using this cell culture system, they demonstrated that when transformed cells arise from a monolayer of normal epithelial cells, the newly emerged transformed cells are apically eliminated. Interestingly, when transformed cells are cultured alone, they remain epithelia, suggesting during this process the interaction between normal and transformed cells is required. This phenomenon is called cell competition.

1.2. Cell Competition in Mammal

1.2.1. in vitro cell competition model

In normal culture systems, when two different types of cells are cultured together, cell sorting occurs and the same type of cells form colonies (Steinberg and Takeichi 1994; Foty and Steinberg 2005; Krieg *et al.* 2008). Therefore, it is difficult to form mosaic pattern when normal and transformed cells are co-cultured. To avoid the cell sorting phenomenon, using Mardin-Darby canine kidney cell lines, Yasuyuki Fujita group has

established a cell culture system, where transformed cells emerges from a monolayer of normal epithelial cells in a tetracycline-inducible manner (Hogan *et al.* 2009). In this system, normal MDCK cells and tetracycline-inducible transforming MDCK cells are mixed at a ratio 50:1. After forming monolayer, we add tetracycline to induce transformation. Using this system, we successfully mimic the initial stage of carcinogenesis, newly emerged transformed cells are surrounded by normal epithelial cells (Fig. 1).

1.2.2. Cell competition at the initial stage of carcinogenesis

Using MDCK cells expressing constitutively active form of Ras in a tetracycline-inducible manner (MDCK-pTR GFP-RasV12), our group reported that when RasV12-transformed cells are surrounded by normal epithelial cells, the majority of RasV12 cells are apically eliminated from epithelial monolayer in an apoptosis-independent manner Hogan *et al.* 2009). We also also demonstrated that MAPK pathway, CDC42, and ROCK activity in RasV12 cells is involved in this process. Importantly, when RasV12 cells are cultured alone, apical extrusion does not occur, indicating that activation of downstream signaling pathways of Ras itself is not sufficient to induce apical extrusion, and the presence of surrounding normal cells is also required. Similar to RasV12 cells, when oncoprotein v-Src-transformed cells are surrounded by normal epithelial cells, v-Src cells are also apically extrude from a monolayer of normal epithelial monolayer (Kajita *et al.* 2010). Apical extrusion of RasV12 cells is observed in mouse small intestine in vivo cell competition mouse model (Kon *et al.* 2017), and apical extrusion of v-Src

expressing cells is observed in the enveloping layer (EVL) of zebrafish embryos (Kajita *et al.* 2010) as well, suggesting that apical extrusion occurs in vivo and is an evolutionarily conserved process in vertebrates for elimination of transformed cells from the epithelium. Moreover, we reported that when cells with mutation in tumor suppressor genes such as Scribble or p53 are surrounded by normal cells, these transformed cells are eliminated by apoptosis or necroptosis (Normal *et al.* 2012; Watanabe *et al.* 2018). These results indicate that cell competition has an important role in protection against cancer.

1.2.3. EDAC (Epithelia Defense Against Cancer)

Apical extrusion of transformed cells does not occur when transformed cells are cultured alone, suggesting that the neighboring normal cells have ability to sense and actively eliminate the transformed cells. To reveal this, Kajita *et al.* performed a biochemical screening, and showed that filamin and vimentin are specifically modulated under the mix culture condition of normal and Src- or RasV12-transformed epithelial cells (Kajita *et al.* 2014). Immunofluorescence analysis demonstrated that both filamin and vimentin are strongly accumulated in the neighboring normal cells at the interface with transformed cells, and positively regulate apical extrusion of transformed cells. Furthermore, we demonstrated that the Rho/Rho kinase pathway regulates filamin accumulation and filamin acts upstream of vimentin in the apical extrusion of transformed cells. These findings suggest that normal epithelial cells recognize and actively eliminate neighboring transformed cells and that filamin is a key mediator in the interaction

between normal and transformed epithelial cells.

1.3. Cell Competition in Drosophila

The interaction between normal and transformed cells during differentiation are studied well by using Drosophila Melanogaster. Drosophila Melanogaster is a reasonable model organism because it is easy to generate transgenic and deletion mutated fries and a lot of mutants that we want could be got from fly bank.

In the early of the 1970's, using wing discs in Drosophila Melanogaster, Morata and Ripoll are reported an interesting cell competition phenomenon that occurs at the interface between normal and Minute-transformed cells (Morata and Ripoll 1975). Minute is a genetic mutant that arisesin ribosomal genes. Homozygous Minute flies ($Minute^{-/-}$) are lethal. Although heterozygous Minute ($Minute^{+/-}$) flies develop slowly and have smaller bristles, they are able to glow and develop to normal adult. Morata and Ripoll observed that when $Minute^{+/-}$ cells are surrounded by normal cells, the $Minute^{+/-}$ cells are eliminated by apoptosis and surrounding normal cells glow as compensation for eliminated cell space. Based on this observation, they thought that this phenomenon is as a result of competition for their survival and they celled this phenomenon "Cell Competition". Importantly, when $Minute^{+/-}$ cells alone are present, cell competition does not occur. Therefore, cell competition is cell-context-dependent manner.

1.4. Warburg Effect

Dr. Otto Warburg, a German physiologist, reported a monumental study

that cancer cells prefer aerobic breakdown of glucose even when they are in the presence of abundant oxygen. Neoplastic transformed cells rewire their metabolism to satisfy demands of growth and proliferation. This metabolic reprogramming is widely recognized as the Warburg effect. The Warburg effect is a robust metabolic hallmark of most tumors, thereby leading to a clinical application such as tumor imaging. Although aerobic glycolysis is a common trait of tumors, its role in cancer development remains a subject to debate. Hence ever since its discovery, the Warburg effect is still an unresolved puzzle; Are metabolic changes drivers of cancer progression or do they just come along for the ride? It is generally conceived that the Warburg effect enhances both of cell survival and metastatic potential of malignant tumors. Despite its intense interest, much less is known about how the metabolic alteration impacts cancer development in the context of different tumor stages. To understand cancer as a metabolic disease, it is necessary to uncover how the metabolic reprogramming occurs at initial stage of carcinogenesis, in other words, at emergence of the first transformed cells.

1.5. AHNAK2

AHNAK2 is a 600 kDa giant protein in human (180 kDa in Dog) and composed of a large number of highly conserved central repeat sequences. AHNAK2 mainly localizes to Z-band regions of cardiomyocytes and cosediment with membrane vesicles containing the dihydropyridine receptor (Komuro *et al.* 2004) AHNAK2 are linked to L-type calcium channels and can be phosphorylated by protein kinase A. Moreover AHNAK2 is predicted to have a PDZ domain within its N-terminal, which may mediate these

interactions. However, there are no reports showing the function or significance of AHNAK2.

1.6. Aim of This Study

Although it comes to be revealed that surrounding normal cells actively eliminate the neighboring transformed cells via EDAC process, the molecular mechanism especially about recognition mechanisms and how energy for apical extrusion cells is generated in RasV12 are still unclear. In the first topic, we focused on metabolic alteration in RasV12 cells during apical extrusion and the difference between metabolic alteration in the first step of carcinogenesis and in the later stage of carcinogenesis. In the second topic, we performed SILAC screening to identify the crucial regulator for cell competition. From these experiments, we try to reveal the mechanism underlying cell competition.

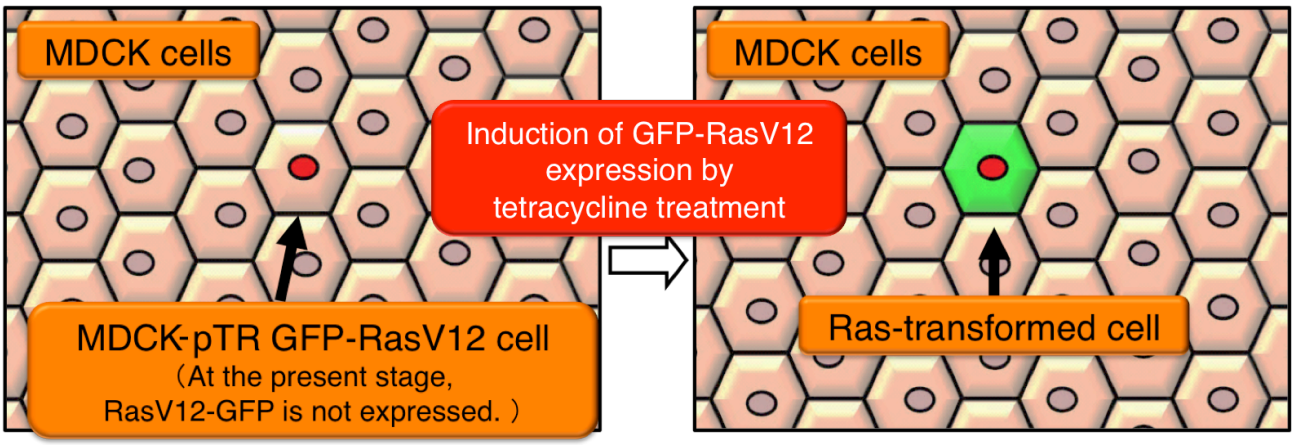

Fig. 1-1 Experimental Design. First, MDCK-pTR GFP-RasV12 cells are mixed with normal cells without tetracycline. After forming monolayer, GFP-RasV12 expression is induced by tetracycline treatment.

Table 1-1. Cell competition phenomena in mammalian cell culture system.

Mutation / Genes	Phenotype	References
Ras	Elimination of RasV12 transformed cells by apical extrusion	Hogan et al. 2009
Src	Elimination of vSrc transformed cells by apical extrusion	Kajita *et al.* 2010
Mahjong	Elimination of Mahjong-knockdown cells by apoptosis	Tamori e*t al.* 2010
Scribble	Elimination of Scribblr-knockdown cells by apoptosis	Norman *et al.* 2012
ErbB2	Elimination of ErbB2 overexpressing cells by apical extrusion	Leung and Brugge 2012
Cdc42	Elimination of constitutively active Cdc42-expressing cells by apical extrusion	Grieve *et al.* 2014
YAP	Elimination of constitutively active YAP-expressing cells by apical extrusion	Chiba *et al.* 2016
p53	Elimination of p53-mutant cells by necroptosis	Watanabe *et al.* 2018

Table 1-2. Interaction between low-fitness cells and high fitness cells in *Drosophila Melanogaster*.

Mutation / Genes	Phenotype	References
Minute	Elimination of Minute$^{+/-}$ cells by apoptosis	Morata and Ripoll 1975
Scribble	Elimination of Scribble-knockdown cells by apoptosis	Richardson *et al.* 2003
dMyc	Elimination of cells with lower level of dMyc by apoptosis	Moreno and Basler 2004 Dela Cova e*t al.* 2004
Vps25	Elimination of Vps25 mutant cells by apoptosis	Thompson *et al.* 2005
Csk	Elimination of Csk-deficient boundary cells by basal exclusion and apoptosis	Vidal *et al.* 2006
Lgl/Mahjong	Elimination of Lgl/Mahjong-knockdown cells by apoptosis	Grzeschik *et al.* 2010 Tamori *et al.* 2010

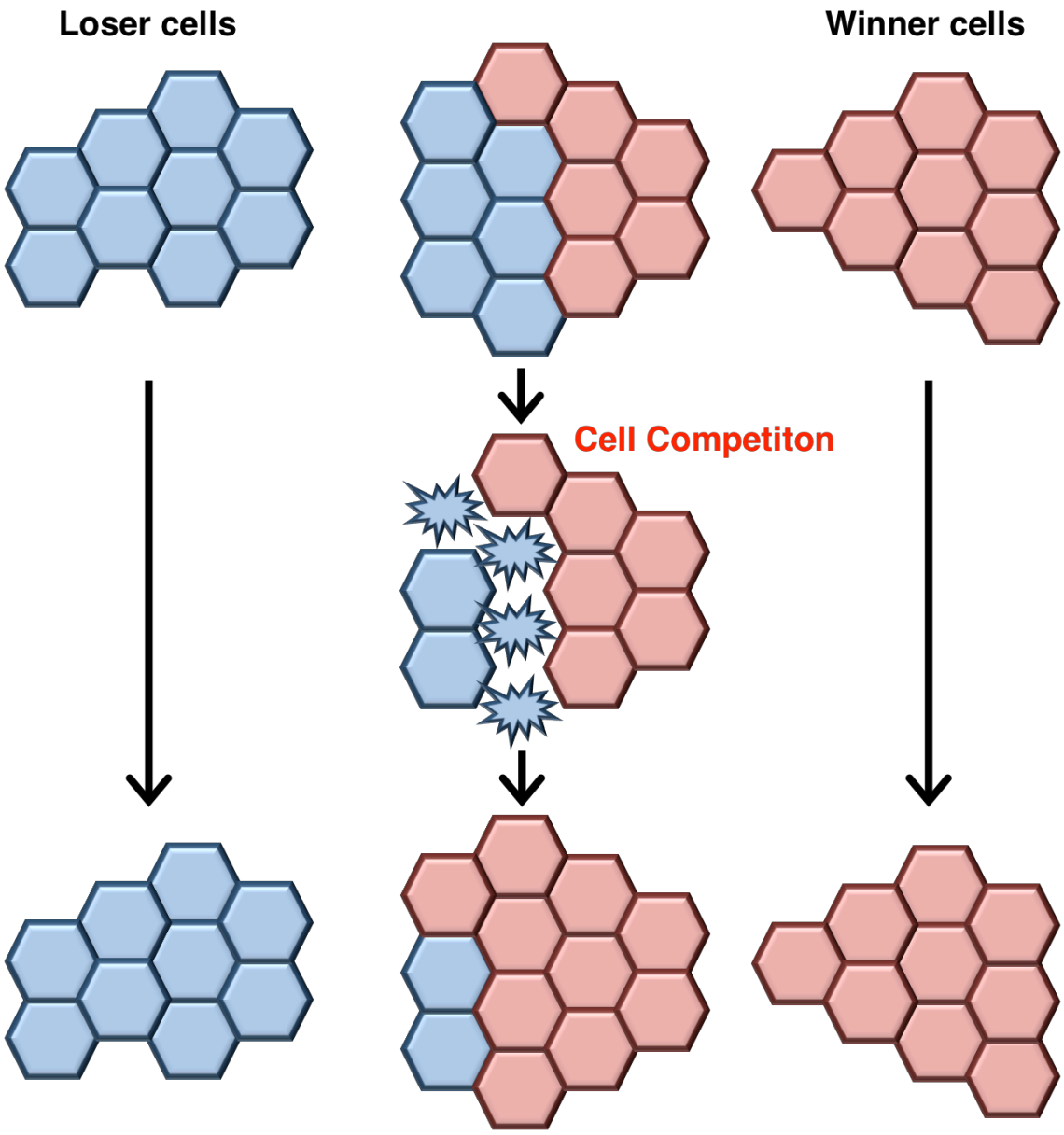

Fig. 1-2 Conceptual Scheme of “Cell Competition”. In cell competition, low-fitness cells (blue) surrounded by themselves survive. On the other hand, when they are surrounded by relative high-fitness cells (red), they are eliminated from epithelial layer. Subsequently, high-fitness cells replace the tissue compensatory proliferation.

1.7. References

Hanahan, D. & Weinberg, R. A. The hallmarks of cancer. Cell 100, 57–70 (2000).

Fialkow, P. J. Clonal origin of human tumors. Biochim. Biophys. Acta. 458, 283–321 (1976).

Nowell, P. C. The clonal evolution of tumor cell populations. Science 194, 23–28 (1976).

Schoenenberger, C. A., Zuk, A., Kendall, D. & Matlin, K. S. Multilayering and loss of apical polarity in MDCK cells transformed with viral K-ras. J. Cell Biol. 112, 873–889 (1991).

Rosenblatt, J., Raff, M. C. & Cramer, L. P. An epithelial cell destined for apoptosis signals its neighbors to extrude it by an actin- and myosin-dependent mechanism. Curr. Biol. 11, 1847–1857 (2001).

Bos, J. L. Ras-like GTPases. Biochim. Biophys. Acta. 1333, M19–31 (1997).
Baena-Lopez, L. A., Pastor-Pareja, J. C. & Resino, J. Wg and Egfr signalling antagonise the development of the peripodial epithelium in Drosophila wing discs. Development 130, 6497–6506 (2003).

Rodriguez-Viciana, P. et al. Role of phosphoinositide 3-OH kinase in cell transformation and control of the actin cytoskeleton by Ras. Cell 89, 457–467 (1997).

Cantrell, D. A. Phosphoinositide 3-kinase signalling pathways. J. Cell Sci. 114, 1439– 1445 (2001).

Karnoub, A. E. & Weinberg, R. A. Ras oncogenes: split personalities. Nature Rev. Mol. Cell Biol. 9, 517–531 (2008).

Kimura, K. et al. Regulation of myosin phosphatase by Rho and Rho-associated kinase (Rho-kinase). Science 273, 245–248 (1996).
Jaffe, A. B. & Hall, A. Rho GTPases: biochemistry and biology. Annu. Rev. Cell Dev. Biol. 21, 247–269 (2005).

Vega, F. M. & Ridley, A. J. Rho GTPases in cancer cell biology. FEBS Lett. 582, 2093–2101 (2008).

Sahai, E., Olson, M. F. & Marshall, C. J. Cross-talk between Ras and Rho signalling pathways in transformation favours proliferation and increased motility. EMBO J. 20, 755–766 (2001).

de la Cova, C., Abril, M., Bellosta, P., Gallant, P. & Johnston, L. A. Drosophila Myc regulates organ size by inducing cell competition. Cell 117, 107–116 (2004).

Moreno, E. & Basler, K. dMyc transforms cells into super-competitors. Cell 117, 117– 129 (2004).

Vidal, M., Larson, D. E. & Cagan, R. L. Csk-deficient boundary cells are eliminated from normal Drosophila epithelia by exclusion, migration, and apoptosis. Dev. Cell 10, 33–44 (2006).

Brumby, A. M. & Richardson, H. E. scribble mutants cooperate with oncogenic Ras or Notch to cause neoplastic overgrowth in Drosophila. EMBO J. 22, 5769–5779 (2003).

Stoker, M. G., Shearer, M. & O'Neill, C. Growth inhibition of polyoma-transformed cells by contact with static normal fibroblasts. J. Cell Sci. 1, 297–310 (1966).

Bignami, M., Rosa, S., La Rocca, S. A., Falcone, G. & Tato, F. Differential influence of adjacent normal cells on the proliferation of mammalian cells transformed by the viral oncogenes myc, ras and src. Oncogene 2, 509–514 (1988).

Alexander, D. B. et al. Normal cells control the growth of neighboring transformed cells independent of gap junctional communication and SRC activity. Cancer Res. 64, 1347–1358 (2004).

Wells, C. M., Walmsley, M., Ooi, S., Tybulewicz, V. & Ridley, A. J. Rac1-deficient macrophages exhibit defects in cell spreading and membrane ruffling but not migration. J. Cell Sci. 117, 1259–1268 (2004).

Hogan, C. et al. Rap1 regulates the formation of E-cadherin-based cell-cell contacts. Mol. Cell. Biol. 24, 6690–6700 (2004).

Shtivelman, E., Cohen, F. E. & Bishop, J. M. (1992) Proc. Natl. Acad. Sci. USA 89, 5472–5476.

Hashimoto, T., Gamou, S., Shimizu, N., Kitajima, Y. & Nishikawa, T. (1995)

Exp. Cell. Res. 217, 258–266.

Hieda, Y., Tsukita, S. & Tsukita, S. (1989) J. Cell Biol. 109, 1511–1518.

Sekiya, F., Bae, Y. S., Jhon, D. Y., Hwang, S. C. & Rhee, S. G. (1999)J. Biol. Chem. 274, 13900–13907.

Haase, H., Podzuweit, T., Lutsch, G., Hohaus, A., Kostka, S., Lindschau, C., Kott, M., Kraft, R. & Morano, I. (1999) FASEB J. 13, 2161–2172.

Chapter 2:

AN ANTI-TUMORIGENIC ROLE OF THE WARBURG EFFECT AT THE EMERGENCE OF TRANSFORMED CELLS

2. An anti-tumorigenic role of the Warburg effect at the emergence of transformed cells

2.1. Introduction

We and other groups have explored the molecular mechanisms of cell competition between normal and RasV12-transformed epithelial cells and revealed that various non-cell-autonomous changes occur in both cells at their interface. For instance, normal epithelial cells accumulate the cytoskeletal protein filamin at the interface with the adjacent transformed cells, thereby actively eliminating them. This implies a notion that normal epithelial cells have anti-tumor activity that does not involve immune cells: a process termed EDAC (epithelial defence against cancer). By contrast, in RasV12-transformed cells that are surrounded by normal cells, the actin-binding protein epithelial protein lost in neoplasm (EPLIN) is accumulated. The accumulated EPLIN then activates the downstream molecules such as protein kinase A (PKA) and myosin II, which positively regulate apical extrusion of RasV12 cells. However, the molecular mechanisms of how EDAC from normal cells affects the neighboring transformed cells and promotes their elimination are still poorly understood. Cellular metabolism is dynamically modulated and adjusted in accordance with various conditions. For example, at the later stage of cancer development, aerobic glycolysis is enhanced in tumor cells, often accompanied by the downregulation of mitochondrial activity; these metabolic changes are called the Warburg effect. However, it is not clearly understood whether cellular metabolism is also affected at the initial stage of

carcinogenesis. In this chapter, we have examined whether and how the metabolic status is regulated at the interface between normal and newly emerging transformed epithelial cells.

2.2. Experimental Procedures

2.2.1. Antibodies and Materials

The following antibodies were used in this study : goat anti-LDHA (sc-27230), mouse anti-Tom20 (sc-17764 clone F10) and mouse anti-EPLIN (sc-136399 clone 20) antibodies from Santa Cruz Biotechnology, mouse anti-Myc (05-724 clone 4A6) and mouse anti-ß-actin (MAB1501R clone C4) antibodies from Millipore, rabbit anti-phospho-PDH antibody (AP1062) from Calbiochem, mouse anti-PDH (ab110330 clone 9H9AF5) and chicken anti-GFP (ab13970) antibodies from Abcam, mouse anti-E-cadherin antibody (610181 clone 36) from BD Transduction and rabbit anti-PDK4 antibody (AP7041B) from ABGENT. Alexa-Fluor-568- and 647-conjugated phalloidin (Life Technologies) were used at 1.0 U ml^{-1}. Alexa-Fluor-568- and 647-conjugated secondary antibodies were from Life Technologies. Hoechst 33342 (Life Technologies) was used at a dilution of 1:5,000. TMRM, MitoSOX, MitoTracker Green and 2-NBDG were obtained from Molecular Probes. The inhibitors radicicol (10 μM), (S)-(–)-blebbistatin (30 μM), KT5720 (4 μM), 3-MA (10 mM), Y27632 (20 μM) and chrysin (100 μM) were from Calbiochem. L-NAME (300 μM) was from Santa Cruz, and cytochalasin D (4 μM), NAC (5 mM), 2-DG (25 mM) and DCA (25 mM) were from Sigma-Aldrich.

2.2.2. Cell culture

MDCK cells were cultured in DMEM supplemented with 10% tetracycline-free FCS, 1% GultaMAX, and 1% penicillin/streptomycin at 37℃ and ambient air supplemented with 5% CO_2. MDCK cells stably expressing

EGFP-RasV12 in a tetracycline- inducible manner (MDCK-pTR GFP-RasV12) were previously established by using the pcDNA4/TO/EGFP-RasV12 plasmid vector and cultured in DMEM supplemented with 0.5 μg ml^{-1} blasticidin (Invitrogen) and 40 μg ml^{-1} Zeocin. To establish MDCK-pTRE3G Myc-RasV12 cells, complementary DNA of Myc-HRasV12 was cloned into BamHI/EcoRI sites of pPB-TRE3G-MCS-CEH-rtTA3-IP, which was constructed by introducing the TRE3G promoter with cloning sites, insulator and rtTA3-expressing elements into a PiggyBac-based vector (SBI). MDCK cells were then transfected with pPB-TRE3G Myc-RasV12 by nucleofection (nucleofector 2b Kit L, Lonza), followed by selection in medium containing 5 μg ml^{-1} blasticidin. MDCK-pTRE3G Myc-RasV12 cells stably expressing FLII^{12}Pglu-700μδ6 were established by co-transfecting MDCK cells with pPB-TRE3G Myc-RasV12 and pPB-FLII^{12}Pglu-700μδ6, followed by the same selection method as above. To establish MDCK-pTR GFP-RasV12 cells stably expressing PDK4 shRNA (PDK4-shRNA1: 5'-GATCCCCGGATTTGGTGGAATTCCATTTCAAGAGAATGGAATTCCAC CAAATCCTTTTTC-3' and 5'-TCGAGAAAAAGGATTTGGTGGAATTCCATTCTCTTGAAATGGAATTC CACCAAATCCGGG-3' or PDK4-shRNA2: 5'-GATCCCCGCATATCGAGTGTCAATATTTCAAGAGAATATTGACACTC GATATGCTTTTTC-3' and 5'-TCGAGAAAAAGCATATCGAGTGTCAATATTCTCTTGAAATATTGACA CTCGATATGCGGG-3') , LDHA shRNA (LDHA-shRNA1: 5'-GATCCCCGCGTAACGTGAACATCTTTTTCAAGAGAAAAGATGTTCAC

GTTACGCTTTTTC-3' and 5'-TCGAGAAAAAGCGTAACGTGAACATCTTTTCTCTTGAAAAAGATGTTCACGTTACGCGGG-3' or LDHA-shRNA2: 5'-GATCCCCCCAAACATCAATATTATTTTTCAAGAGAAAATAATATTGATGTTTGGTTTTTC-3' and 5'-TCGAGAAAAACCAAACATCAATATTATTTTCTCTTGAAAAATAATATTGATGTTTGGGGG-3') or luciferase shRNA(5'-GATCCCCTGAAACGATATGGGCTGAATTCAAGAGATTCAGCCCATATCGTTTCATTTTTC-3' and 5'-TCGAGAAAAATGAAACGATATGGGCTGAATCTCTTGAATTCAGCCCATATCGTTTCAGGG-3'), or MDCK cells stably expressing PDH shRNA (PDH-shRNA1: 5'-GATCCCCGGAAATTGCCGTGTATCTTTTCAAGAGAAAGATACACGGCAATTTCCTTTTTC-3' and 5'-TCGAGAAAAAGGAAATTGCCGTGTATCTTTCTCTTGAAAAGATACACGGCAATTTCCGGG-3' or PDH-shRNA2: 5'-GATCCCCGCAAATCAGTGGATCAAGTTTCAAGAGAACTTGATCCACTGATTTGCTTTTTC-3' and 5'-TCGAGAAAAAGCAAATCAGTGGATCAAGTTCTCTTGAAACTTGATCCACTGATTTGCGGG-3') or luciferase shRNA in a tetracycline-inducible manner, each shRNA sequence was cloned into the BglII/XhoI site of pSUPER.neo + gfp (for the former three shRNAs) or pSUPERIOR.neo + gfp (for the latter two shRNAs) (Oligoengine). For tetracycline-inducible MDCK cell lines, 2 μg ml^{-1} of tetracycline (Sigma-Aldrich) was used to induce expression of proteins or shRNAs except for MDCK-pTRE3G Myc-RasV12

cells, for which 1 μg ml^{-1} of doxycycline (Sigma-Aldrich) was used. MDCK-pTR filamin A shRNA cells were incubated with tetracycline for 48 h to induce sufficient knockdown prior to co-incubation with MDCK-pTR GFP-RasV12 cells. For immunofluorescence, cells were plated onto collagen gel-coated coverslips. Type I collagen (Cellmatrix Type I-A) was obtained from Nitta Gelatin and was neutralized on ice to a final concentration of 2 mg ml^{-1} according to the manufacturer's instructions. The CellTracker dyes CMTPX (red dye), CMFDA (green dye) and CMAC (blue dye) (Life Technologies) were used according to the manufacturer's instructions.

2.2.3. CRISPR/Cas9-based generation of *PDK4*-knockout cells

Guide sequences of PDK4 single-guide RNA 1 (sgRNA1) and sgRNA 2 targeting Canis PDK4 were designed on exons 1 and 9, respectively. PDK4 sgRNA sequences (PDK4 sgRNA1, 5'-GCTTCGTGATGCGCAGCGC-3' ; PDK4 sgRNA2,5' -ACGGCACCAACGCCTGTGA-3') were introduced into the pCDH-EF1-Hygro-sgRNA vector using primers. First, MDCK cells were infected with lentivirus carrying pCW-Cas9, and were cultured in the 500 ng ml^{-1} puromycin-containing medium. The tetracyclineinducible MDCK-Cas9 cells were transfected with the pCDH-EF1-PDK4 sgRNA1 and 2 by nucleofection, followed by selection in medium containing 200 μg ml^{-1} of hygromycin, and subjected to limiting dilution. Indels on the PDK4 exons in each monoclone were analysed by direct sequencing using. To generate PDK4-deleted cells carrying doxycyclineinducible GFP-RasV12, pPB-TRE3G GFP-RasV12 was introduced into the PDK4- deleted cells by nucleofection and antibiotic selection. In addition to the $PDK4^{-/-}$ MDCK-pTRE3G

GFP-RasV12 cells, we generated PDK4$^{+/+}$ MDCK-pTRE3G GFP-RasV12 cells as a control cell line.

2.2.4. Immunofluorescence and western blotting

For immunofluorescence, MDCK-pTR GFP-RasV12, MDCK-pTR cSrcY527F-GFP, MDCK-pTR scribble shRNA, MDCK-pTRE3G Myc-RasV12, MDCK-pTR GFP-RasV12 PDK4 shRNA, MDCK-pTRE3G GFP-RasV12 PDK4 sgRNA, MDCK-pTR PDH shRNA, MDCK-pTR GFP-RasV12 EPLIN shRNA, MDCK-pTR GFP-RasV12 LDHA shRNA or MDCK-pTR GFP-RasV12 luciferase shRNA cells were mixed with MDCK, MDCK-pTR filamin A shRNA or MDCK-pTR luciferase shRNA cells at a ratio of 1:50 and plated onto collagen-coated coverslips. The mixture of cells was incubated for 8–12 h, followed by tetracycline or doxycycline treatment for 16 h, except for analyses of apical extrusions, which were examined after 24 h of tetracycline or doxycycline addition. Cells were fixed with 4% paraformaldehyde (PFA) in PBS and permeabilized with 0.5% TritonX-100 in PBS, then blocked with 1% BSA in PBS. All primary antibodies were used at 1:100, and all secondary antibodies were used at 1:200. To monitor the mitochondrial activity or superoxide production, cells were loaded with 50 nM TMRM or 5 μM MitoSOX respectively for 30 min and subjected to microscopic observation or quantitatively analysed with a CellInsight image cytometer (Thermo Fisher Scientific). The ratiometric images of TMRM and MitoTracker Green were obtained by incubating cells with 200 nM MitoTracker Green for 2 h, briefly washed, and then loaded with 50 nM TMRM. The 2-NBDG uptake was examined by incubating cells with glucose-free DMEM for 2 h followed by

addition of 100 μM 2-NBDG for 30 min. Immunofluorescence images were analysed with the Olympus FV1000 or FV1200 system and Olympus FV10-ASW software. Images were quantified with the MetaMorph software (Molecular Devices). Western blotting was carried out as previously described. Primary antibodies were used at 1:1,000. The western blotting data were analysed using ImageQuant LAS4010 (GE Healthcare).

2.2.5. FRET analysis

Glucose FRET experiments were carried out as follows, MDCK-pTRE3G Myc-RasV12 cells stably expressing FLII^{12}Pglu-700μδ6 were co-cultured with MDCK cells at a ratio of 1:50 or cultured alone on a collagen gel in 35 mm diameter, glass-bottom dishes (Matsunami Glass). At 16 h after doxycycline addition, a differential interference contrast (DIC) image and cyan fluorescent protein (CFP) and FRET fluorescence images were recorded. FRET efficiency was calculated as a quotient of background-subtracted FRET and CFP images and is presented in an intensity-modified display mode with the MetaMorph software. In the intensity-modified display mode, eight colours from red to blue are used to represent the FRET efficiency. To evaluate the ATP level, MDCK-pTRE3G Myc-RasV12 cells were transiently transfected with ATeam probe57, stained with CMTPX, and co-cultured with MDCK cells at ratio of 1:50 or cultured alone on a collagen gel in 35 mm diameter, glass-bottom dishes. At 16 h after doxycycline addition, FRET efficiency was examined as described above.

2.2.6. Electron microscopy

MDCK-pTR GFP-RasV12 cells were cultured alone or co-cultured with MDCK cells in collagen-gel-coated, grid-imprinted plastic dishes (μ-Dish 35 mm Grid-500, Ibidi Corporation). After tetracycline treatment for 24 h, cells were fixed in 2% glutaraldehyde in HEPES buffer (30 mM HEPES, 0.1 M NaCl and 2 mM CaCl2 (pH 7.4)), and fluorescence and DIC images of GFP-RasV12 cells and the surrounding cells were captured together with the underlying, numbered grid information. Cells were then post-fixed in 2% osmium tetroxide in 0.1 M imidazole (pH 7.4) and stained with 1% uranyl acetate (UA) before being dehydrated and embedded in Araldite–Epon resin (Electron Microscopy Sciences). During these procedures, GFP fluorescence was lost, but the grid was imprinted onto the resin. Subsequently, GFP-RasV12 cells and the two or three rows of surrounding MDCK cells were selected and excised, while referring to the grid information, morphology of the cells and captured images. Ultrathin sections of the trimmed sample were poststained with UA and lead citrate, and cells were imaged with an electron microscope (JEM-1400; JEOL) operating at 80 kV.

2.2.7. Quantitative real-time PCR

MDCK-pTR GFP-RasV12 cells or a 10:1 mixed culture of MDCK and MDCK-pTR GFP-RasV12 cells were cultured at a density of 2×10^7 cells on collagen-coated 15 cm dishes (Greiner-Bio-One). After incubation with tetracycline for 16 h, GFP-positive RasV12 cells and GFP-negative MDCK cells were separated with an analytical flow cytometer. Total RNA was extracted from the isolated cells using Trizol (Thermo Fisher Scientific) and an RNeasy Mini Kit (QIAGEN) and reverse transcribed using a QuantiTect

Reverse Transcription Kit (QIAGEN). GeneAce SYBR qPCR Mix (NIPPON GENE) was used to perform qPCR using the StepOne system (Thermo Fisher Scientific). The primer sequences used are listed in Supplementary Table 1. We used ß-actin as a reference gene to normalize data.

2.2.8. Lactate assay

For lactate assay, MDCK cells, MDCK-pTR GFP-RasV12 cells, MDCK-pTR GFP-RasV12 LDHA shRNA cells or a 1:1 mix of MDCK and MDCKpTR GFP-RasV12 or MDCK-pTR GFP-RasV12 LDHA shRNA cells were cultured at a density of 6.5×10^5 cells on collagen-coated 12-well dishes (Falcon) in DMEM containing neither phenol red nor FCS. The culture medium was replaced with fresh medium at 12 h after tetracycline addition and collected 12 h later. Samples were subjected to measurement of lactate concentration using a lactate assay kit (BioVision).

2.2.9. Statistics and reproducibility

For data analyses, unpaired two-tailed Student t-tests were used to determine P-values. P-values less than 0.05 were considered to be significant. No statistical method was used to predetermine sample size. All results were reproduced with at least two independent experiments.

2.3. Results

2.3.1. Warburg-effect-like metabolic changes occur in RasV12-transformed cells that are surrounded by normal cells

To examine the involvement of metabolic regulation in cell competition, we first examined mitochondrial energy metabolism at the interface between normal and RasV12-transformed epithelial cells. TMRM (tetramethylrhodamine methyl ester) is a positively charged red fluorescent dye that accumulates in active mitochondria according to the negative membrane potential gradient across their inner membranes. We found that the TMRM fluorescence, but not the fluorescence of a control dye CMTPX, was strongly reduced in RasV12-transformed epithelial cells surrounded by normal epithelial cells when compared with that in RasV12-transformed cells cultured alone or in green fluorescent protein (GFP)-expressing cells surrounded by normal cells (Fig. 2-1). A comparable phenomenon was also observed in Src-transformed cells, but not in scribble-knockdown cells (Fig. 2-2). The decreased incorporation of TMRM was observed in both apically extruding and extruded RasV12 cells (Fig. 2-3). The mix ratio of normal and RasV12 cells affected the TMRM incorporation in RasV12 cells; the decreased TMRM incorporation was clearly observed at 50:1 or 10:1, but occurred less frequently at 4:1 or 1:1. This is compatible with the previous report demonstrating that the proportion of winner–loser cells profoundly influences the occurrence of cell competition. The non-cell-autonomous downregulation of mitochondrial membrane potential was also confirmed by using MitoSOX, an indicator for mitochondrial superoxide production that

reflects mitochondrial ATP production (Fig. 2-4). Immunofluorescence of the mitochondrial resident protein Tom20 or MitoTracker Green fluorescence, which is incorporated into mitochondria in a membrane-potential-independent manner, showed that the number of mitochondria was not altered in RasV12 cells surrounded by normal cells (Fig. 2-5 and 6). In addition, by electron microscopic analyses, mitophagosome-like structures were frequently observed in RasV12 cells that were surrounded by normal epithelial cells (Fig. 2-7). Collectively, these data imply that the decreased TMRM incorporation results not from a change in mitochondrial mass, but from a change in mitochondrial function. Furthermore, we found that incorporation of the glucose analogue 2-deoxy-2-[(7-nitro-2,1,3-benzoxadiazol-4-yl) amino]-D-glucose (2-NBDG) was enhanced in RasV12 cells surrounded by normal cells (Fig. 2-8), suggesting that uptake of glucose is enhanced in a non-cell-autonomous fashion. Moreover, expression of lactate dehydrogenase A (LDHA), which converts pyruvate to lactate, was significantly increased in RasV12-transformed cells that were surrounded by normal cells (Fig. 2-9 and 10). Accordingly, lactate secretion was higher in RasV12 cells than normal cells, and was further enhanced when RasV12 cells were surrounded by normal cells (Fig. 2-11). This non-cell-autonomous increase in lactate secretion was abolished when LDHA was knocked down in RasV12 cells (Fig. 2-11). These data indicate that the interaction with the neighboring normal epithelial cells potentiates the Warburg-effect-like metabolic changes in transformed cells: downregulation of mitochondrial function and enhanced aerobic glycolysis.

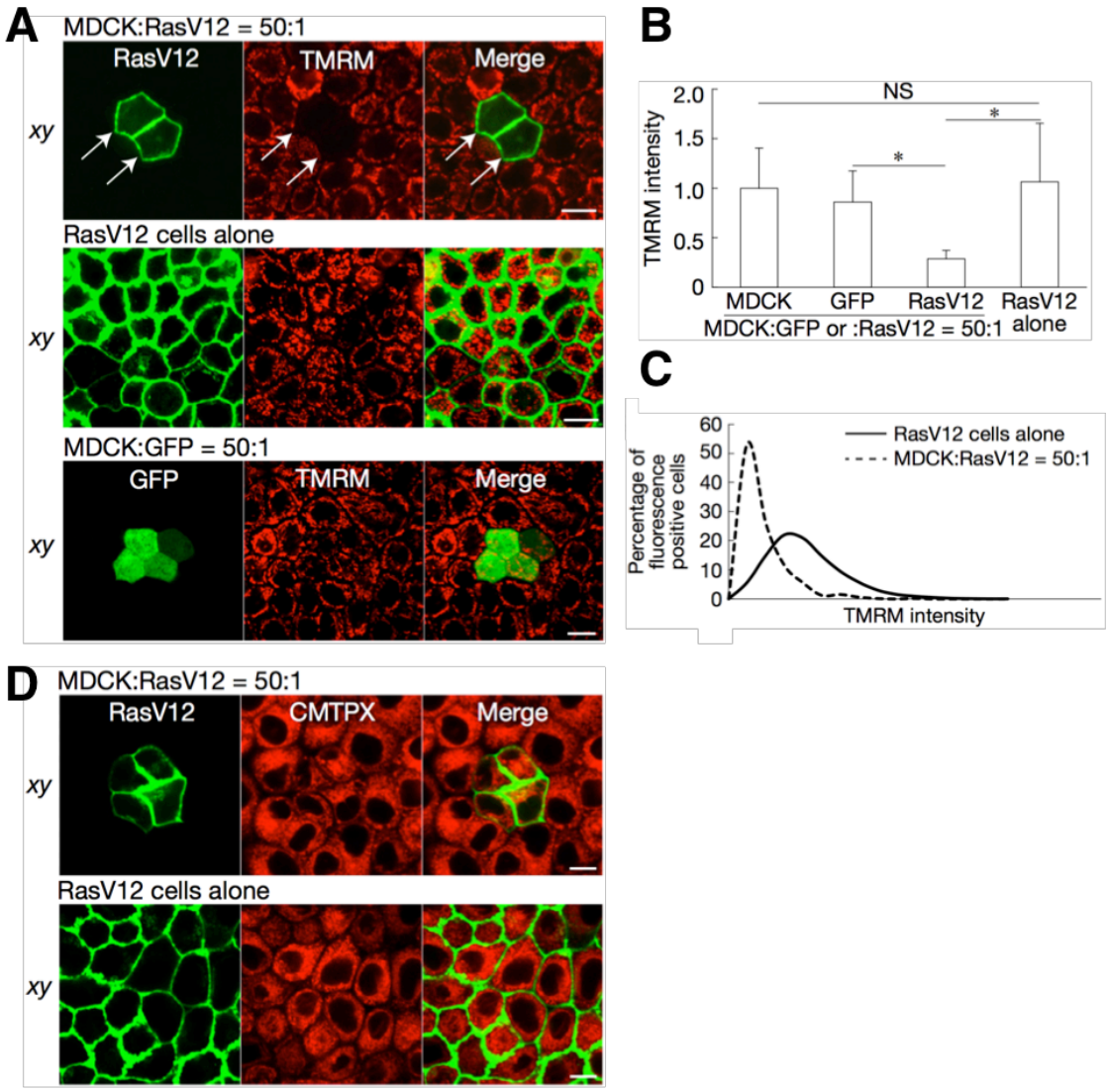

Fig. 2-1 Mitochondrial membrane potential is diminished in RasV12- transformed cells that are surrounded by normal epithelial cells. (**A**) Confocal microscopy images of MDCK-pTR GFP-RasV12 or MDCK-pTR GFP cells mixed with normal MDCK cells, or cultured alone. Cells were loaded with 50 nM TMRM (red). (**B**) Quantification of the fluorescence intensity of TMRM. Data are mean ± s.e.m. Values are expressed as a ratio relative to MDCK. **P* < 0.001, unpaired two-tailed *t* -test; *n* = 92, 24, 53 and 60 cells pooled from three independent experiments. (**C**) Measurement of fluorescence intensity of TMRM using an image cytometer in MDCK-pTR GFP-RasV12 cells mixed with normal MDCK cells or cultured alone. Cells were loaded with 50 nM TMRM. (**D**) CMTPX incorporation in RasV12-transformed cells. MDCK-pTR GFP-RasV12 cells were mixed with normal MDCK cells or cultured alone, and loaded with 5 μM CMTPX (red). Scale bars, 10 μm (**A**, **D**)

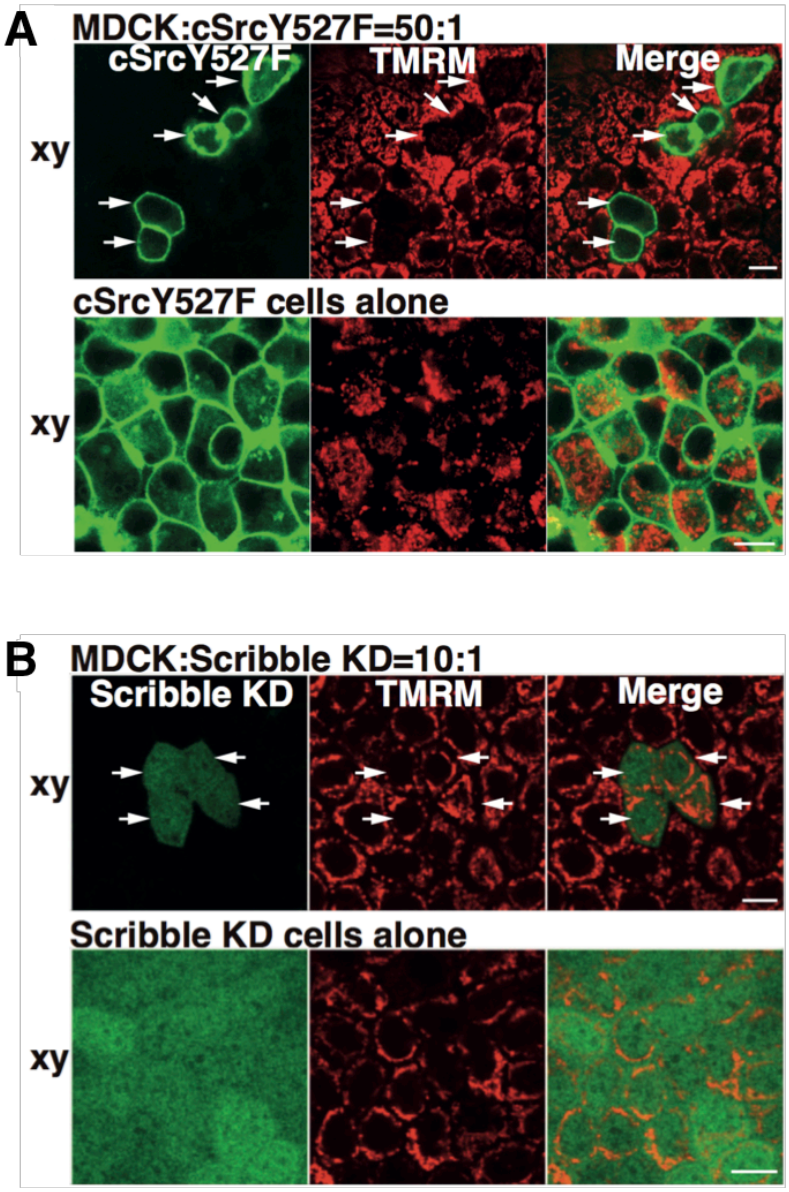

Fig. 2-2 The mitochondrial membrane potential is decreased in Src-transformed cells but not in Scribble-knockdown cells when they are surrounded by normal cells. (**A**) TMRM incorporation in Src-transformed cells. MDCK-pTR cSrcY527F-GFP cells were mixed with normal MDCK cells or cultured alone, and loaded with 50 nM TMRM (red). Arrows indicate Src-transformed cells showing diminished fluorescence intensity of TMRM. (**B**) TMRM incorporation in Scribble-knockdown cells. MDCK-pTR Scribble-shRNA cells were mixed with normal MDCK cells or cultured alone, and incubated with tetracycline for 48 h and loaded with 50 nM TMRM (red). Arrows indicate Scribble-knockdown cells showing the comparable fluorescence intensity of TMRM to that in the surrounding normal cells. Scale bars, 10 μm (**A**, **B**)

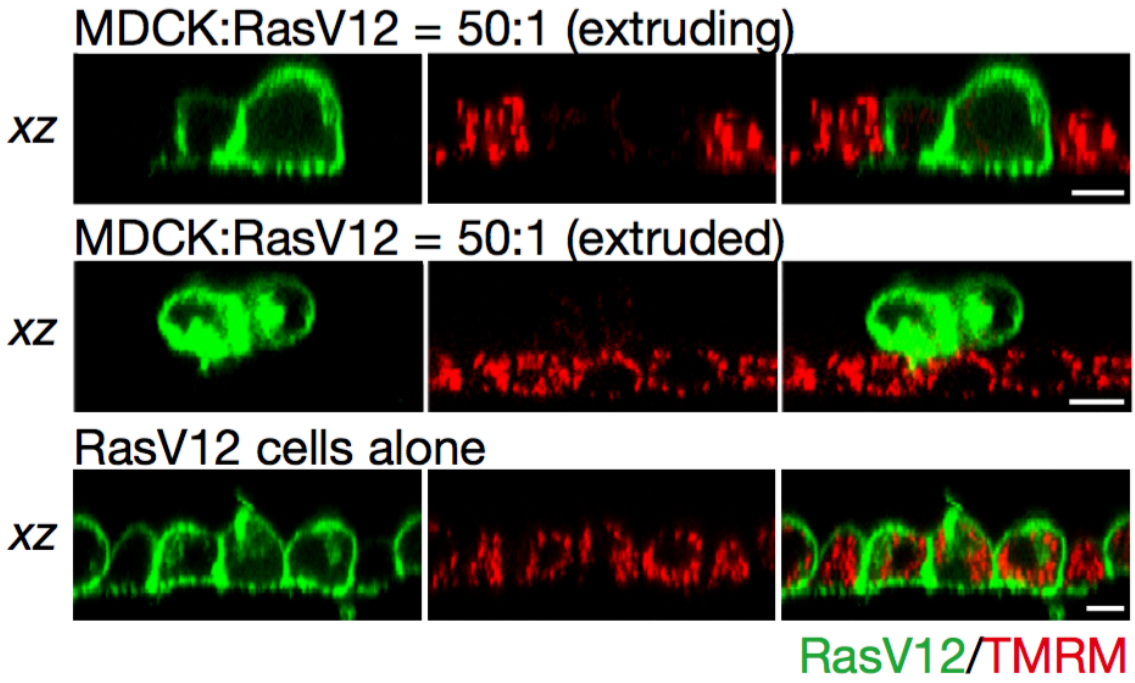

Fig. 2-3 The decreased incorporation of TMRM was observed in both apically extruding and extruded RasV12 cells. Confocal microscopy images of *xz* sections of apically extruding or extruded RasV12-transformed cells surrounded by normal cells and of RasV12-transformed cells cultured alone. Scale bars, 10 μm.

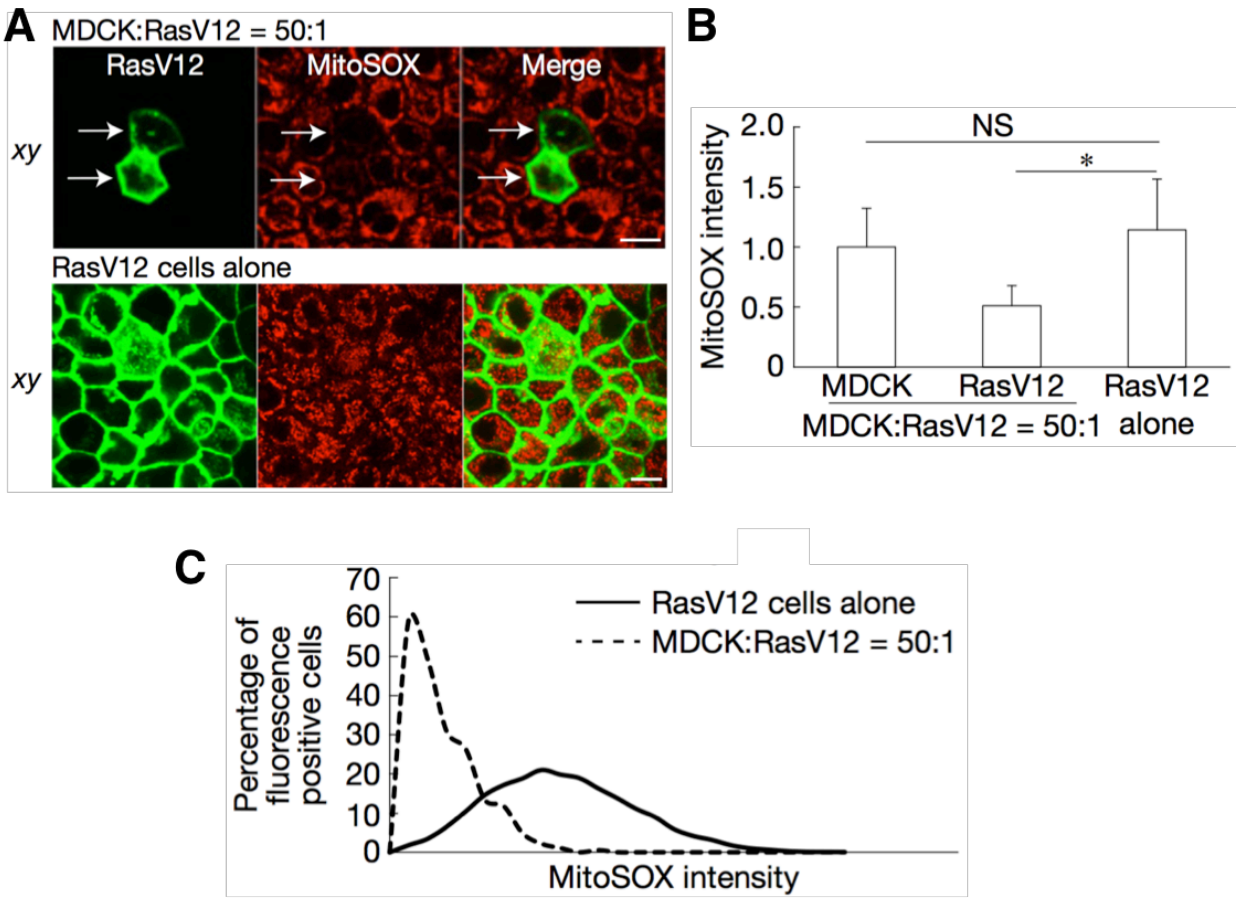

Fig. 2-4 Incorporation of MitoSOX in RasV12-transformed cells surrounded by normal cells. (**A**) Confocal microscopy images of MDCK-pTR GFP-RasV12 or MDCK-pTR GFP cells mixed with normal MDCK cells, or cultured alone. Cells were loaded with 5 μM MitoSOX (red). Scale bars, 10 μm. (**B**) Quantification of the fluorescence intensity of MitoSOX. Data are mean ± s.e.m. Values are expressed as a ratio relative to MDCK. *$P < 0.001$, unpaired two-tailed t-test; $n = 52$, 45 and 31 cells pooled from three independent experiments. (**C**) Measurement of fluorescence intensity of TMRM using an image cytometer in MDCK-pTR GFP-RasV12 cells mixed with normal MDCK cells or cultured alone. Cells were loaded with 5 μM MitoSOX.

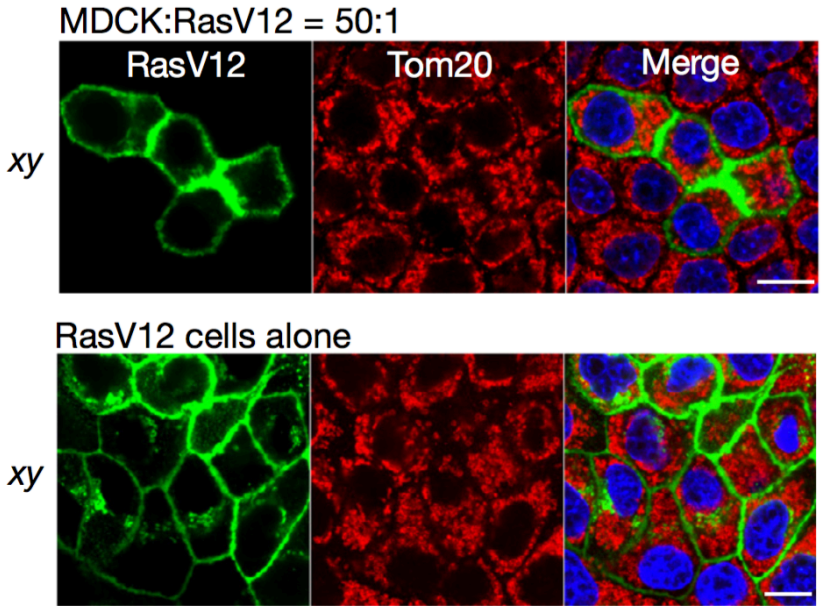

Fig. 2-5 Immunofluorescence images of Tom20. MDCK-pTR GFP-RasV12 cells were mixed with normal MDCK cells or cultured alone, and were stained with Hoechst 33342 (blue) and anti-Tom20 antibody (red). Scale bars, 10 μm.

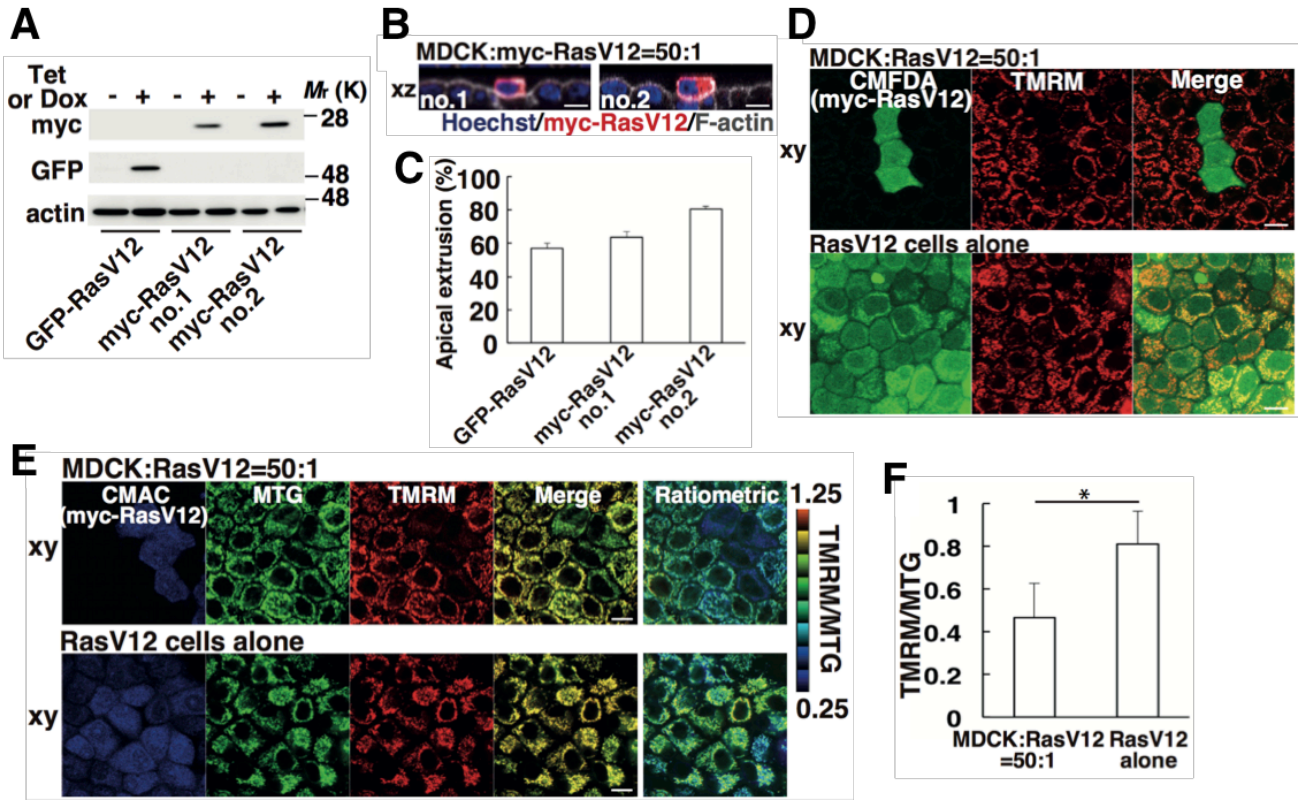

Fig. 2-6 The number of mitochondria was not altered in RasV12 cells surrounded by normal cells. (**A**) Establishment of doxycycline-inducible myc-RasV12 MDCK cell lines. Doxycycline-induced expression of myc-RasV12 proteinis determined by western blotting. (**B**) Immunofluorescence images of xz sections of myc-RasV12 MDCK cells surrounded by normal MDCK cells. (**C**) Quantification of the apical extrusion of myc-RasV12 cells. Data are mean ± s.e.m.. n=2 independent experiments. These data demonstrate that myc-RasV12 cells are apically extruded when surrounded by normal cells, similarly for GFP-RasV12 cells. (**D**) TMRM incorporation in myc-RasV12 cells. MDCK-pTRE3G myc-RasV12 cells were fluorescently labelled with CMFDA dye (green), and co-cultured with normal MDCK cells or cultured alone, and loaded with 50 nM TMRM (red). This result shows that non-cell-autonomous reduction of TMRM incorporation also occurs in myc-RasV12 cells. (**E**) Immunofluorescence and ratiometric images of MitoTracker Green (MTG) and TMRM. MDCK-pTRE3G myc-RasV12 cells were fluorescently labelled with CMAC dye (blue), and co-cultured with normal MDCK cells or cultured alone. Cells were incubated with 200 nM MTG for 2 h, washed briefly and subsequently loaded with 50 nM TMRM for 30 min. Scale bars, 10 μm (**B**, **D**, **E**). (**F**) Quantification of the ratio of TMRM to MTG. Data are mean ± s.e.m.. *P<0.001, unpaired two-tailed t-test; n=50 and 36 cells pooled from three independent experiments.

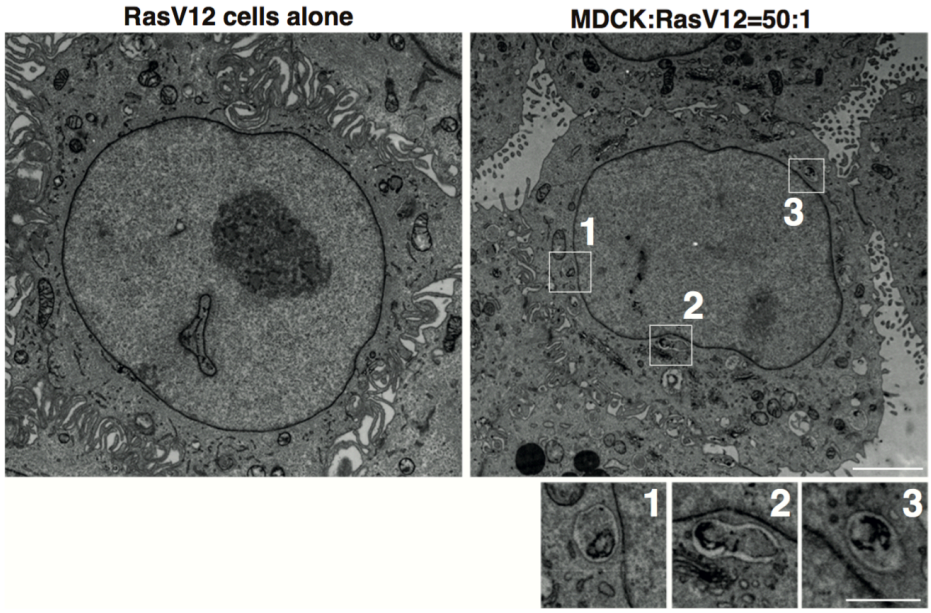

Fig. 2-7 Mitophagosome-like structures are frequently observed in RasV12 cells that are surrounded by normal epithelial cells. Electron microscopic images of MDCK-pTR GFP-RasV12 cells cultured alone or surrounded by normal cells. The areas in the white boxes are shown below at higher magnification, demonstrating mitophagosome-like structures. In RasV12 cells surrounded by normal cells, on average 0.65 mitophagosome-like structures in a single RasV12 cell per slice (51 slices); in RasV12 cells cultured alone, on average 0.01 mitophagosome-like structures in a single RasV12 cell per slice (84 slices). Scale bars, 2 μm (upper panels) and 0.5 μm (lower panels).

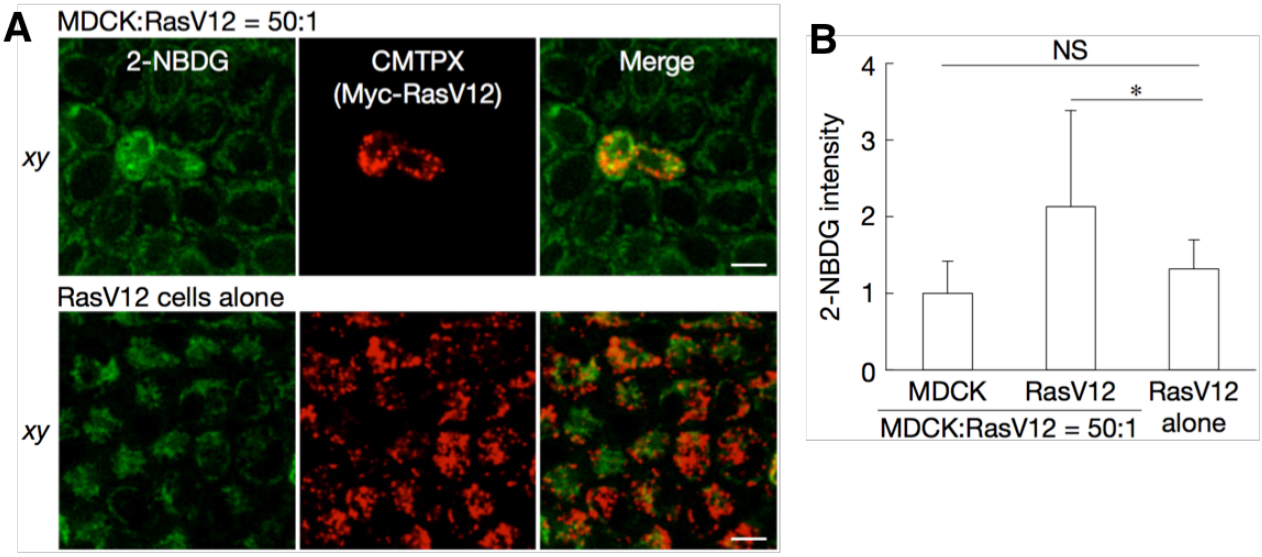

Fig. 2-8 Warburg-effect-like metabolic changes in RasV12-transformed cells that are surrounded by normal cells. (**A**) 2-NBDG incorporation in Myc-RasV12 cells. MDCK-pTRE3G Myc-RasV12 cells co-cultured with MDCK cells or cultured alone were loaded with 100 μM 2-NBDG. Scale bars, 10 μm. (**B**) Quantification of the fluorescence intensity of 2-NBDG. Data are mean ± s.e.m. Values are expressed as a ratio relative to MDCK. **P* < 0.001, unpaired two-tailed *t* -test; *n* = 66, 66 and 48 cells pooled from three independent experiments.

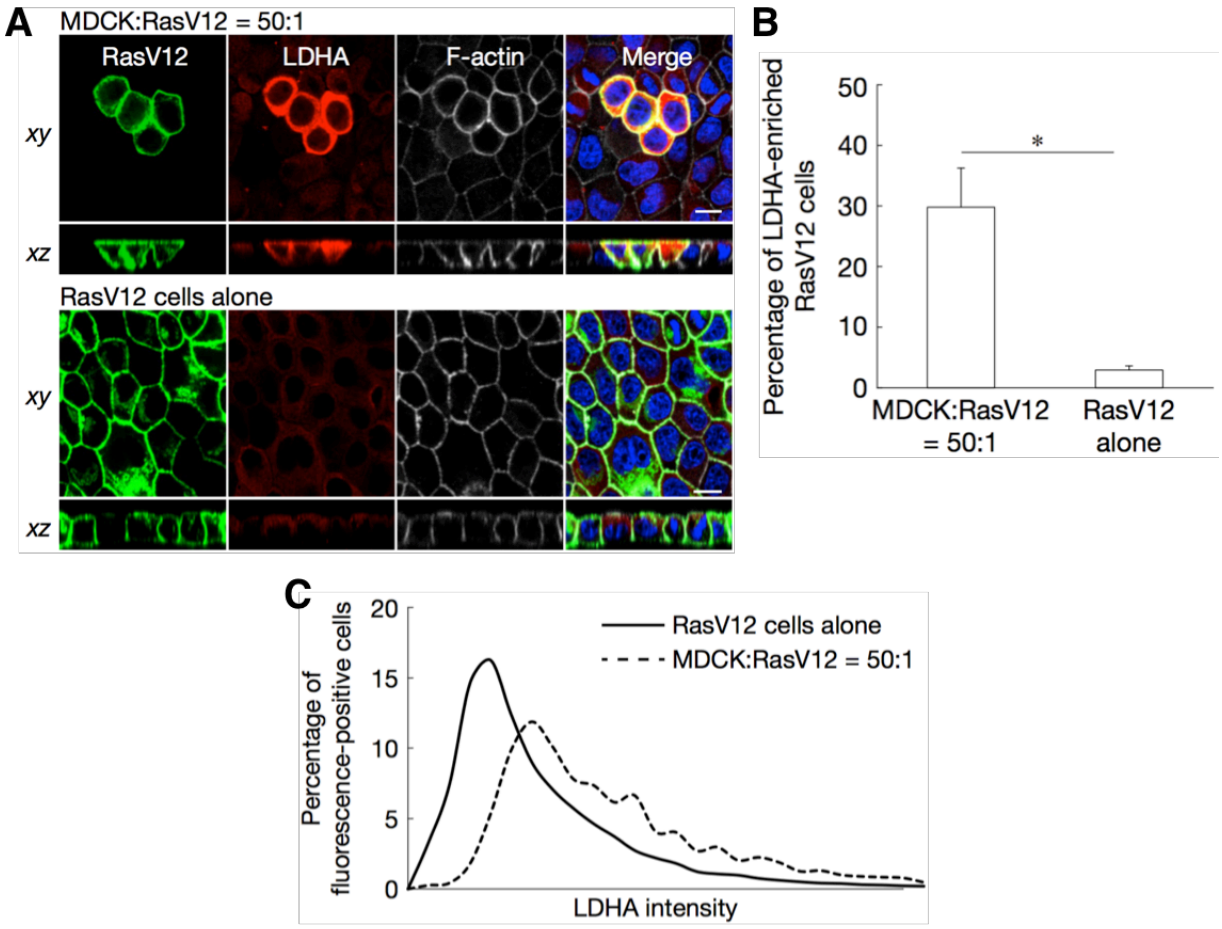

Fig. 2-9 Accumulation of LDHA in RasV12-transformed cells surrounded by normal cells. (**A**) Immunofluorescence images of LDHA. MDCK-pTR GFP-RasV12 cells were mixed with normal MDCK cells or cultured alone, and were stained with Hoechst 33342 (blue), anti-LDHA antibody (red) and Alexa-Fluor-647-conjugated phalloidin (white). Scale bars, 10 μm. (**B**) Quantification of the percentage of LDHA-enriched RasV12-transformed cells. Data are mean ± s.e.m. $*P < 0.05$, unpaired two-tailed *t* -test; *n* = two independent experiments. (**C**) The measurement of fluorescence intensity of LDHA using an image cytometer in MDCK-pTR GFP-RasV12 cells mixed with normal MDCK cells or cultured alone. Cells were stained with Hoechst 33342 and anti- LDHA antibody.

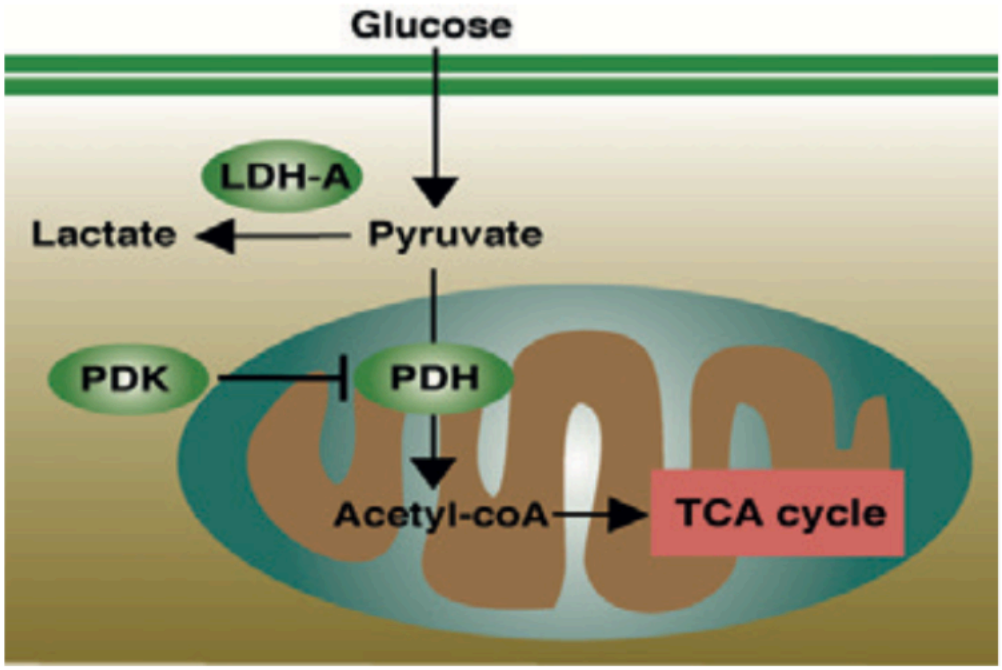

Fig. 2-10 The illustration for the mode of action of PDK and LDHA.

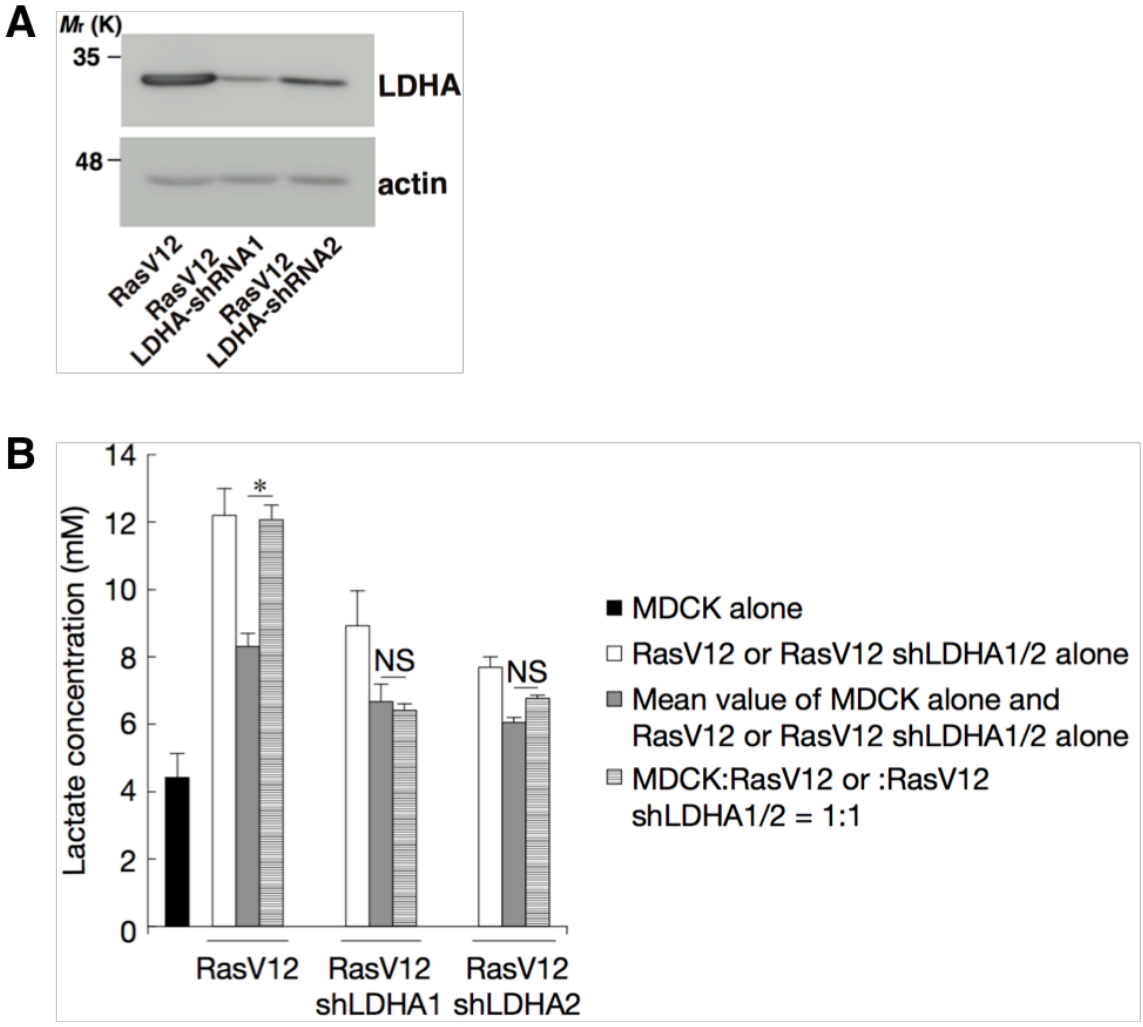

Fig. 2-11 Lactate secretion in the mix culture condition. (**A**) Establishment of MDCK-pTR GFP-RasV12 cells stably expressing LDHA-shRNA1 or -shRNA2. Knockdown of LDHA is confirmed by western blotting. (**B**) Lactate concentration in the conditioned medium at 12–24h after tetracycline addition. The mean values of the indicated single cultures are also shown as the grey bars. Data are mean ± s.e.m. *P < 0.001, unpaired two-tailed t -test; n = five independent experiments for MDCK alone, RasV12 alone and MDCK:RasV12 = 1:1, two independent experiments for RasV12 shLDHA1 alone and MDCK:RasV12 shLDHA1 = 1:1, and three independent experiments for RasV12 shLDHA2 alone and MDCK:RasV12 shLDHA2 = 1:1.

2.3.2. PDK4 plays a crucial role in the decreased mitochondrial membrane potential and apical extrusion of RasV12-transformed cells surrounded by normal cells

To reveal the molecular mechanism that causes the Warburg-effect-like phenomenon, we examined expression of various metabolic enzymes by quantitative real-time PCR (qrtPCR) and found that expression of pyruvate dehydrogenase kinase 4 (PDK4) was significantly elevated in RasV12-transformed cells when they were co-cultured with normal cells (Fig. 2-12). PDK4 phosphorylates and thus inactivates pyruvate dehydrogenase (PDH), which catalyses conversion of pyruvate to acetyl-CoA, thereby blocking the entry into the tricarboxylic acid cycle (Fig.2-10). Indeed, phosphorylation of PDH was also enhanced in RasV12 cells when they were surrounded by normal cells (Fig. 2-13). To examine the functional involvement of PDK4, we established RasV12-transformed cells stably expressing PDK4 short hairpin RNA (shRNA) (Fig. 2-14) and CRISPR-edited PDK4-knockout RasV12-transformed cells (Fig. 2-15). PDK4 knockdown or knockout suppressed PDH phosphorylation and significantly restored TMRM incorporation in RasV12 cells surrounded by normal cells (Fig. 2-16 and 17), suggesting that upregulation of PDK4 is, at least partly, responsible for the decreased mitochondrial membrane potential. PDK4 knockdown or knockout also suppressed LDHA accumulation (Fig. 2-18). Interestingly, PDK4 knockdown or knockout drastically suppressed apical extrusion of RasV12 cells, while promoting formation of basal protrusions that extended beneath the neighboring normal cells (Fig. 2-19 and 20). Dichloroacetate (DCA) is a specific inhibitor of the PDK family, of which

upregulation is often observed in the late stage of cancer. Therefore, DCA has been intensively tested in clinical trials for treatment of malignant cancer including glioblastoma and various solid tumors. We found that treatment of DCA caused an effect comparable to that induced by PDK4 knockdown or knockout: suppression of PDH phosphorylation (Fig. 2-21), restoration of TMRM incorporation (Fig. 2-22) and suppression of apical extrusion and promotion of basal protrusions (Fig. 2-23). We also demonstrated that another PDK inhibitor, radicicol, phenocopied the effect of DCA (Fig. 2-24). DCA treatment also suppressed elevated LDHA expression in RasV12 cells surrounded by normal cells (Fig. 2-21). In contrast, knockdown of LDHA in RasV12 cells did not affect TMRM incorporation (Fig. 2-25), suggesting that decreased mitochondrial membrane potential causes LDHA upregulation. Moreover, knockdown of LDHA moderately suppressed apical extrusion (Fig. 2-26). These results imply that the PDK4-mediated Warburg-effect-like metabolic alteration influences the behavior of transformed cells and promotes their elimination from epithelia. When PDH-knockdown cells were surrounded by normal cells, apical extrusion did not occur (Fig. 2-27), indicating that downregulation of mitochondrial membrane potential alone is not sufficient to cause apical extrusion. Thus, while the non-cell-autonomously induced metabolic changes play an indispensable role in the elimination of transformed cells, additional, unidentified molecular mechanisms, which need to be explored in future studies, are also involved in this process.

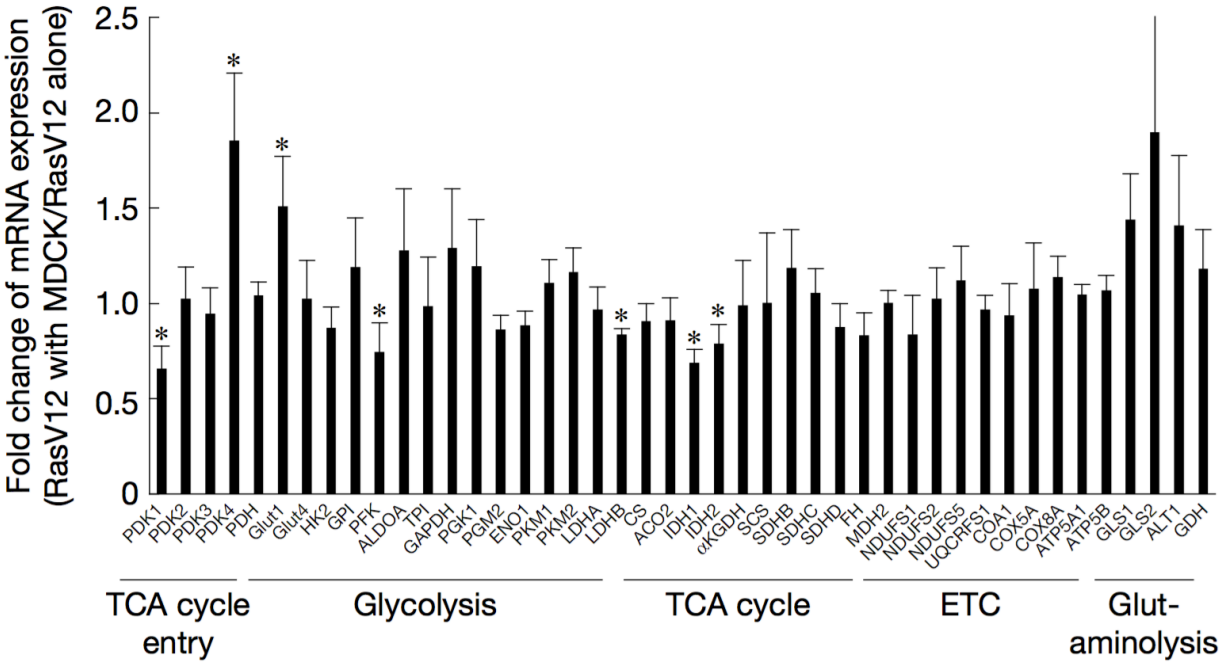

Fig. 2-12 PDK4 expression is upregulated in RasV12-transformed cells surrounded by normal cells. qrtPCR analysis of various metabolic enzymes in RasV12-transformed cells surrounded by normal cells. MDCK-pTR GFP-RasV12 cells were co-cultured with normal MDCK cells or cultured alone. GFP-positive RasV12 cells were selectively collected by FACS and subjected to qPCR analysis. Values are shown as fold change in RasV12 cells surrounded by normal cells relative to RasV12 cells cultured alone. Data are mean ± s.e.m. **P* < 0.05, unpaired two-tailed *t* -test; *n* = three or four independent experiments.

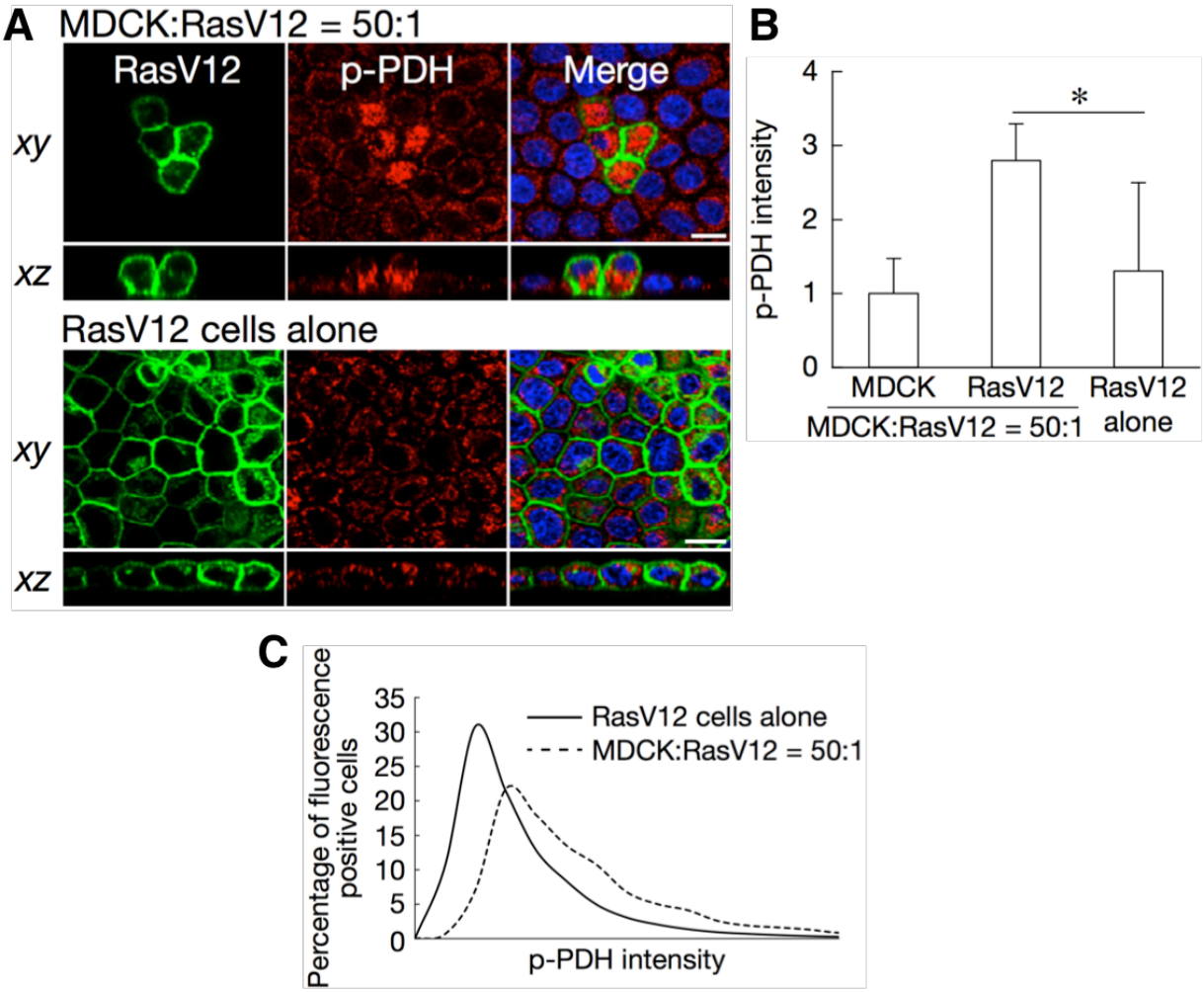

Fig. 2-13 The phosphorylation of PDH is upregulated in RasV12-transformed cells surrounded by normal cells. (**A**) Immunofluorescence images of phosphorylated PDH. MDCK-pTR GFP-RasV12 cells were mixed with normal MDCK cells or cultured alone, and were stained with Hoechst 33342 (blue) and anti-p-PDH antibody (red). Scale bars, 10 μm. (**B**) Quantification of the fluorescence intensity of p-PDH. Data are mean ± s.e.m. Values are expressed as a ratio relative to MDCK. **P* < 0.005, unpaired two-tailed *t* -test; *n* = 93, 147 and 89 cells pooled from three independent experiments. (**C**) Measurement of fluorescence intensity of p-PDH using an image cytometer in MDCK-pTR GFP-RasV12 cells mixed with normal MDCK cells or cultured alone. Cells were stained with Hoechst 33342 and anti-p-PDH antibody.

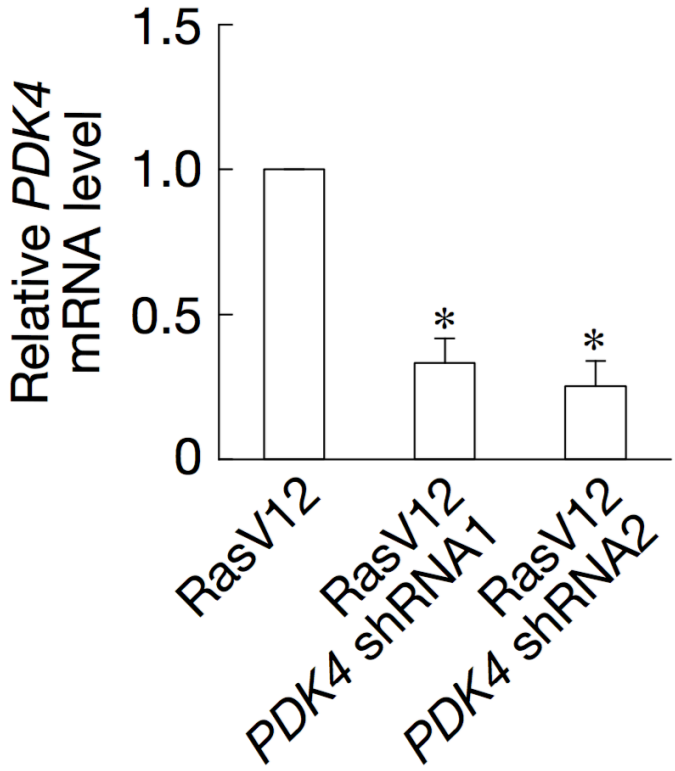

Fig. 2-14 Establishment of MDCK-pTR GFP-RasV12 cells stably expressing *PDK4* shRNA1 or *PDK4* shRNA2. Knockdown of *PDK4* was confirmed by qrtPCR. Data are mean ± s.e.m. **P* < 0.01, unpaired two-tailed *t* -test; *n* = three independent experiments.

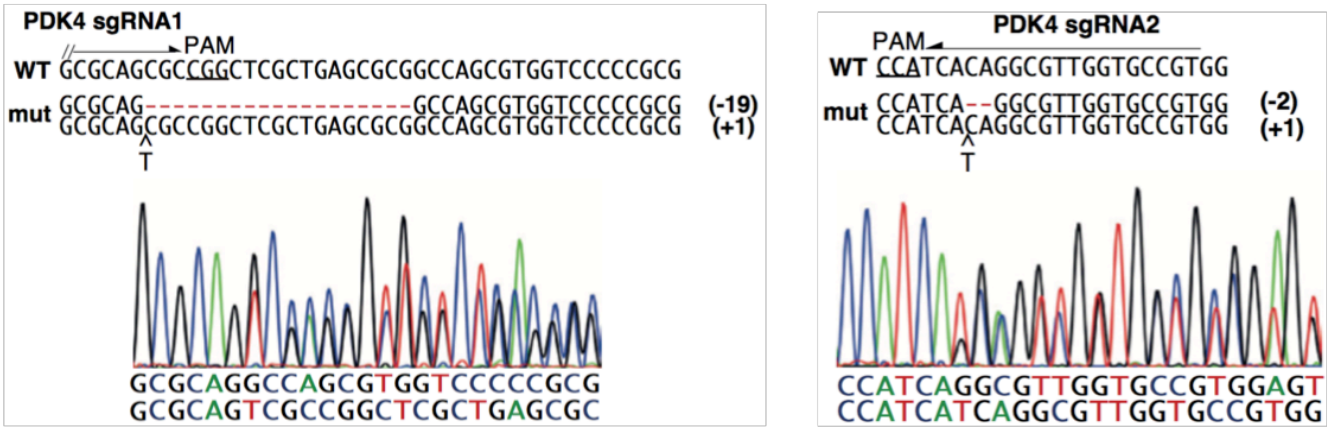

Fig. 2-15 Establishment of MDCK-pTRE3G GFP-RasV12 PDK4 sgRNA1 or PDK4 sgRNA2. A targeting scheme and DNA sequences of the wild type and PDK4-null MDCK-pTRE3G GFP-RasV12 cell lines. PAM motifs are underlined. The red spacing indicates a deleted nucleotide.

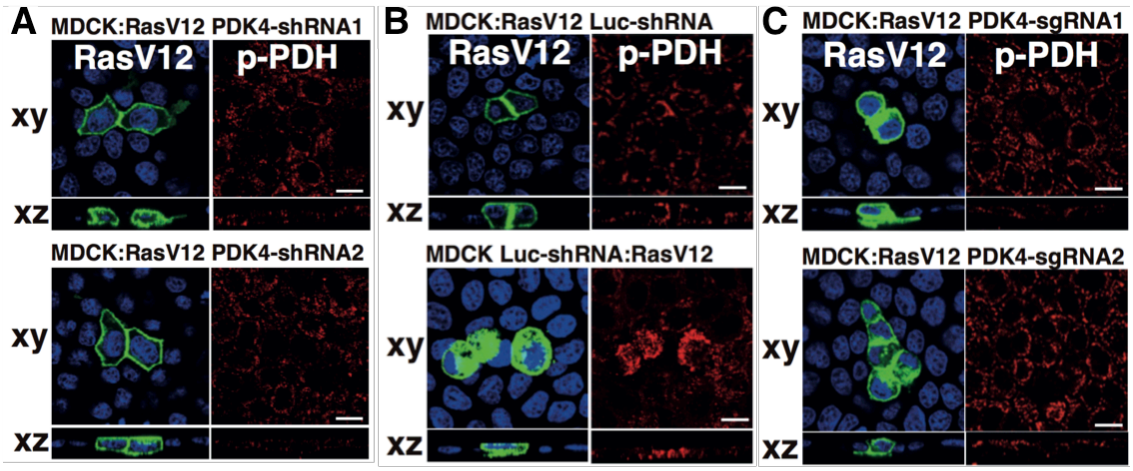

Fig. 2-16 Effect of PDK4-knockdown or -knockout on p-PDH. MDCK-pTR GFP-RasV12 PDK4-shRNA cells (**A**), MDCK-pTR GFP-RasV12 Luciferase-shRNA cells (**B**) or MDCK-pTRE3G GFP-RasV12 PDK4-sgRNA cells (**C**) were mixed with normal MDCK cells or MDCK-pTR Luciferase-shRNA cells. Cells were stained with Hoechst 33342 (blue) and anti-p-PDH (red). Scale bars, 10 μm.

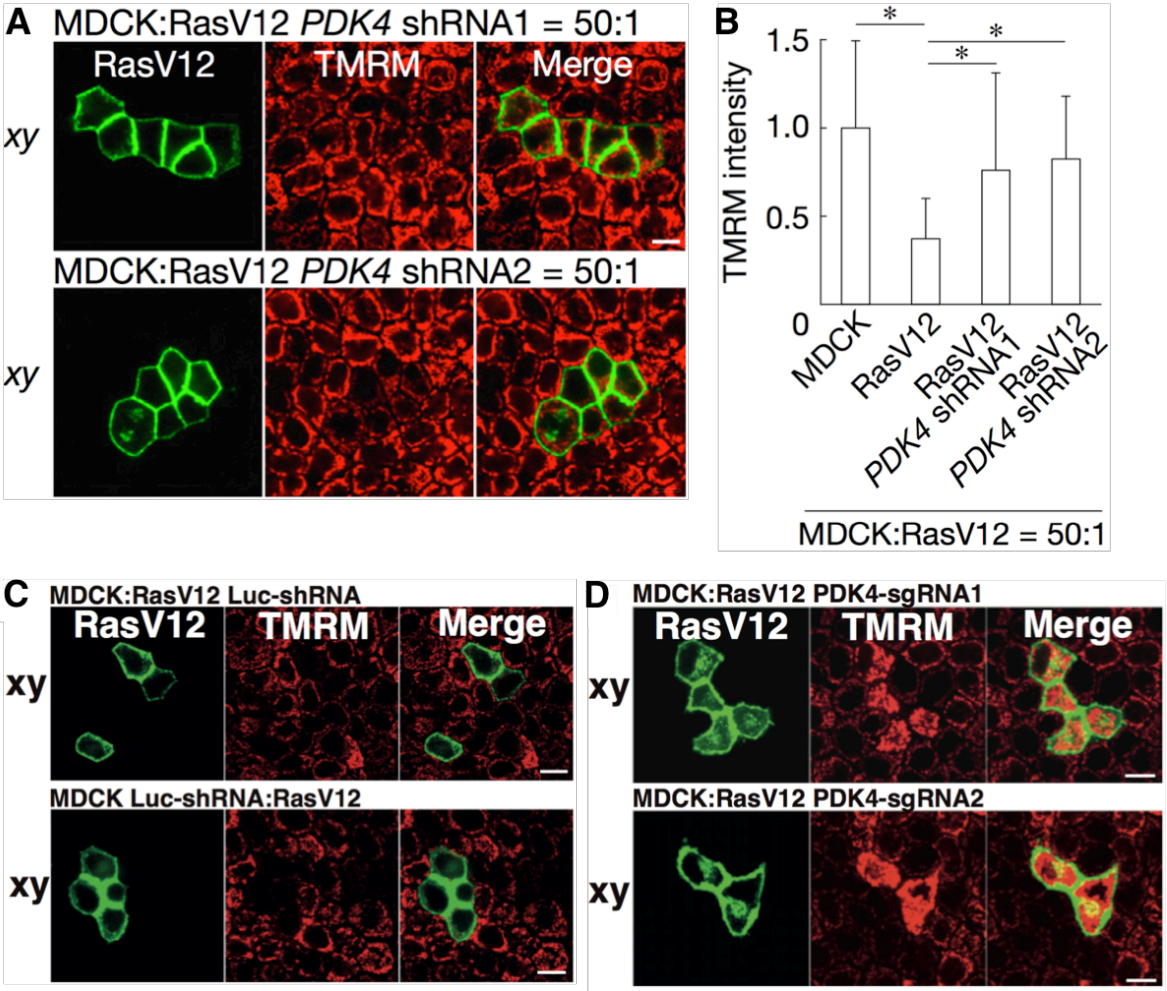

Fig. 2-17 Effect of PDK4-knockdown or -knockout on TMRM incorporation. MDCK-pTR GFP-RasV12 PDK4-shRNA cells (**A**), MDCK-pTR GFP-RasV12 Luciferase-shRNA cells (**C**) or MDCK-pTRE3G GFP-RasV12 PDK4-sgRNA cells (**D**) were mixed with normal MDCK cells or MDCK-pTR Luciferase-shRNA cells. Cells were loaded with 50 nM TMRM (red). Scale bars, 10 μm. (**B**) Quantification of the fluorescence intensity of TMRM. Data are mean ± s.e.m. Values are expressed as a ratio relative to MDCK. **P* < 0.001, unpaired two-tailed *t* -test; *n* = 92, 92, 97 and 102 cells pooled from three independent experiments.

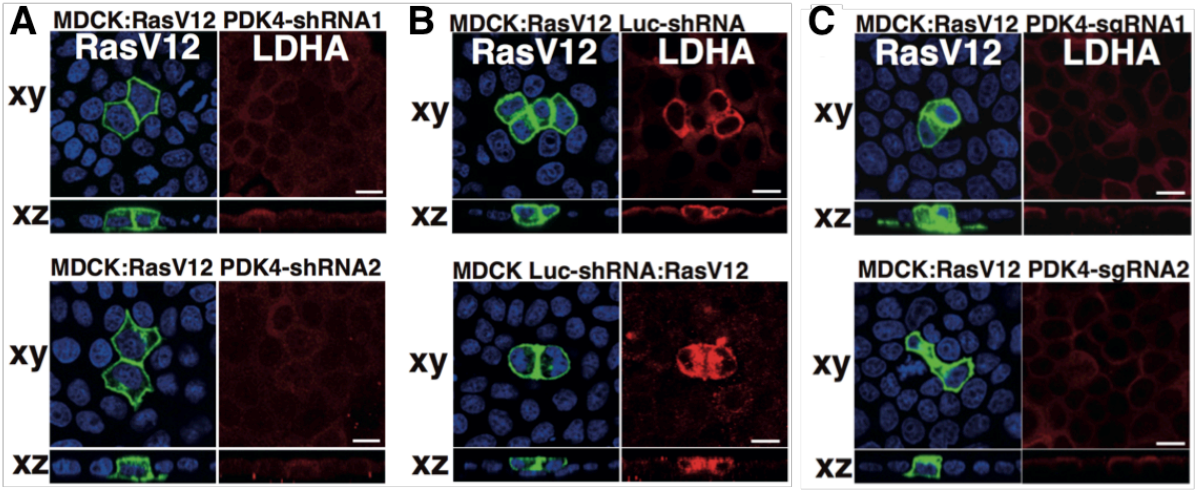

Fig. 2-18 Effect of PDK4-knockdown or -knockout on LDHA. MDCK-pTR GFP-RasV12 PDK4-shRNA cells (**A**), MDCK-pTR GFP-RasV12 Luciferase-shRNA cells (**B**) or MDCK-pTRE3G GFP-RasV12 PDK4-sgRNA cells (**C**) were mixed with normal MDCK cells or MDCK-pTR Luciferase-shRNA cells. Cells were stained with Hoechst 33342 (blue) and anti-LDHA (red). Scale bars, 10 μm.

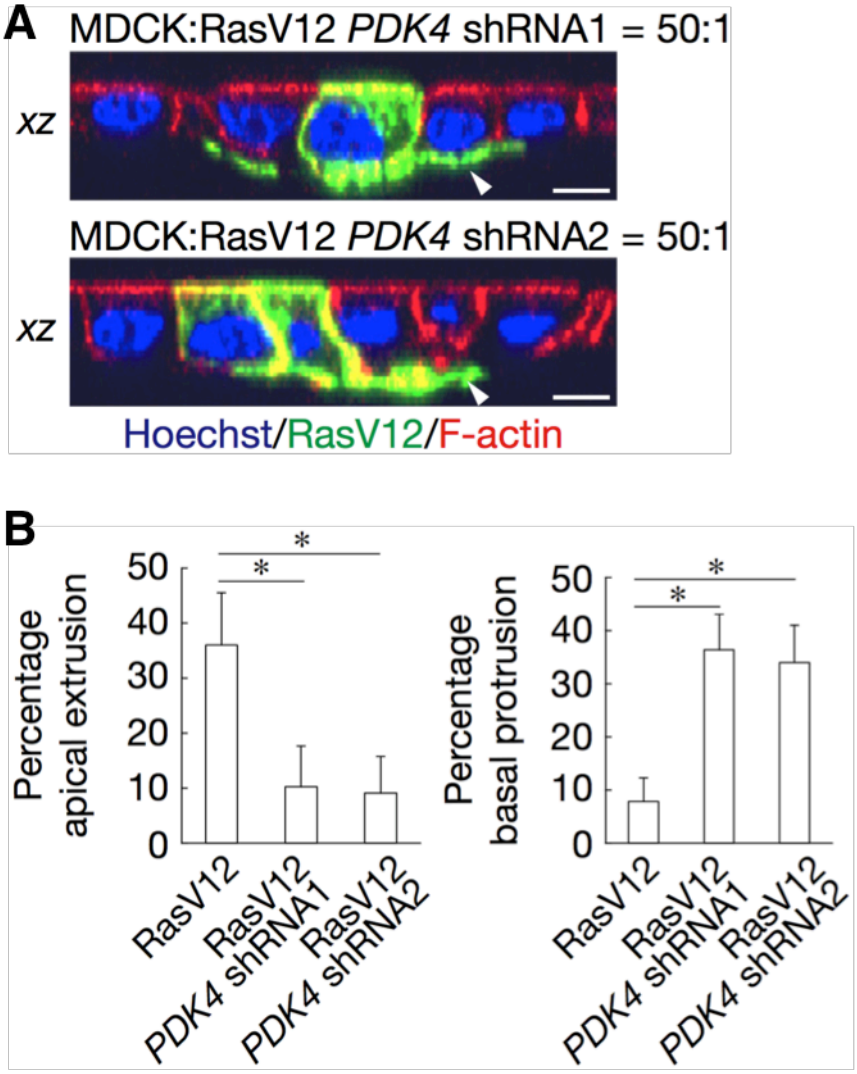

Fig. 2-19 Effect of PDK4-knockdown on apical extrusion. (**A**) Immunofluorescence images of *xz* sections of MDCK-pTR GFP-RasV12 *PDK4* shRNA1 or *PDK4* shRNA2 cells surrounded by normal MDCK cells. Arrowheads indicate the basal protrusion. Scale bars, 10 μm. (**B**) Quantification of the apical extrusion and basal protrusion formation. Data are mean ± s.e.m. **P* < 0.05, unpaired two-tailed *t* -test; *n* = three independent experiments.

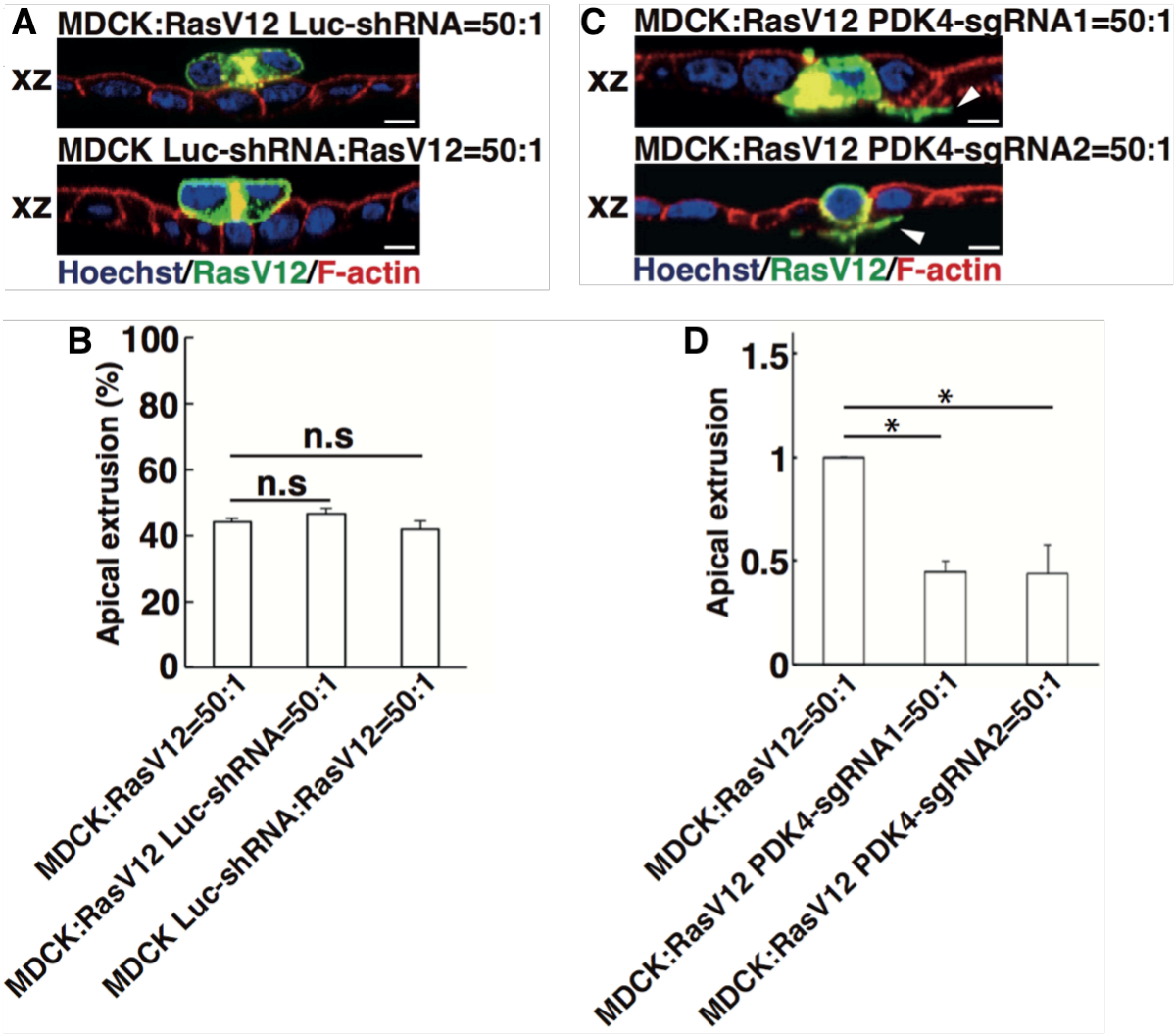

Fig. 2-20 Effect of PDK4-knockout on apical extrusion. (**A**) Immunofluorescence images of xz sections of MDCK-pTR GFP-RasV12 Luciferase-shRNA cells surrounded by normal MDCK cells or of MDCK-pTR GFP-RasV12 cells surrounded by MDCK-pTR Luciferase-shRNA cells. (**B**) Quantification of apical extrusion of RasV12 cells mixed with MDCK cells, RasV12 Luc-shRNA cells mixed with MDCK cells or RasV12 cells mixed with MDCK Luc-shRNA cells. Data are mean ± s.e.m.. **P*<0.05, unpaired two-tailed t-test; n=3 independent experiments. (**C**) Immunofluorescence images of xz sections of MDCK-pTRE3G GFP-RasV12 PDK4-sgRNA1 or -sgRNA2 cells surrounded by normal MDCK cells. Arrowheads indicate basal protrusions. Scale bars, 10 µm. (**D**) Quantification of the apical extrusion of MDCK-pTRE3G GFP-RasV12 PDK4-sgRNA1 or -sgRNA2 cells. Data are mean ± s.e.m.. Values are expressed as a ratio relative to MDCK:RasV12=50:1. **P*<0.05, unpaired two-tailed t-test; n=3 independent experiments.

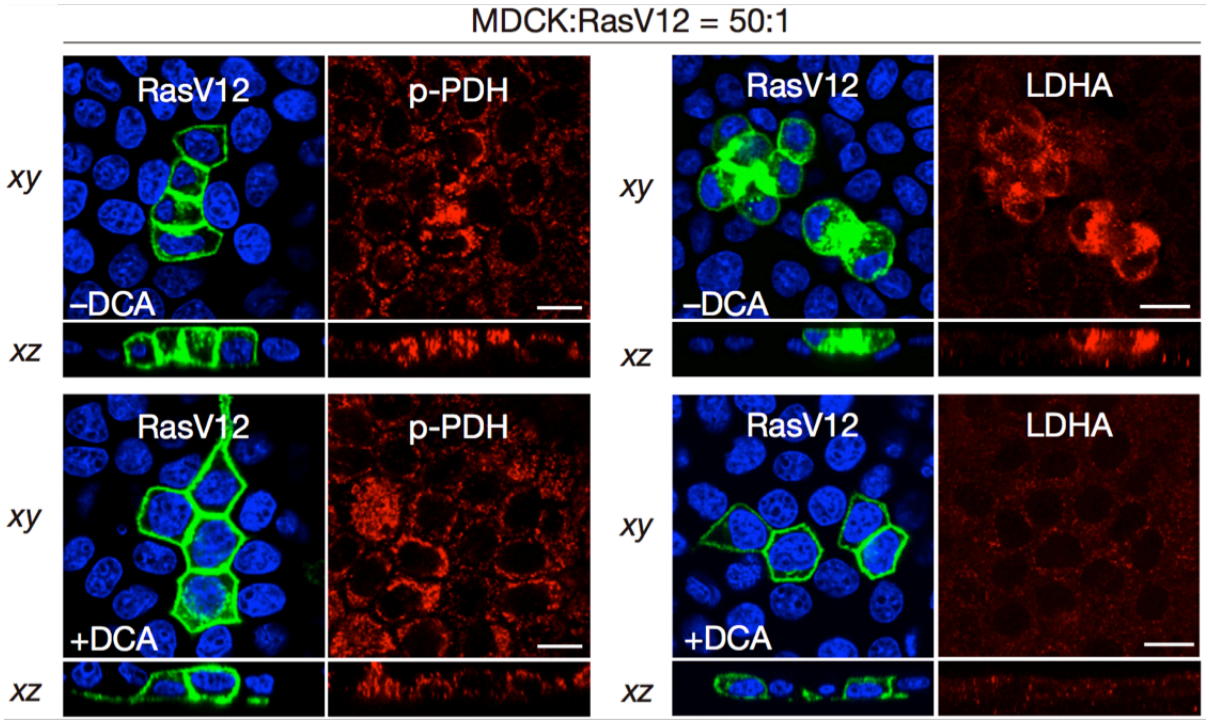

Fig. 2-21 Effect of DCA on p-PDH or LDHA. MDCK-pTR GFP-RasV12 cells were mixed with normal MDCK cells in the absence or presence of 25 mM DCA. Cells were stained with Hoechst 33342 (blue) and anti-p-PDH or anti-LDHA antibody (red). Scale bars, 10 μm.

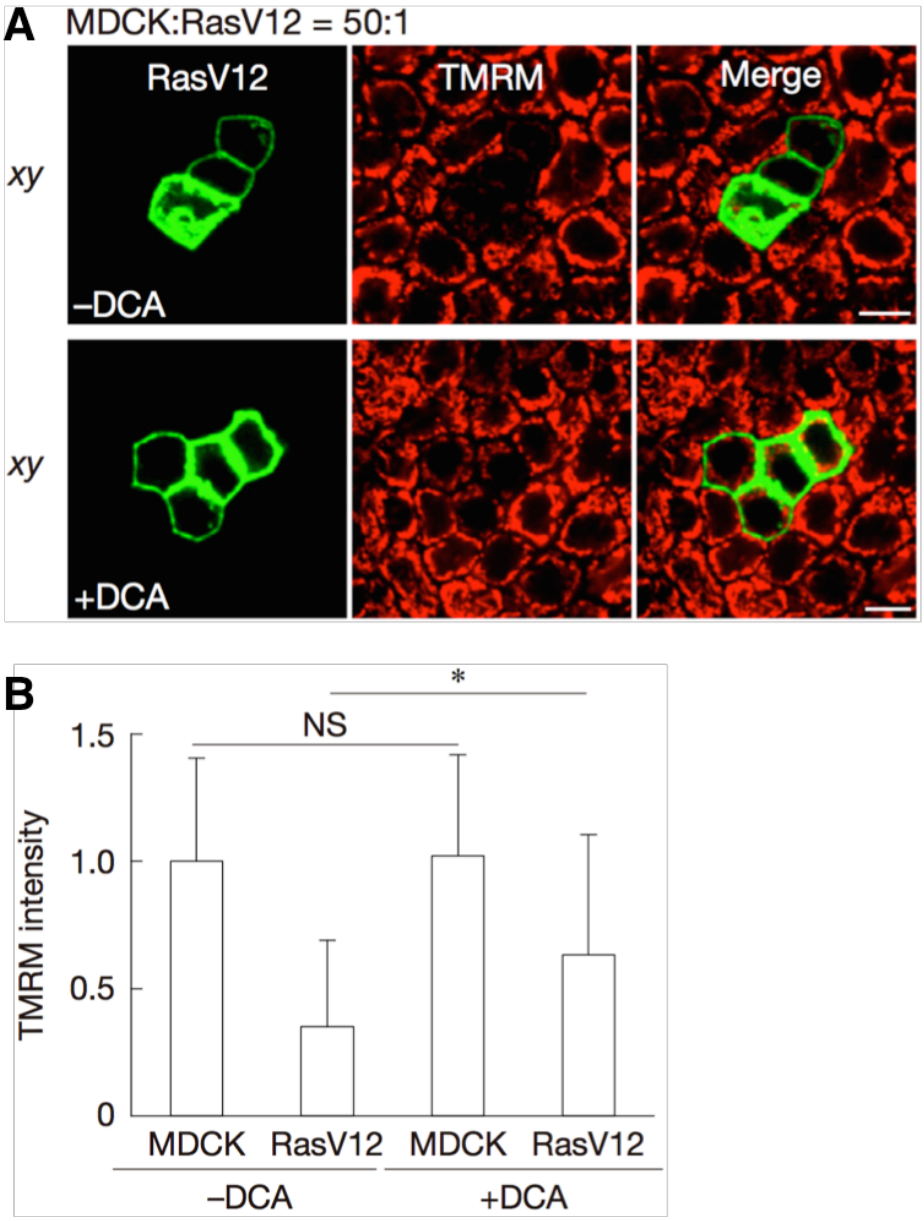

Fig. 2-22 Effect of DCA on TMRM incorporation of RasV12-transformed cells. (**A**) MDCK-pTR GFP-RasV12 cells were co-cultured with normal MDCK cells in the absence or presence of 25 mM DCA and incubated with 50 nM TMRM (red). Scale bars, 10 μm. (**B**) Quantification of the fluorescence intensity of TMRM. Data are mean ± s.e.m. Values are expressed as a ratio relative to MDCK (-DCA). $^{*}P < 0.001$, unpaired two-tailed *t* -test; n=84, 82, 98 and 90 cells pooled from three independent experiments.

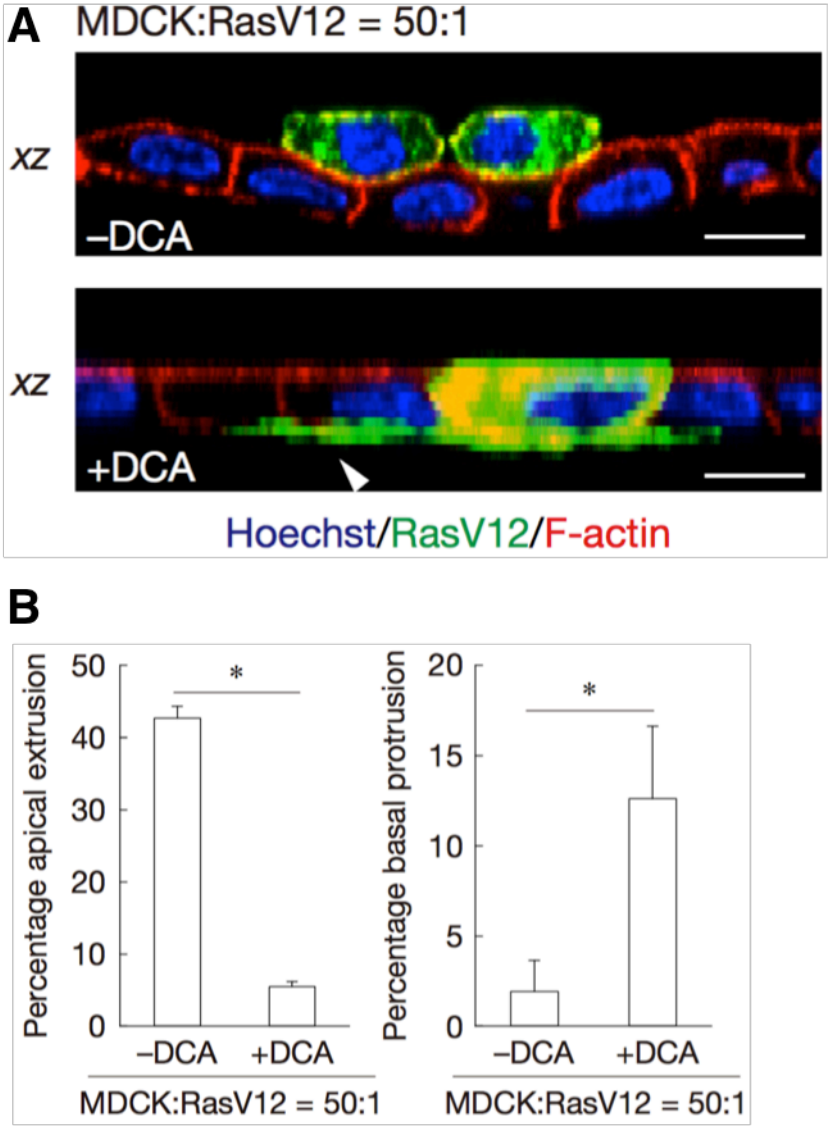

Fig. 2-23 Effect of DCA on apical extrusion of RasV12-transformed cells. (**A**) Immunofluorescence images of *xz* sections of MDCK-pTR GFP-RasV12 cells surrounded by normal MDCK cells in the absence or presence of DCA. An arrowhead indicates the basal protrusion. Scale bars, 10 μm. (**B**) Quantification of the apical extrusion and basal protrusion formation of RasV12 cells in the absence or presence of DCA. Data are mean ± s.e.m. $*P < 0.05$, unpaired two-tailed *t* -test; *n* = three independent experiments.

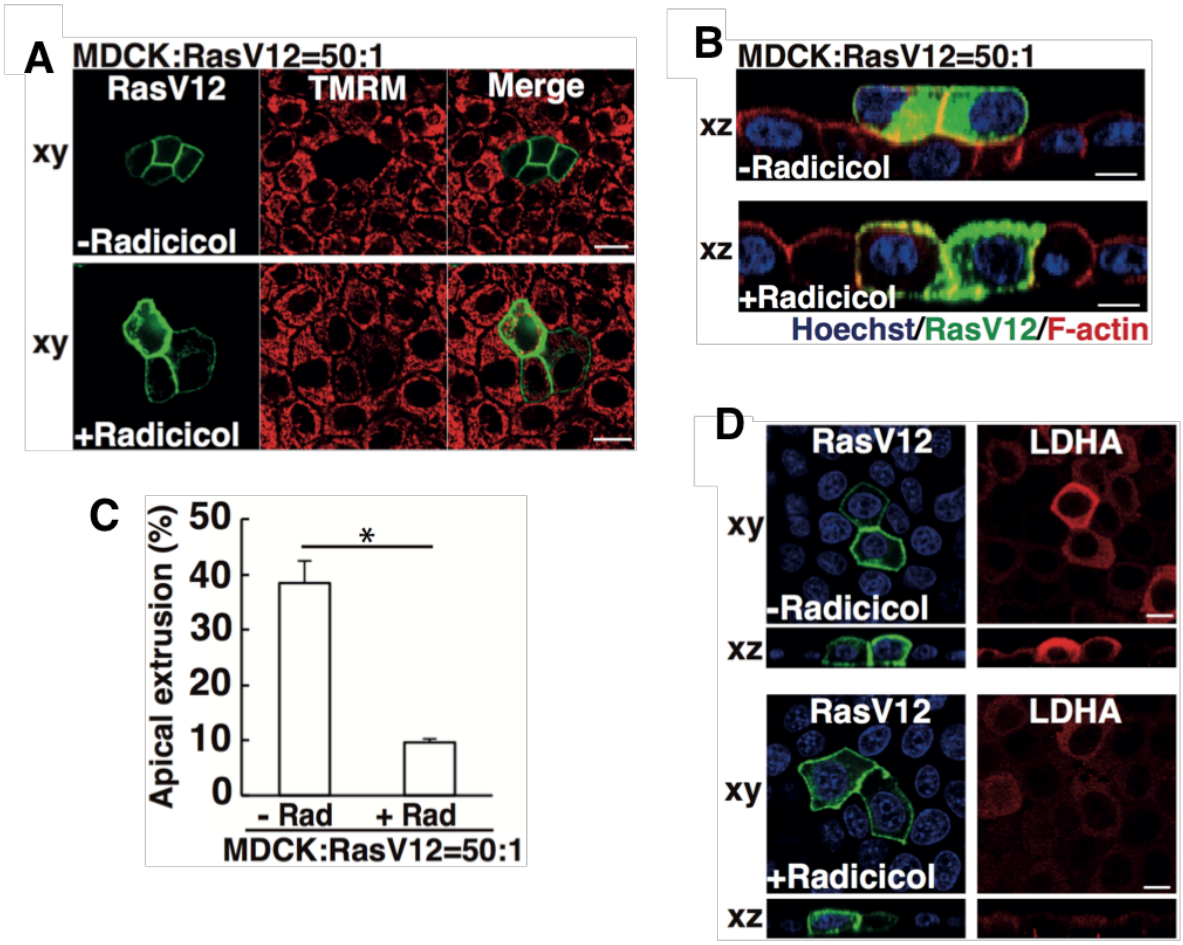

Fig. 2-24 PDK inhibitor Radicicol restores TMRM incorporation and suppresses apical extrusion of RasV12-transformed cells surrounded by normal cells. (**A**) Effect of Radicicol on TMRM incorporation of RasV12-transformed cells. MDCK-pTR GFP-RasV12 cells were co-cultured with normal MDCK cells in the absence or presence of 10 μM Radicicol and incubated with 50 nM TMRM (red). (**B**) Immunofluorescence images of xz sections of MDCK-pTR GFP-RasV12 cells surrounded by normal MDCK cells in the absence or presence of Radicicol. (**C**) Quantification of the effect of Radicicol on apical extrusion. Data are mean ± s.e.m.. *P<0.01, unpaired two-tailed t-test; n=3 independent experiments. (**D**) Effect of Radicicol on LDHA in RasV12-transformed cells that are surrounded by normal cells. MDCK-pTR GFP-RasV12 cells were mixed with normal MDCK cells in the absence or presence of Radicicol. Cells were stained with Hoechst 33342 (blue) and anti-LDHA antibody (red). Scale bars, 10 μm.

.

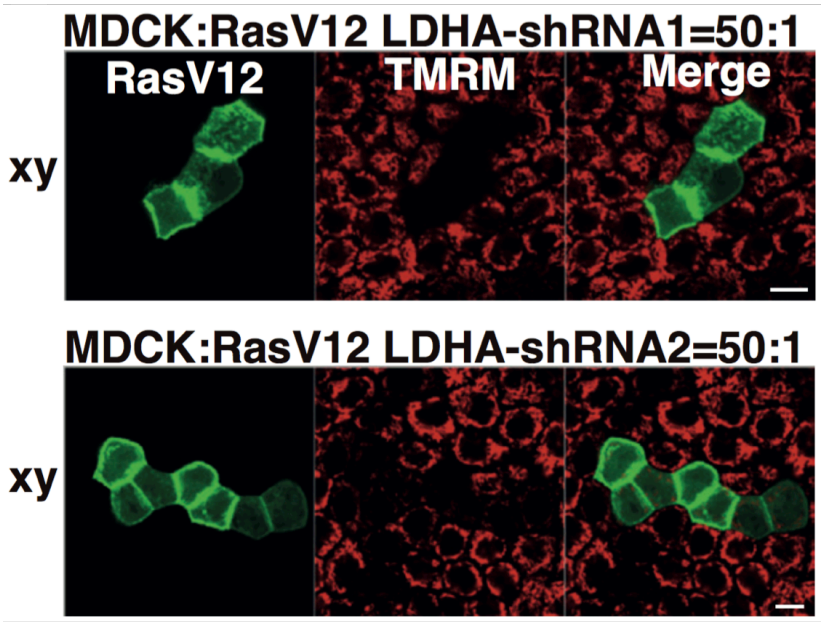

Fig. 2-25 Effect of LDHA-knockdown on TMRM incorporation. MDCK-pTR GFP-RasV12 LDHA-shRNA1 or -shRNA2 cells were mixed with normal MDCK cells and loaded with 50 nM TMRM (red). Scale bars, 10 μm.

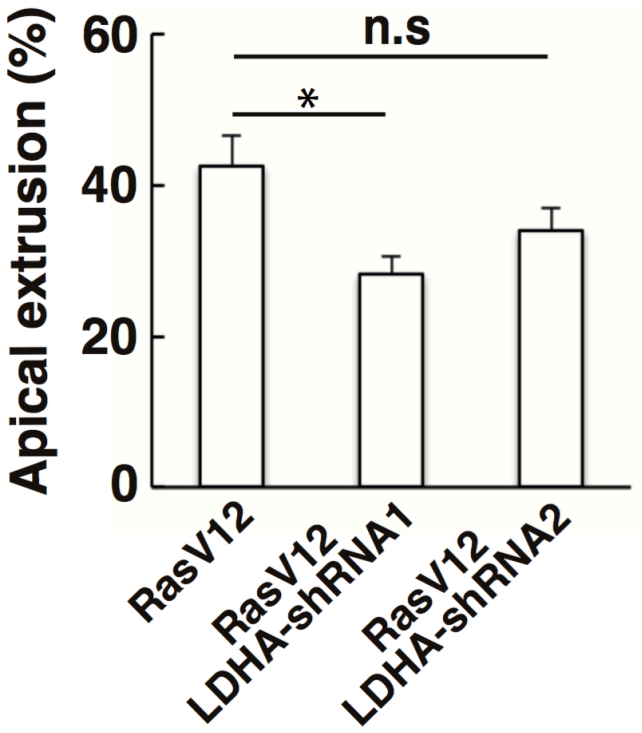

Fig. 2-26 Effect of LDHA-knockdown on apical extrusion. Quantification of the apical extrusion of MDCK-pTR GFP-RasV12 LDHA-shRNA1 or -shRNA2 cells. Data are mean ± s.e.m.. *P<0.05, unpaired two-tailed t-test; n=3 independent experiments.

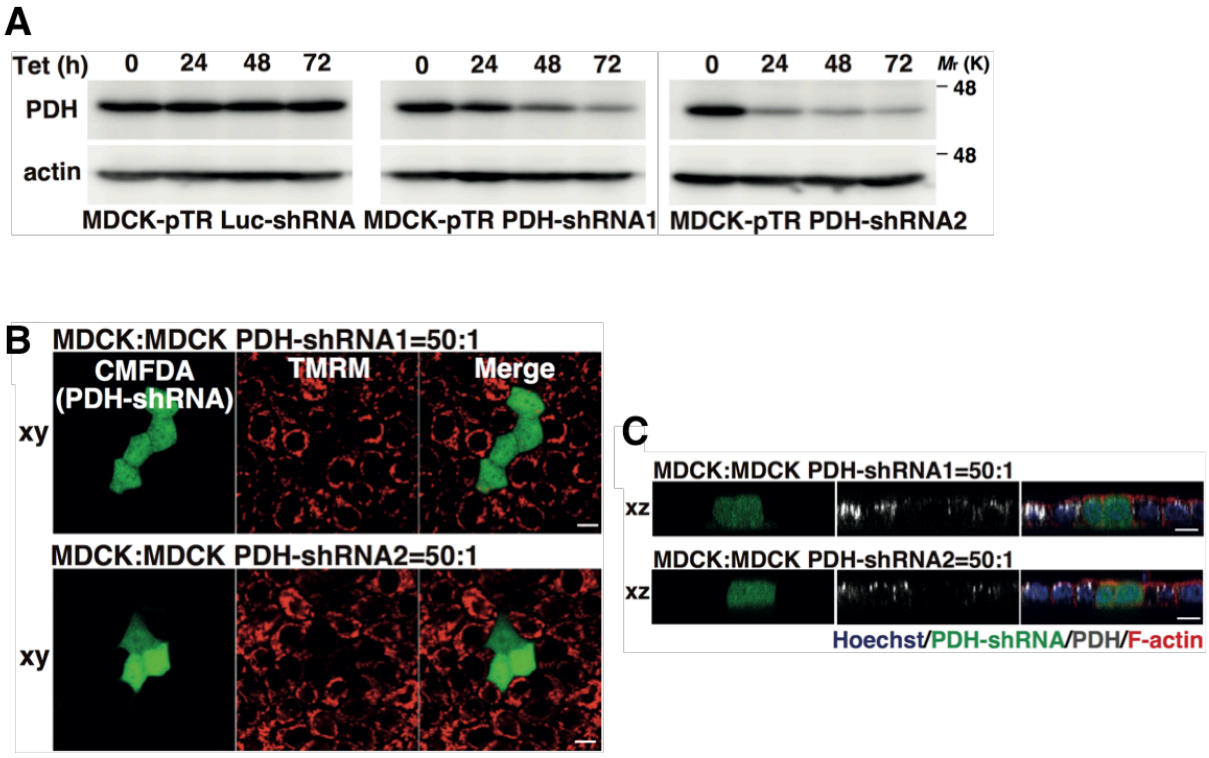

Fig. 2-27 (**A**) Establishment of tetracycline-inducible PDH-knockdown MDCK cell lines. Effect of tetracycline on expression of PDH protein is determined by western blotting. (**B**) TMRM incorporation in PDH-knockdown cells. MDCK-pTR PDH-shRNA1 or -shRNA2 cells were fluorescently labelled with CMFDA dye (green), and co-cultured with normal MDCK cells. Cells were incubated with tetracycline for 48 h, and loadedwith 50 nM TMRM (red). (**C**) Immunofluorescence images of xz sections of MDCK-pTR PDH-shRNA cells surrounded by normal MDCK cells at 72 h after tetracycline addition. Scale bars, 10 μm.

2.3.3. EDAC and EPLIN act upstream of the Warburg-effect-like metabolic changes in RasV12 cells surrounded by normal cells

We further examined the molecular mechanism underlying the Warburg-effect-like phenomenon. In a previous study, we demonstrated that EPLIN accumulates in RasV12-transformed cells surrounded by normal cells and plays a positive role in the apical extrusion via activation of the downstream molecules PKA and myosin II. We found that knockdown of EPLIN in RasV12 cells significantly restored mitochondrial membrane potential (Fig. 2-28). In addition, EPLIN knockdown suppressed PDK4 upregulation, phosphorylation of PDH and LDHA accumulation (Fig. 2-29). These data indicate that EPLIN is a crucial upstream regulator of the Warburgeffect-like metabolic changes. Furthermore, we examined the effect of various inhibitors on TMRM incorporation and apical extrusion. Concerning downstream molecules of EPLIN, the PKA inhibitor KT5720 reverted TMRM incorporation, whereas the myosin II inhibitor blebbistatin did not (Fig. 2-30). The other tested inhibitors (cytochalasin D, NAC, 3-MA, Y27632, L-NAME) did not affect TMRM incorporation (Fig. 2-30), indicating the specific effect of KT5720 on TMRM incorporation. Furthermore, KT5720 did not significantly affect expression of PDK4. These data suggest that EPLIN regulates those metabolic changes via PDK4- and PKA-dependent pathways (Fig. 2-33). It was previously reported that normal epithelial cells can recognize and actively eliminate the neighboring transformed cells, in which filamin in the normal cells plays an important role, at least partly, by inducing the accumulation of EPLIN in transformed cells; this tumor-suppressing process is called EDAC. When RasV12 cells were

surrounded by EDAC-deficient filamin-knockdown cells, TMRM incorporation in RasV12 cells was restored, and instead promoted in comparison with that in the surrounding knockdown cells (Fig. 2-31). In addition, knockdown of filamin in the surrounding normal cells substantially suppressed phosphorylation of PDH and accumulation of LDHA (Fig. 2-32). Collectively, these data demonstrate that EDAC from normal cells induces the metabolic alterations of the neighboring transformed cells via EPLIN, thereby promoting elimination of the transformed cells from epithelia (Fig. 2-33).

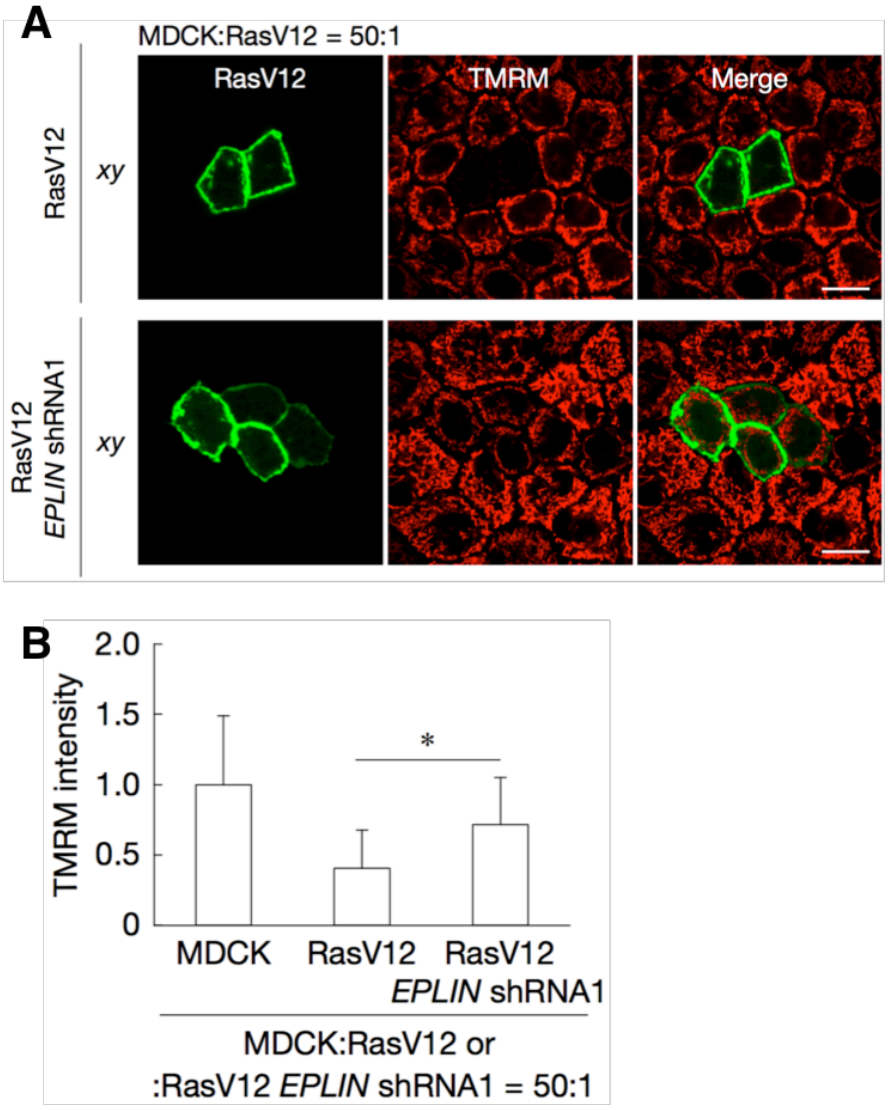

Fig. 2-28 Effect of EPLIN-knockdown on TMRM incorporation. (**A**) TMRM incorporation in *EPLIN*-knockdown RasV12-transformed cells. MDCK-pTR GFP-RasV12 cells or MDCK-pTR GFP-RasV12 *EPLIN* shRNA1 cells were co-cultured with normal MDCK cells and loaded with 50nM TMRM (red). Scale bars, 10 μm. (**B**) Quantification of the fluorescence intensity of TMRM. Data are mean ± s.e.m. Values are expressed as a ratio relative to MDCK. **P* < 0.001, unpaired two-tailed *t* -test; *n* = 64, 21 and 45 cells pooled from two independent experiments.

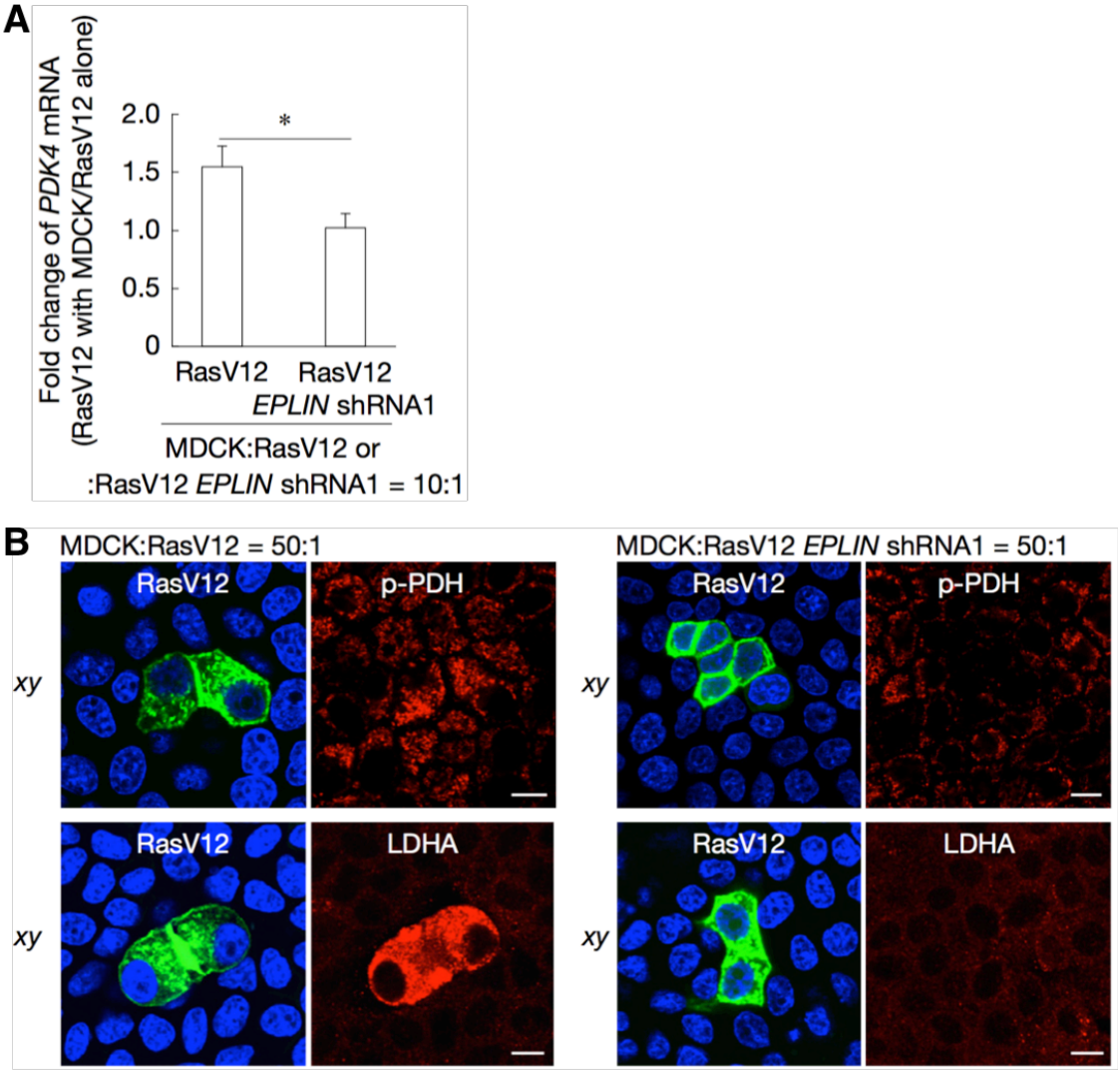

Fig. 2-29 Effect of EPLIN-knockdown on PDK4, p-PDH or LDHA in RasV12 cells surrounded by normal cells. (**A**) MDCK-pTR GFP-RasV12 cells or MDCK-pTR GFP-RasV12 *EPLIN* shRNA1 cells were co-cultured with normal MDCK cells or cultured alone. GFP-positive RasV12 cells were selectively collected by FACS and subjected to qPCR analysis. Values are shown as fold change in RasV12 cells surrounded by normal cells relative to RasV12 cells cultured alone. Data are mean ± s.e.m. $*P < 0.05$, unpaired two-tailed *t* -test; *n* = three independent experiments. (**B**) MDCK-pTR GFP-RasV12 cells or MDCK-pTR GFP-RasV12 *EPLIN* shRNA1 cells were co-cultured with normal MDCK cells. Cells were stained with Hoechst 33342 (blue) and anti-p-PDH or anti-LDHA antibody (red). Scale bars, 10 μm.

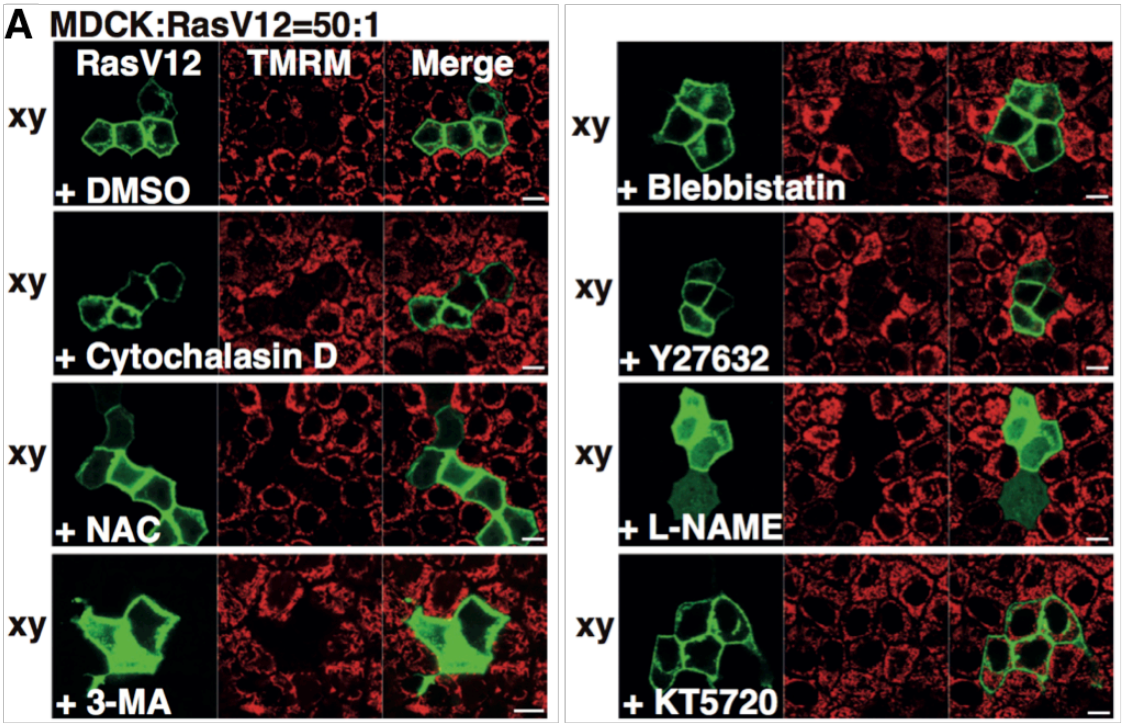

B

Inhibitor	Target	Extrusion	TMRM incorporation
Blebbistatin	Myosin- II	↓*	No effect
Cytochalasin D	Actin polymerization	↓*	No effect
Y27632	Rho kinase	↓*	No effect
NAC	ROS	No effect	No effect
L-NAME	NOS	ND	No effect
3-MA	Autophagy	↓*	No effect
KT5720	PKA	ND	↑*

Fig. 2-30 Effect of various inhibitors on TMRM incorporation. (**A**) MDCK-pTR GFP-RasV12 cells were co-cultured with normal MDCK cells in the presence of various inhibitors and loaded with TMRM (red). Each inhibitor inhibits the following molecule or cellular process; Blebbistatin: myosin-II, Cytochalasin D: actin polymerization, Y27632: Rho kinase, NAC: reactive oxygen species, L-NAME: nitrogen oxide synthase, 3-MA: autophagy, KT5720: PKA. Scale bars, 10 μm. (**B**) Effect of various inhibitors on apical extrusion of RasV12-transformed cells and on TMRM incorporation in RasV12-transformed cells that are surrounded by normal cells. *: statistically significant (unpaired two-tailed t-test); ND: not done; Grey box: our published observations.

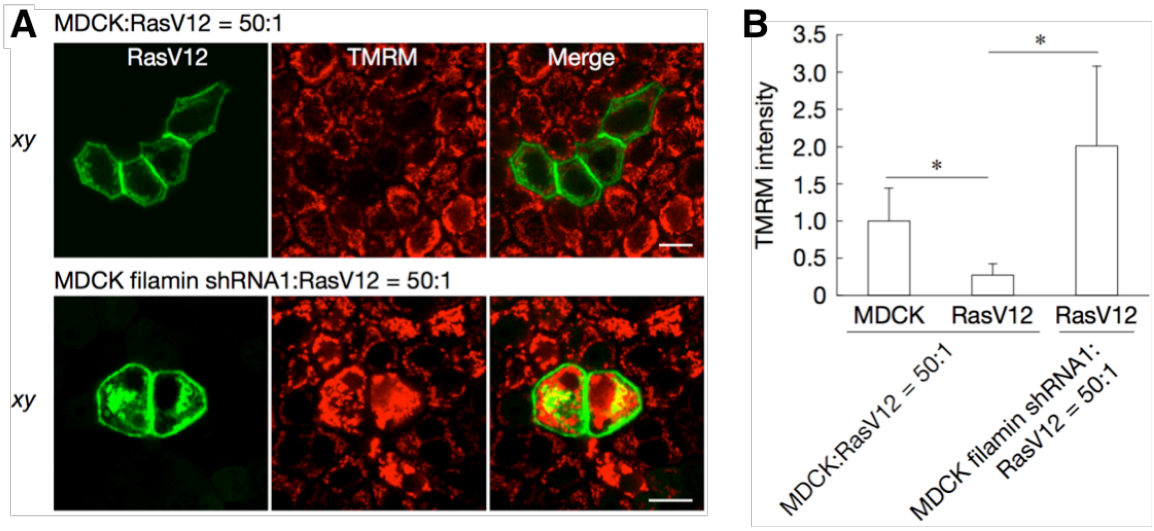

Fig. 2-31 Effect of filamin-knockdown in the surrounding normal cells on TMRM incorporation. (**A**) TMRM incorporation in RasV12-transformed cells surrounded by filamin-knockdown cells. MDCK-pTR GFP-RasV12 cells were co-cultured with MDCK cells or MDCK-pTR filamin shRNA1 cells, and loaded with 50nM TMRM. Scale bars, 10 μm. (**B**) Quantification of the fluorescence intensity of TMRM. Data are mean ± s.e.m. Values are expressed as a ratio relative to MDCK. *P < 0.001, unpaired two-tailed t -test; n = 50, 41 and 42 cells pooled from three independent experiments.

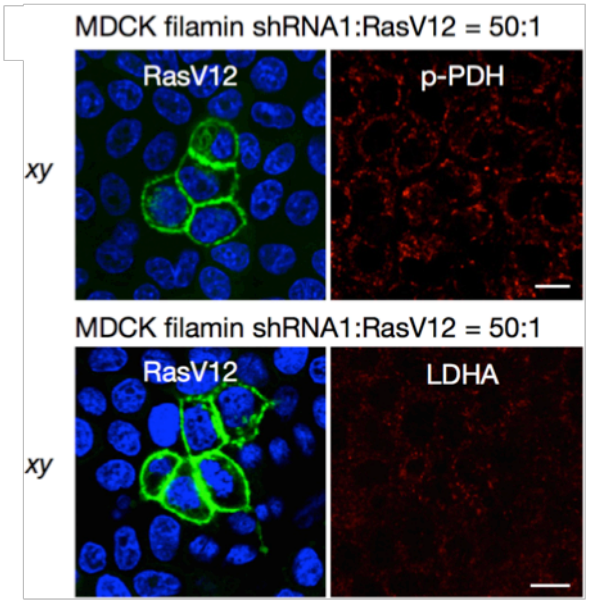

Fig. 2-32 Effect of filamin knockdown in the surrounding normal cells on PDH phosphorylation or LDHA accumulation in RasV12-transformed cells. MDCK-pTR GFP-RasV12 cells were co-cultured with MDCK-pTR filamin shRNA1 cells. Cells were stained with Hoechst 33342 (blue) and anti-p-PDH or anti-LDHA antibody (red). Scale bars, 10 μm.

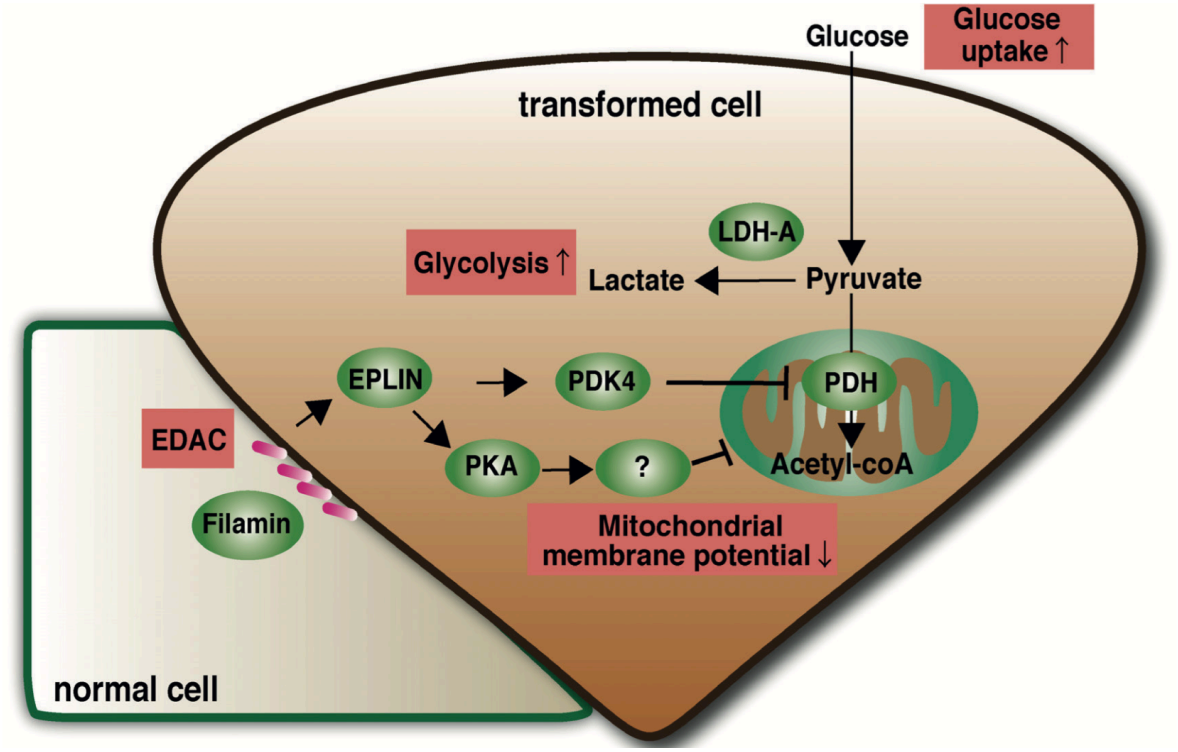

Fig. 2-33 A schematic model for molecular mechanisms of the Warburg effect-like metabolic changes in transformed cells that are surrounded by normal cells.

2.3.4. Upregulation of the glycolytic pathway plays a positive role in the elimination of RasV12-transformed cells

What is the functional significance of EDAC-induced Warburg-effect-like metabolic changes in the apical elimination of transformed cells? The metabolic shift from mitochondrial oxidative phosphorylation to glycolysis can affect various cellular processes, such as glucose metabolism, ATP production and resistance to reactive oxygen species (ROS)-mediated oxidative stress. Using a glucose FRET (fluorescence resonance energy transfer) probe, we found that intracellular glucose concentration was substantially diminished in RasV12 cells surrounded by normal cells (Fig. 2-34), indicating that intracellular glucose is exhausted via massively elevated glycolysis despite the increased glucose uptake (Fig. 2-8). The comparable glucose metabolic condition is also reported in the conventional Warburg effect. In addition, the result with the FRET-based ATP sensor (ATeam) showed that the ATP level was moderately increased in RasV12-transformed cells that were surrounded by normal cells (Fig. 2-35), suggesting that the ATP production is fully compensated and even promoted by the enhanced glycolytic pathway. To further understand the functional significance of this process, we examined the effect of a hexokinase inhibitor, 2-deoxy-D-glucose (2-DG). Addition of 2-DG diminished the non-cell-autonomously upregulated ATP level (Fig. 2-35) and significantly suppressed apical extrusion of RasV12 cells surrounded by normal cells (Fig. 2-36), indicating that the upregulation of the glycolytic pathway plays a positive role in the elimination of transformed cells. The ATP production speed via glycolysis is far greater than that via mitochondria, hence the

metabolic shift to glycolysis may be of benefit to transformed cells by supporting the prompt energy supply required for the dynamic process of apical extrusion. Note that 2-DG could inhibit both oxidative and fermentative glucose metabolism. To further clarify the metabolic alterations during apical extrusion, additional experiments are required in future studies.

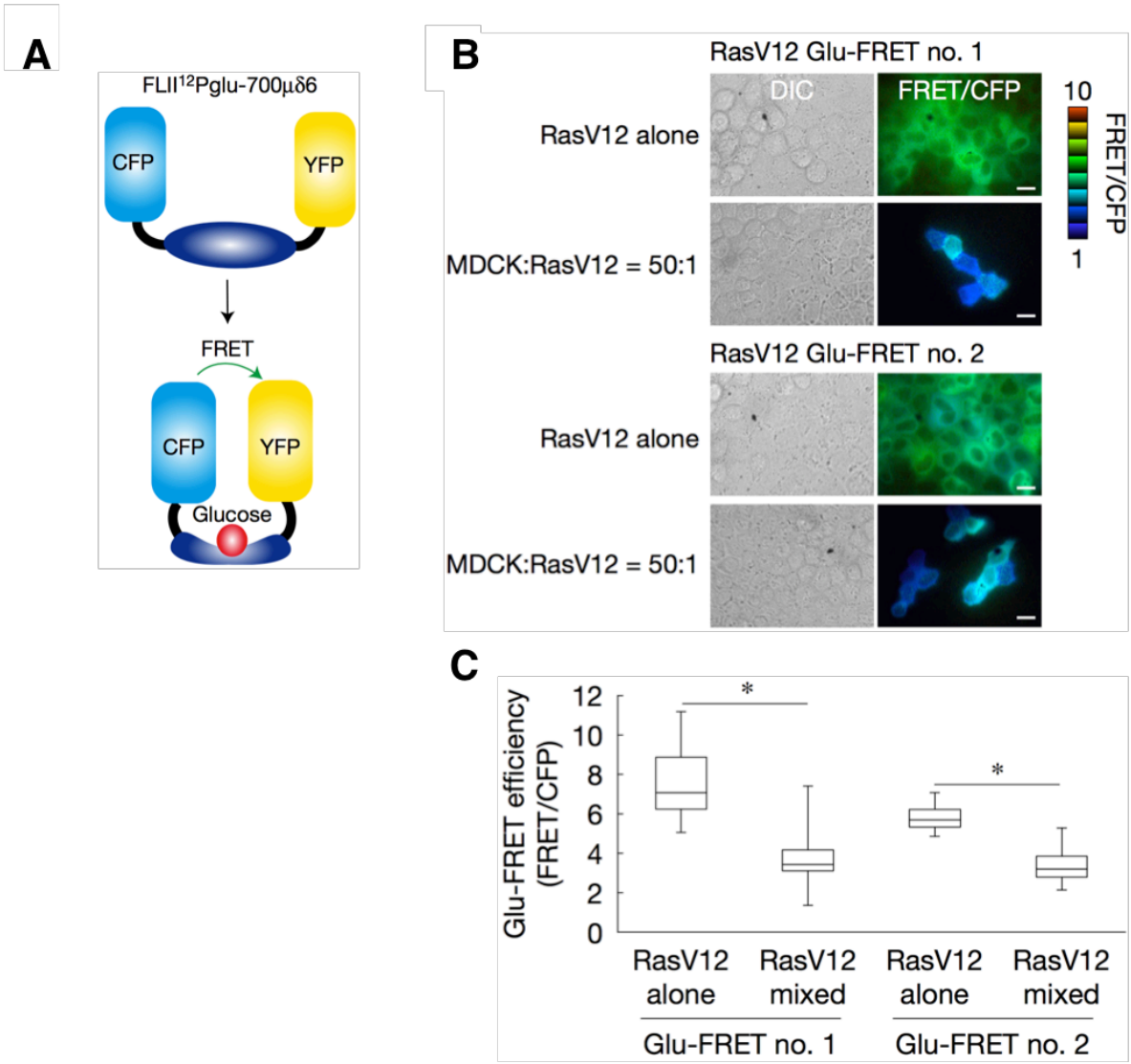

Fig. 2-34 FRET analyses for intracellular glucose. (**A**) Schematic diagram for glucose FRET. YFP, yellow fluorescent protein. (**B**) Glucose FRET images. MDCK-pTRE3G Myc-RasV12 cell lines stably expressing FLII12Pglu-700μδ6 (RasV12 Glu-FRET no. 1 or no. 2) were co-cultured with MDCK cells or cultured alone with doxycycline for 16 h and then analysed by dual-emission fluorescence microscopy. FRET/CFP ratio images were generated to represent FRET efficiency. Scale bars, 10 μm. (**C**) Quantification of glucose FRET efficiency (FRET/CFP). The box plots represent values from the 25th (bottom) to the 75th (top) percentiles, with the median as the horizontal line. *$P < 0.001$, unpaired two-tailed t -test; n = 40, 61, 41 and 68 cells pooled from three independent experiments.

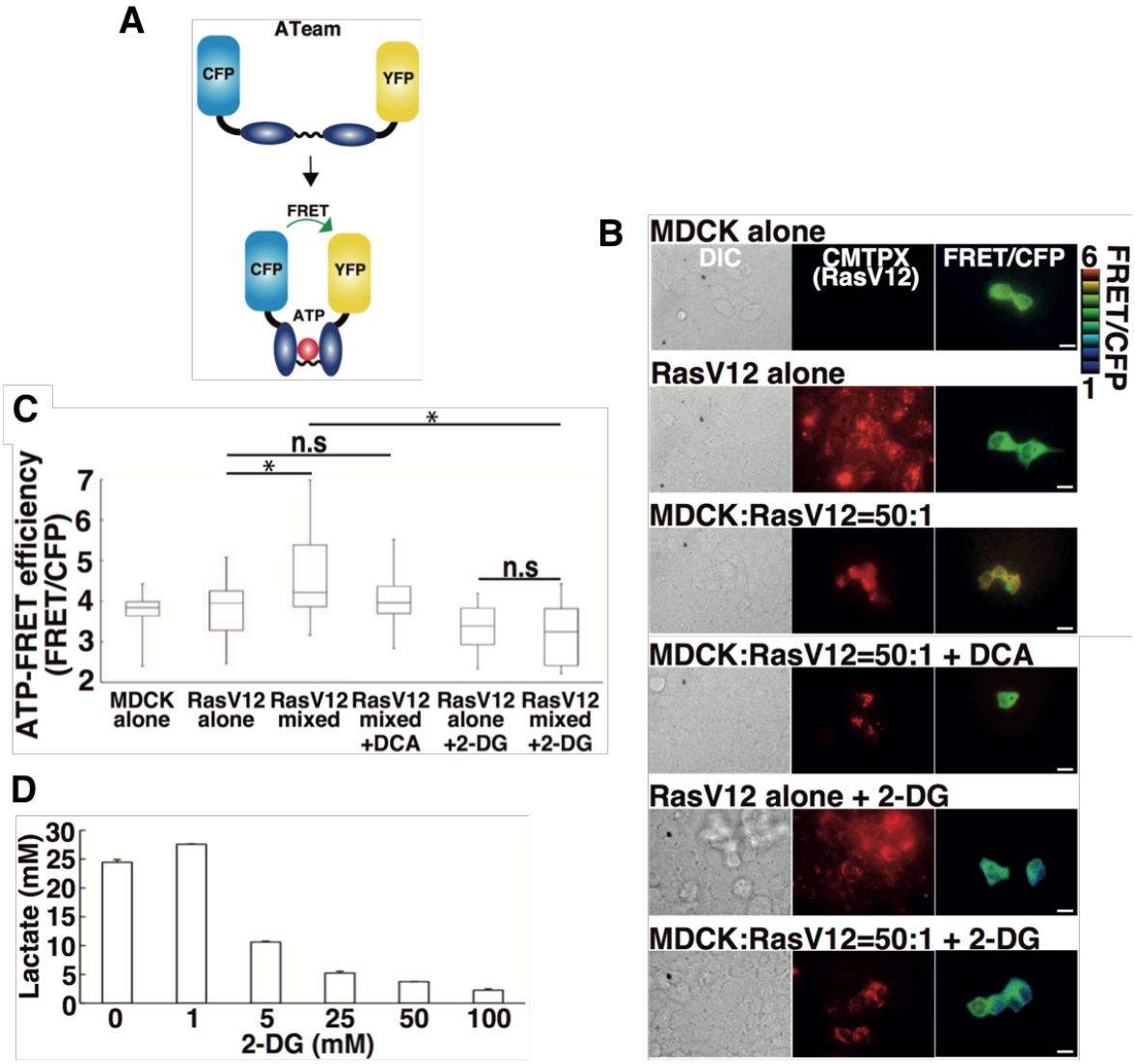

Fig. 2-35 Effect of various inhibitors on FRET analyses for ATP. (**A**) Schematics for ATP-FRET (ATeam). (**B**) ATP-FRET images. MDCK or MDCK-pTRE3G myc-RasV12 cells transiently expressing ATeam were stained with CMTPX and co-cultured with MDCK cells or cultured alone with doxycycline for 16 h in the absence or presence of DCA or 2-DG and then analysed by dual-emission fluorescence microscopy. FRET/CFP ratio images were generated to represent FRET efficiency. Scale bars, 10 μm. (**C**) Quantification of ATP-FRET efficiency ratio (FRET/CFP). The box plots represent values from the 25th (bottom) to the 75th (top) percentiles, with the median as the horizontal line. **P*<0.001, unpaired two-tailed t-test; n=50, 34, 32, 32, 15 and 15 cells pooled from two independent experiments. (**D**) Effect of 2-DG on lactate production in RasV12-transformed cells. MDCK-pTRE3G myc-RasV12 cells were incubated with the indicated concentration of 2-DG for 24 h, and lactate concentration in the culture media was measured. Data are mean ± s.e.m. from three independent experiments.

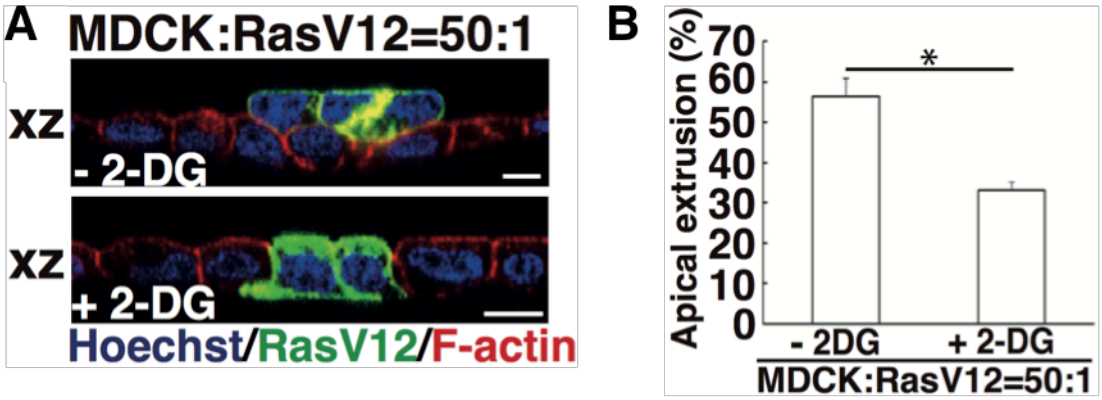

Fig. 2-36 Effect of 2-DG on apical extrusion of RasV12-transformed cells. MDCK-pTR GFP-RasV12 cells were co-cultured with normal MDCK cells in the absence or presence of 25 mM 2-DG. (**A**) Immunofluorescence images of xz sections of MDCK-pTR GFP- RasV12 cells surrounded by normal MDCK cells in the absence or presence of 2-DG. Scale bars, 10 μm. (**B**) Quantification of the effect of 2-DG on apical extrusion. Data are mean ± s.e.m.. *P<0.01, unpaired two-tailed t-test; n=3 independent experiments.

2.4. Discussion

As described above, newly emerging transformed cells are apically eliminated by the surrounding normal cells through PDK4-mediated the Warburg effect-like metabolic shift. This suggests a novel mechanism for the inception of the Warburg effect-induced tumor suppressive process, and is in stark contrast to the historical view in which the Warburg effect plays a positive role in promoting cancer progression (hereafter referred as conventional Warburg effect). However, the EDAC-induced metabolic changes share many aspects with the conventional Warburg effect. For instance, cells display increased uptake of glucose and higher production of lactate. The aerobic glycolysis was originally viewed as a compensatory mechanism for dysfunctional respiration, and reduced mitochondrial activity is observed in EDAC-induced metabolic reprogramming. Nevertheless, it should be noted that several accumulating studies have argued that mitochondrial activity normally functions in substantial cases of cancers, suggesting that mitochondrial impairment is not always associated with the Warburg effect phenotype. The conventional Warburg effect can be provoked through activation centered on hypoxia-inducible factor 1α (HIF-1α)-related genes such as glucose transporters (GLUTs), hexokinase 1/2 (HK1/2), pyruvate kinase M2 (PKM2), PDK1/3 and LDHA. Given the intimate link between HIF-1α and aerobic glycolysis, we thoroughly investigated the involvement of HIF-1α activity in cell competition. However, there was no obvious evidence that HIF-1α activity is promoted in transformed cells co-cultured with normal cells. Instead of PDK1/3, PDK4 was identified as one of prime molecules to enhance aerobic glycolysis during the process of

EDAC (Fig. 2-33). Best documented to upregulate expression of PDK4 is proliferator-activated receptor (PPAR) family. It is very intriguing that expression of PPARγ is very susceptible to mechanical stimuli as compressive force results in a reduction in PPARγ expression. Furthermore, EPLIN has been proposed to function as a mechanosensor by sensing actomyosin fibers at adherens junctions, suggesting that mechanical forces exerted by normal cells against transformed cells would underlie the induction of metabolic reprogramming. Whether the PPAR transcriptional complex is involved in the EDAC process remains unclear at present, which should be addressed in future studies. Interestingly, upon detachment from extracellular matrix (ECM), cells display enhanced expression of PDK4, leading to a metabolic impairment. This implies that the PDK4 activation is closely associated with a dissociation phenotype irrespective of oncogenic status of cells. Taken together, these findings indicate that PDK4-mediated mitochondrial activity generally affects the biological behavior of cells dissociated from an epithelial layer.

Tumor cells are subjected to a remarkable array of pressures in a harsh condition such as hypoxia and scarce of nutrient. The Warburg effect was initially considered as adaptation to such environment. It has been postulated that the Warburg effect confers neoplastic cells with many biological advantages to sustain the uncontrolled proliferation. First, the enhanced glucose consumption serves to produce cellular building blocks (e.g., nucleotides, amino acids and lipids) to meet the requirement of rapid proliferating cancer cells. The increase in glycolytic flux allows glycolytic intermediates such as gluose-6-phosphate or fructose-6-phosphate which can

be used for nucleotide synthesis, whereas 3-phosphoglycerate and pyruvate are key precursors in the biogenesis of several amino acids. Under the condition of increased aerobic glycolysis, citrate converted from acetyl-CoA is exported from the mitochondria. In the cytosol citrate is delivered as acetyl-CoA for synthesis of fatty acids where ß-nicotinamide adenine dinucleotide 2'-phosphate, reduced (NADPH) is required for this step. It is currently unknown how the production rate of these macromolecules is altered and whether it accounts for the biological consequence of the EDAC-induced Warburg effect.

In addition to these biosynthetic functions, the rewiring of metabolic status also affects the generation of reactive oxygen species (ROS). There is enormous evidence that large amounts of glycolytic intermediates are diverted to the pentose phosphate pathway (PPP) to produce reducing equivalents in the form of NADPH. NADPH is a major cellular antioxidant which maintains glutathione in a reduced state to secure the redox balance. The electron transport chain (ETC) is a major source of ROS production as leaky electrons react with oxygen to produce superoxide across the respiratory chain. Given that transformed cells are inherently under increased oxidative stress as a result of higher rate of proliferation, downregulated mitochondrial activity as an antioxidant mechanism is proposed to function to lower oxidative burden, which potentiates cell viability. In this regard, it is tempting to assume that the PDK4-mediated reduction of mitochondrial redox potential is beneficial for cells to negate oxidative stress induced by EDAC. However, the opposite model of mitochondrial function in that it counteracts ROS through NADPH

production by isocitrate dehydrogenase 2 (IDH2), a TCA cycle enzyme, has been recently put forward. In addition, it has been implicated that ROS is a vital regulator for the cellular activity, as not only does ROS production cause DNA damage, but also function as a signaling molecule. For instance, ROS has been shown to inactivate phosphatases such as phosphatase and tensin homolog (PTEN) or protein tyrosine phosphatases. From this perspective, EDAC-induced ROS might have a function as a mediator to transduce downstream signal(s). Future studies aimed at delineating how the redox status alters in transformed cells during cell competition are necessary.

In mitochondrial oxidative phosphorylation (OXPHOS), oxidation of one glucose produces 36 molecules of adenosine 5'-triphosphate (ATP), whereas glycolysis in cytosol generates 2 ATP. Thus, aerobic glycolysis appears at first glance to be an inefficient means to generate ATP as mitochondrial oxidative phosphorylation can maximize ATP production. However, the ATP production by glycolysis is up to 100 times faster than that of OXPHOS. Hence if extracellular glucose is abundant, the metabolic shift to glycolysis would allow cells to meet acute energy demand. In line with this concept, our group found that the intracellular ATP level is profoundly higher in RasV12 cells surrounded by normal cells compared to RasV12 cells cultured alone based on the analysis of FRET-based ATP imaging. The facts that myosin-II-driven contraction, PKA activation and enhanced endocytosis in transformed cells are required to force them out of epithelia suggest that rapid ATP production might provide free energy for transformed cells to sustain those biological reactions.

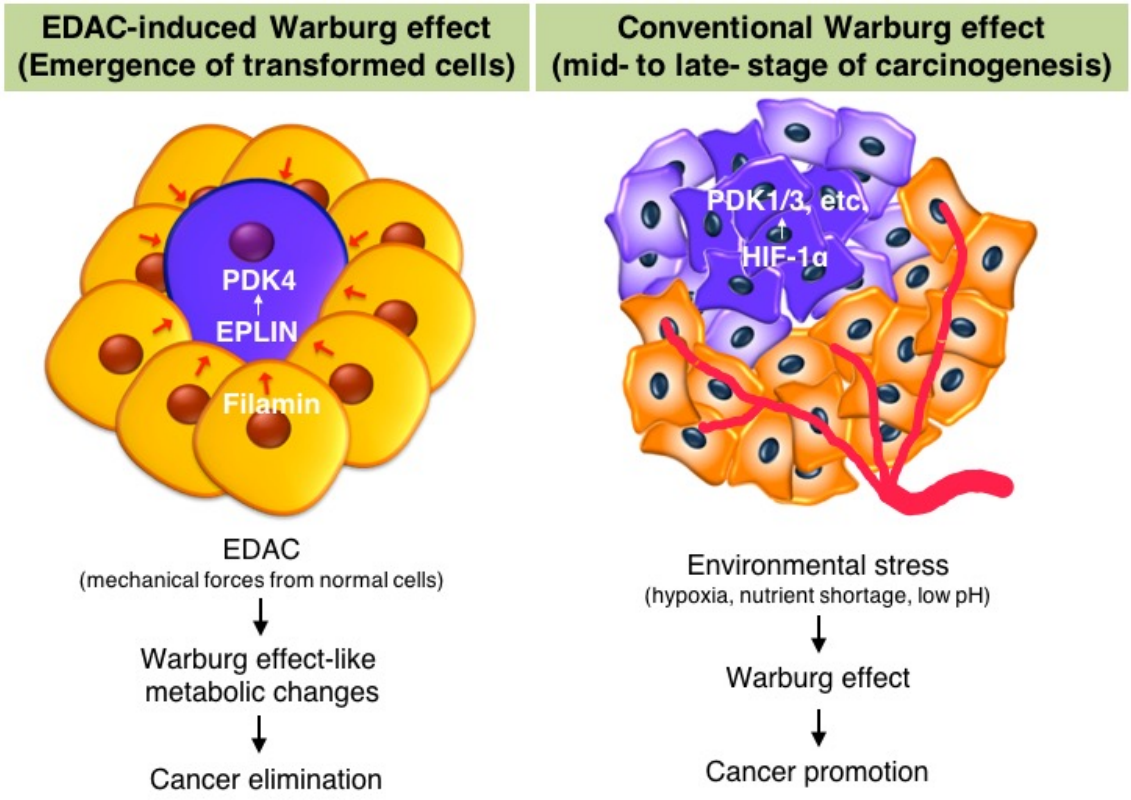

Fig. 2-37 A schematic representation of difference between EDAC-induced Warburg effect and conventional Warburg effect**.** In the EDAC-induced Warburg effect, a mechanical force generated from surrounding normal cells cause the Warburg effect-like metabolic changes in transformed cells via FilaminA-EPLIN-PDK4 pathway. This metabolic shift results in elimination of transformed cells. In contrast, at mid– to late- stage of carcinogenesis environmental stresses such as hypoxia, scarce of nutrients and low pH induce the Warburg effect in cancer cells, resulting in a selective advantage for survival, invasion and metastasis.

2.5. References

Hanahan, D. & Weinberg, R. A. Hallmarks of cancer: the next generation. Cell 144, 646–674 (2011).

Fialkow, P. J. Clonal origin of human tumors. Biochim. Biophys. Acta 458, 283–321 (1976).

Nowell, P. C. The clonal evolution of tumor cell populations. Science 194, 23–28 (1976).

Morata, G. & Ripoll, P. Minutes: mutants of Drosophila autonomously affecting cell division rate. Dev. Biol. 42, 211–221 (1975).

de la Cova, C., Abril, M., Bellosta, P., Gallant, P. & Johnston, L. A. Drosophila myc regulates organ size by inducing cell competition. Cell 117, 107–116 (2004).

Moreno, E. & Basler, K. dMyc transforms cells into super-competitors. Cell 117, 117–129 (2004).
Tamori, Y. *et al.* Involvement of Lgl and Mahjong/VprBP in cell competition. PLoS Biol. 8, e1000422 (2010).

Karim, F. D. & Rubin, G. M. Ectopic expression of activated Ras1 induces hyperplastic growth and increased cell death in Drosophila imaginal tissues. Development 125, 1–9 (1998).

Brumby, A. M. & Richardson, H. E. scribble mutants cooperate with oncogenic Ras or Notch to cause neoplastic overgrowth in Drosophila. EMBO J. 22, 5769–5779 (2003).

Hogan, C. *et al.* Characterization of the interface between normal and transformed epithelial cells. Nat. Cell Biol. 11, 460–467 (2009).

Kajita, M. *et al.* Interaction with surrounding normal epithelial cells influences signalling pathways and behaviour of Src-transformed cells. J. Cell Sci. 123, 171–180 (2010).
Wu, S. K. *et al.* Cortical F-actin stabilization generates apical-lateral patterns of junctional contractility that integrate cells into epithelia. Nat. Cell Biol. 16, 167–178 (2014).

Leung, C. T. & Brugge, J. S. Outgrowth of single oncogene-expressing cells from suppressive epithelial environments. Nature 482, 410–413 (2012).

Norman, M. *et al.* Loss of Scribble causes cell competition in mammalian cells. J. Cell Sci. 125, 59–66 (2012).

Kajita, M. *et al.* Filamin acts as a key regulator in epithelial defence against transformed cells. Nat. Commun. 5, 4428 (2014).

Ohoka, A. *et al.* EPLIN is a crucial regulator for extrusion of RasV12-transformed cells. J. Cell Sci. 128, 781–789 (2015).

Vander Heiden, M. G., Cantley, L. C. & Thompson, C. B. Understanding the Warburg effect: the metabolic requirements of cell proliferation. Science 324, 1029–1033 (2009).

Sciacovelli, M., Gaude, E., Hilvo, M. & Frezza, C. The metabolic alterations of cancer cells. Methods Enzymol. 542, 1–23 (2014).

Koppenol, W. H., Bounds, P. L. & Dang, C. V. Otto Warburg's contributions to current concepts of cancer metabolism. Nat. Rev. Cancer 11, 325–337 (2011).

Cairns, R. A., Harris, I. S. & Mak, T. W. Regulation of cancer cell metabolism. Nat. Rev. Cancer 11, 85–95 (2011).

Warburg, O. On the origin of cancer cells. Science 123, 309–314 (1956).

Levayer, R., Hauert, B. & Moreno, E. Cell mixing induced by myc is required for competitive tissue invasion and destruction. Nature 524, 476–480 (2015).

Kato, M., Li, J., Chuang, J. L. & Chuang, D. T. Distinct structural mechanisms for inhibition of pyruvate dehydrogenase kinase isoforms by AZD7545, dichloroacetate, and radicicol. Structure 15, 992–1004 (2007).

Wynn, R. M. *et al.* Pyruvate dehydrogenase kinase-4 structures reveal a metastable open conformation fostering robust core-free basal activity. J. Biol. Chem. 283, 25305–25315 (2008).

Sutendra, G. *et al.* Mitochondrial activation by inhibition of PDKII suppresses HIF1a signaling and angiogenesis in cancer. Oncogene 32, 1638–1650 (2013).

Koukourakis, M. I. *et al.* Pyruvate dehydrogenase and pyruvate dehydrogenase kinase expression in non small cell lung cancer and tumor-associated stroma. Neoplasia 7, 1–6 (2005).

Hur, H. *et al.* Expression of pyruvate dehydrogenase kinase-1 in gastric cancer as a potential therapeutic target. Int. J. Oncol. 42, 44–54 (2013).

Lu, C. W. *et al.* Overexpression of pyruvate dehydrogenase kinase 3 increases drug resistance and early recurrence in colon cancer. Am. J. Pathol. 179, 1405–1414 (2011).

Chu, Q. S. *et al.* A phase I open-labeled, single-arm, dose-escalation, study of dichloroacetate (DCA) in patients with advanced solid tumors. Invest. New Drugs 33, 603–610 (2015).

Dunbar, E. M. *et al.* Phase 1 trial of dichloroacetate (DCA) in adults with recurrent malignant brain tumors. Invest. New Drugs 32, 452–464 (2014).

Strum, S. B. *et al.* Case report: sodium dichloroacetate (DCA) inhibition of the "Warburg Effect" in a human cancer patient: complete response in non-Hodgkin's lymphoma after disease progression with rituximab-CHOP. J. Bioenerg. Biomembr. 45, 307–315 (2013).
Garon, E. B. *et al.* Dichloroacetate should be considered with platinum-based chemotherapy in hypoxic tumors rather than as a single agent in advanced non-small cell lung cancer. J. Cancer Res. Clin. Oncol. 140, 443–452 (2014).

Kami, K. *et al.* Metabolomic profiling of lung and prostate tumor tissues by capillary electrophoresis time-of-flight mass spectrometry. Metabolomics 9, 444–453 (2013).

Shestov, A. A. *et al.* Quantitative determinants of aerobic glycolysis identify flux through the enzyme GAPDH as a limiting step. eLife 3, e03342 (2014).

Tang, X. *et al.* A joint analysis of metabolomics and genetics of breast cancer. Breast Cancer Res. 16, 415 (2014).

Pfeiffer, T., Schuster, S. & Bonhoeffer, S. Cooperation and competition in the evolution of ATP-producing pathways. Science 292, 504–507 (2001).

Sato, T. *et al.* Single Lgr5 stem cells build crypt-villus structures in vitro without a mesenchymal niche. Nature 459, 262–265 (2009).

Imajo, M., Ebisuya, M. & Nishida, E. Dual role of YAP and TAZ in renewal of the intestinal epithelium. Nat. Cell Biol. 17, 7–19 (2015).

Semenza, G. L., Roth, P. H., Fang, H. M. & Wang, G. L. Transcriptional regulation of genes encoding glycolytic enzymes by hypoxia-inducible factor 1. J. Biol. Chem. 269, 23757–23763 (1994).

Gordan, J. D., Thompson, C. B. & Simon, M. C. HIF and c-Myc: sibling rivals for control of cancer cell metabolism and proliferation. Cancer Cell 12, 108–113 (2007).

Kim, J. W., Tchernyshyov, I., Semenza, G. L. & Dang, C. V. HIF-1-mediated expression of pyruvate dehydrogenase kinase: a metabolic switch required for cellular adaptation to hypoxia. Cell Metab. 3, 177–185 (2006).

Papandreou, I., Cairns, R. A., Fontana, L., Lim, A. L. & Denko, N. C. HIF-1 mediates adaptation to hypoxia by actively downregulating mitochondrial oxygen consumption. Cell Metab. 3, 187–197 (2006).

Kluza, J. *et al.* Inactivation of the HIF-1alpha/PDK3 signaling axis drives melanoma toward mitochondrial oxidative metabolism and potentiates the therapeutic activity of pro-oxidants. Cancer Res. 72, 5035–5047 (2012).

Atsumi, T. *et al.* High expression of inducible 6-phosphofructo-2-kinase/fructose2,6-bisphosphatase (iPFK-2; PFKFB3) in human cancers. Cancer Res. 62, 5881–5887 (2002).

Christofk, H. R. *et al.* The M2 splice isoform of pyruvate kinase is important for cancer metabolism and tumor growth. Nature 452, 230–233 (2008).

Wu, W. & Zhao, S. Metabolic changes in cancer: beyond the Warburg effect. Acta Biochim. Biophys. Sin. 45, 18–26 (2013).

Semenza, G. L. HIF-1: upstream and downstream of cancer metabolism. Curr. Opin. Genet. Dev. 20, 51–56 (2010).

de la Cova, C. *et al.* Supercompetitor status of Drosophila Myc cells requires p53 as a fitness sensor to reprogram metabolism and promote viability. Cell Metab. 19, 470–483 (2014).

Chapter 3:

IDENTIFICATION OF THE CRUCIAL REGULATOR OF CELL COMPETITION BY SILAC-SCREENING

3. Identification of the crucial regulator of cell competition by SILCA-screening

3.1. Introduction

Epithelial tissues covers the outside of our body and the cells in epithelial tissue are very closely packed together, suggesting that epithelial cells play a role in a barrier between inside our body and outside our body. From these information, epithelial cell homeostasis such as cell death or imbalance should be regulated precisely. In a previous study, Hogan *et al.* reported that when RasV12-transformed cells are surrounded by normal epithelial cells, the RasV12 cells are apically eliminated from an epithelial monolayer (Hogan *et al.* 2009). Interestigly, when RasV12 cells are cultured alone, the phenomenon does not occur, suggesting that cell-cell interaction and recognition between normal and transformed cells are important for apical elimination in epithelium. However, the recognition mechanism under this process is still unclear. Kajita *et al.* also reported that filamin, an actin binding protein, accumulates in normal cells at the interface with neighboring transformed cells and positively regulates elimination of transformed cells (Kajita *et al.* 2014). This result suggests that mechanical forces is involved in maintenance of epithelial homeostasis. In this study, we have examined how epithelial cells sense imbalance or heterogeneity of epithelial layer caused by the mixture of normal and transformed cells and how mechanical force is regulated during this step.

3.2. Experimental Procedures

3.2.1. Antibodies and Materials

The following antibodies were used in this study: rabbit anti-phospho-PKA substrate (RRXS*/T*) (9624) and rabbit anti-phospho(Ser) PKC Substrate (2261) antibodies from Cell Signaling Technology, rabbit anti-phospho-AHNAK2 and rabbit anti-AHNAK2 antibodies were we generated. Alexa-Fluor-647-conjugated phalloidin (Life Technologies) were used at 1.0 U ml^{-1}. Alexa-Fluor-568-conjugated secondary antibodies were from Life Technologies. Hoechst 33342 (Life Technologies) was used at a dilution of 1:5,000 for fixed samples, 1:4,000 for living cells. The inhibitors BIM-I (10 μM), KT5720 (4 μM), Y27632 (20 μM), Go6976 (10 μM) were from Calbiochem. LY294002 (10 μM) was Millipore, U73122 (10 μM) was from abcam, and SP600125 (10 μM) was from Sigma-Aldrich.

3.2.2. Cell culture

MDCK cells were cultured in DMEM supplemented with 10% tetracycline-free FCS, 1% GultaMAX, and 1% penicillin/streptomycin at 37℃ and ambient air supplemented with 5% CO_2. MDCK cells stably expressing EGFP-RasV12 in a tetracycline-inducible manner (MDCK-pTR GFP-RasV12) were previously established by using the pcDNA4/TO/EGFP-RasV12 plasmid vector and cultured in DMEM supplemented with 0.5 μg ml^{-1} blasticidin (Invitrogen) and 40 μg ml^{-1} Zeocin. To establish MDCK-pTRE3G Myc-RasV12 cells, complementary DNA of Myc-HRasV12 was cloned into BamHI/EcoRI sites of

pPB-TRE3G-MCS-CEH-rtTA3-IP, which was constructed by introducing the TRE3G promoter with cloning sites, insulator and rtTA3-expressing elements into a PiggyBac-based vector (SBI). MDCK cells were then transfected with pPB-TRE3G Myc-RasV12 by nucleofection (nucleofector 2b Kit L, Lonza), followed by selection in medium containing 5 μg ml^{-1} blasticidin. To establish MDCK stably expressing GCaMP6S, complementary DNA of GCaMP6S was cloned into BamHI/EcoRI sites of pPB-EF1-MCS, which was constructed by introducing the EF1 promoter with cloning sites into a PiggyBac-based vector (SBI). MDCK cells were then transfected with pPB-EF1-MCS-IRES-Neo-GCaMP6S by nucleofection (nucleofector 2b Kit L, Lonza), followed by selection in medium containing 800 μg ml^{-1} G418 (Calbiochem). To establish MDCK GCaMP6S cells expressing TRPC1 shRNA in a tetracycline-inducible manner (TRPC1-shRNA1: 5'-CCGGGAGAAATGCTGTTACCATACTCGAGTATGGTAACAGCATTTCTCTTTTTG-3' and 5'-AATTCAAAAAGAGAAATGCTGTTACCATACTCGAGTATGGTAACAGCATTTCTC-3' or TRPC1-shRNA2: 5'-CCGGTGCTTAGTGCATCGTTATCCTCGAGGATAACGATGCACTAAGCATTTTTG-3' and 5'-AATTCAAAAATGCTTAGTGCATCGTTATCCTCGAGGATAACGATGCACTAAGCA-3') each shRNA sequence was cloned into the BglII/XhoI site of pSUPERIOR.neo + gfp (Oligoengine). To establish MDCK cells expressing AHNAK2 shRNA in a tetracycline-inducible manner (AHNAK2-shRNA1: 5'-GATCCCCGGACTACAACGCTCAGGTTTTCAAGAGAAACCTGAGCGTTG

TAGTCCTTTTTC-3' and 5'-TCGAGAAAAAGGACTACAACGCTCAGGTTTCTCTTGAAAACCTGAGCGTTGTAGTCCGGG-3' or AHNAK2-shRNA2: 5'-GATCCCCGCATATCGAGTGTCAATATTTCAAGAGAATATTGACACTCGATATGCTTTTTC-3' and 5'-TCGAGAAAAAGCAAGTTCAAACTGCCAAATCTCTTGAATTTGGCAGTTTGAACTTGCGGG-3') each shRNA sequence was cloned into the BglII/XhoI site of pSUPERIOR.neo + gfp (Oligoengine). For tetracycline-inducible MDCK cell lines, 2 μg ml^{-1} of tetracycline (Sigma-Aldrich) was used to induce expression of proteins or shRNAs except for MDCK-pTRE3G Myc-RasV12 cells, for which 1 μg ml^{-1} of doxycycline (Sigma-Aldrich) was used. For immunofluorescence, cells were plated onto collagen gel-coated coverslips. Type I collagen (Cellmatrix Type I-A) was obtained from Nitta Gelatin and was neutralized on ice to a final concentration of 2 mg ml^{-1} according to the manufacturer's instructions.

3.2.3. Immunofluorescence

For immunofluorescence, MDCK-pTR GFP-RasV12, MDCK-pTR cSrcY527F-GFP, MDCK-pTR scribble shRNA, MDCK-pTRE3G Myc-RasV12, cells were mixed with MDCK, MDCK-pTR AHNAK2 shRNA, MDCK GCaMP6S cells or MDCK GCaMP6S TRPC1 shRNA cells at a ratio of 1:1 and plated onto collagen-coated coverslips. The mixture of cells was incubated for 8–12 h, followed by tetracycline or doxycycline treatment for 6 h, except for analyses of apical extrusions, which were examined after 24 h of tetracycline or doxycycline addition. Cells were fixed with 4%

paraformaldehyde (PFA) in PBS and permeabilized with 0.5% TritonX-100 in PBS, then blocked with 1% BSA in PBS. All primary antibodies were used at 1:100, and all secondary antibodies were used at 1:200. Immunofluorescence images were analysed with the Olympus FV1000 or FV1200 system and Olympus FV10-ASW software. Images were quantified with the MetaMorph software (Molecular Devices).

3.2.4. Time-lapse Microscopic observation

For time-lapse analyses, MDCK cells were co-cultured with MDCK-pTR GFP-RasV12 cells or MDCK cells at a ratio of 1:1. Subsequently, time-lapse observation was carried out for 8 h in the L-15 medium containing 2 μg/mL tetracycline by the Olympus FV1000 system and Olympus FV10-ASW software. Images were quantified with the MetaMorph software (Molecular Devices).

3.2.5. PDMS-based cell stretch assay

MDCK GCaMP6S or MDCK GCaMP TRPC1 shRNA cells were plated onto a stretched flexible polydimethylsiloxane (PDMS) membranes (STB-100-04 : STREX). Before plating, the clamped PDMS membranes were coated with 25 μg ml^{-1} fibronectin/PBS (Sigma-Aldrich) for 1 h at 37°C. The cells pre-treated with tetracycline for 48 h (MDCK GCaMP6S TRPC1 shRNA) were allowed to adhere for 24 h and then the membrane was stretched by 10%. The cells were fixed in 4% PFA/PBS 10 min after stretch and processed for immunofluorescence.

3.2.6. Stable isotope labeling with amino acids in cell culture

For SILAC labeling experiments, cells were maintained in DMEM minus L-Lysine and L-Arginine (CIL) supplemented with 10% dialyzed FCS and 1% penicillin/streptomycin (Gibco). In addition, 50 μg ml^{-1} of a L-lysine and L-arginine (CIL), and 200 μg ml-1 of a L-proline (Sigma) were added to medium. After two weeks of SILAC labeling, 2×10^7 cells were plated into a 145-mm dish, cultured without tetracycline for 8-12 h, and treated with 2 mg ml^{-1} tetracycline for 6 or 8 h. Then fixed cells with liquid-N2. Protein identification by mass spectrometry was performed by a collaborator, Mr. Takashi Hayashi (Otsuka Pharmaceutical Co., Ltd.).

3.2.7. Quantitative real-time PCR

Total RNA was extracted from the isolated cells using Trizol (Thermo Fisher Scientific) and reverse transcribed using a QuantiTect Reverse Transcription Kit (QIAGEN). GeneAce SYBR qPCR Mix (NIPPON GENE) was used to perform qPCR using the StepOne system (Thermo Fisher Scientific). The primer sequences used are as shown below. We used ß-actin as a reference gene to normalize data.

Target	Sequence	
Dog AHNAK2	Forward	GGGATGGACACCAGAAAGAA
	Reverse	GCGTGGACACTGTAATGGTG
Dog TRPC1	Forward	CATGAGGCAGAAGATGCAAA
	Reverse	TGCAAATGCAGTCTTCAGG
Dog ACTINβ	Forward	GGCACCCAGCACAATGAAG
	Reverse	ACAGTGAGGCCAGGATGGAG

3.2.8. Statistics and reproducibility

For data analyses, unpaired two-tailed Student t-tests were used to determine P-values. P-values less than 0.05 were considered to be significant. No statistical method was used to predetermine sample size. All results were reproduced with at least two independent experiments.

3.3. Results

3.3.1. SILAC screening for phosphorylated proteins in the mix culture of normal and RasV12- or Src-transformed cells

To reveal the recognition mechanisms that function in the early stage of cell competition between normal and transformed cells, we performed a quantitative mass spectrometric analysis. Using stable isotope labeling with amino acids in cell culture (SILAC)-based quantitative proteomics, we examined proteins whose phosphorylation level is altered in the mixture of normal and RasV12- or cSrcY527F-transformed cells. We used MDCK cells expressing GFP-RasV12 or cSrcY527F-GFP in a tetracycline inducible manner. Two types of isotope-labeled arginine and lysine were used - heavy (Arg 10, Lys 8) for labeling mono-culture of normal and RasV12 or cSrcY527F cells, and medium (Arg 6, Lys 4) for labeling mix-culture (Fig. 3-1). Medium-labeled normal MDCK and RasV12 or cSrcY527F cells were mixed, whereas heavy-labeled MDCK and RasV12 or cSrcY527F cells were cultured alone (Fig. 3-1). Followed by a 6 or 10 hours induction of RasV12 or cSrcY527F expression with tetracycline, the cells were combined and the amounts of heavy- and medium-labeled peptides were compared by quantitative mass spectrometry; the ratio of medium to heavy label (M:H ratio) was calculated for each peptide (Fig. 3-2). And we identified AHNAK2 as one of the proteins whose phosphorylation level is upregulated at the highest level in the mix culture conditions compared to alone culture condition in all 4 conditions (Ras 6/10 hours, Src 6/10 hours) (Fig. 3-2).

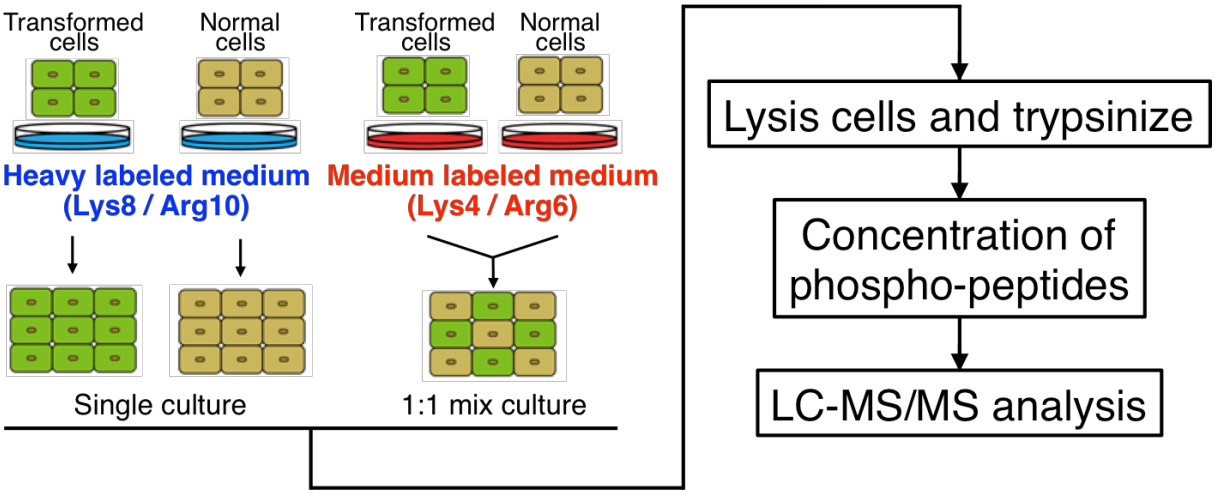

Fig. 3-1 SILAC screening for phosphorylated proteins in the mixture of normal and RasV12- or cSrcY527F-transformed cells. A schematic image for SILAC screening. MDCK cells and MDCK-pTR GFP-RasV12 cells and MDCK-pTR cSrcY527F-GFP cells were labeled with medium (Arg 6, Lys 4) for 1:1 mix culture or heavy (Arg 10, Lys 8) for alone culture. These cells were incubated for 12 hours after seeding. And then they were incubated with tetracycline for 6 or 10 hours.

Name	phosphosite	M:H ratio			
		MDCK:RasV12 =1:1 mix		MDCK:cSrcY527F =1:1 mix	
		6 hours	10 hours	6 hours	10 hours
AHNAK2 Uncharacterized protein	S564,S732,S914, S1096,S1264,S1446	16.313	14.549	3.795	4.735
TPD52L2 tumor protein D52-like 2	S189	4.719	5.019	2.074	45.8
CAD carbamoyl-phosphate synthetase 2, aspartate transcarbamylase, and dihydroorotase	S1827	8.302	2.491	2.752	5.794
EPS8 epidermal growth factor receptor pathway substrate 8	S665	2.649	2.648	3.154	4.974
CTNNA1 catenin (cadherin-associated protein), alpha 1, 102kDa	S641	8.772	1.949	1.81	5.02
PRRC2C proline-rich coiled-coil 2C	S2063	1.825	2.449	1.837	5.707
CDC42EP4 CDC42 effector protein (Rho GTPase binding) 4	S118	3.001	1.86	2.351	5.439

Fig. 3-2 The list of identified proteins that are significantly phosphorylated in the mixture of MDCK and RasV12 cells or cSrcY527F cells. M:H ratio indicates the ratio of mixed-culture compared to mono-culture.

3.3.2. Phosphorylation of AHNAK2 is upregulated in normal cells mixed with RasV12-transformed cells and plays a crucial role in apical extrusion

To validate the result of phospho-SILAC screening, we generated antibody that recognizes the phosphorylated-AHNAK2 specifically and performed immunofluorescence. We found that phosphorylation of AHNAK2 in a cytosol was upregulated in normal epithelial cells mixed with RasV12-transformed cells compared to normal cells alone (Fig. 3-3). A comparable phenomenon was also observed in Src-transformed cells, but not in scribble-knockdown cells (Fig. 3-4). On the other hand, the expression level of AHNAK2 was not upregulated in normal cells mixed with RasV12 cells (Fig. 3-5), indicating that phosphorylation of AHNAK2, but not expression, was upregulated in normal epithelial cells mixed with RasV12- or cSrcY527F-transformed cells. To examine the involvement of AHNAK2 in apical extrusion, we established normal cells expressing AHNAK2 short hairpin RNA (shRNA) in a tetracycline inducible manner (Fig. 3-6). AHNAK2 knockdown in surrounding normal cells suppressed apical extrusion of RasV12 cells, while promoting formation of basal protrusions that extended beneath the neighboring normal cells (Fig. 3-6), suggesting that AHNAK2 in surrounding normal cells is important for apical extrusion of RasV12 cells.

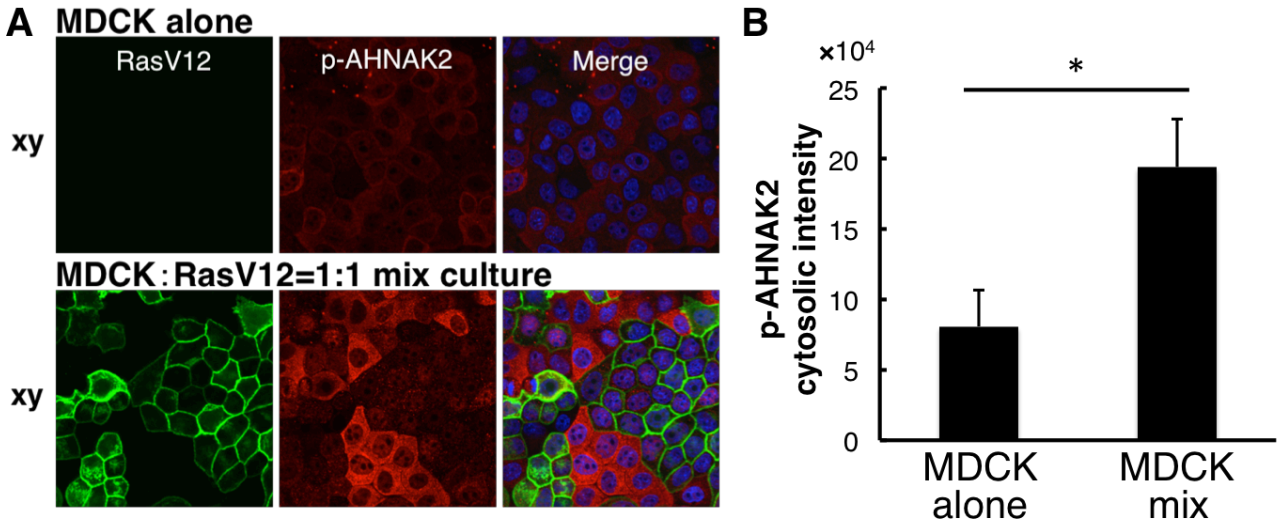

Fig. 3-3 The phosphorylation of AHNAK2 is upregulated in normal cells mixed with RasV12-transformed cells. (**A**) Immunofluorescence images of phosphorylated AHNAK2. Normal MDCK cells were mixed with MDCK-pTR GFP-RasV12 cells or cultured alone for 6 hours, and were stained with Hoechst 33342 (blue) and anti-p-AHNAK2 antibody (red). (**B**) Quantification of the fluorescence intensity of cytosolic p-AHNAK2. Data are mean ± s.e.m. $^{*}P < 0.01$, unpaired two-tailed t -test; n = three independent experiments.

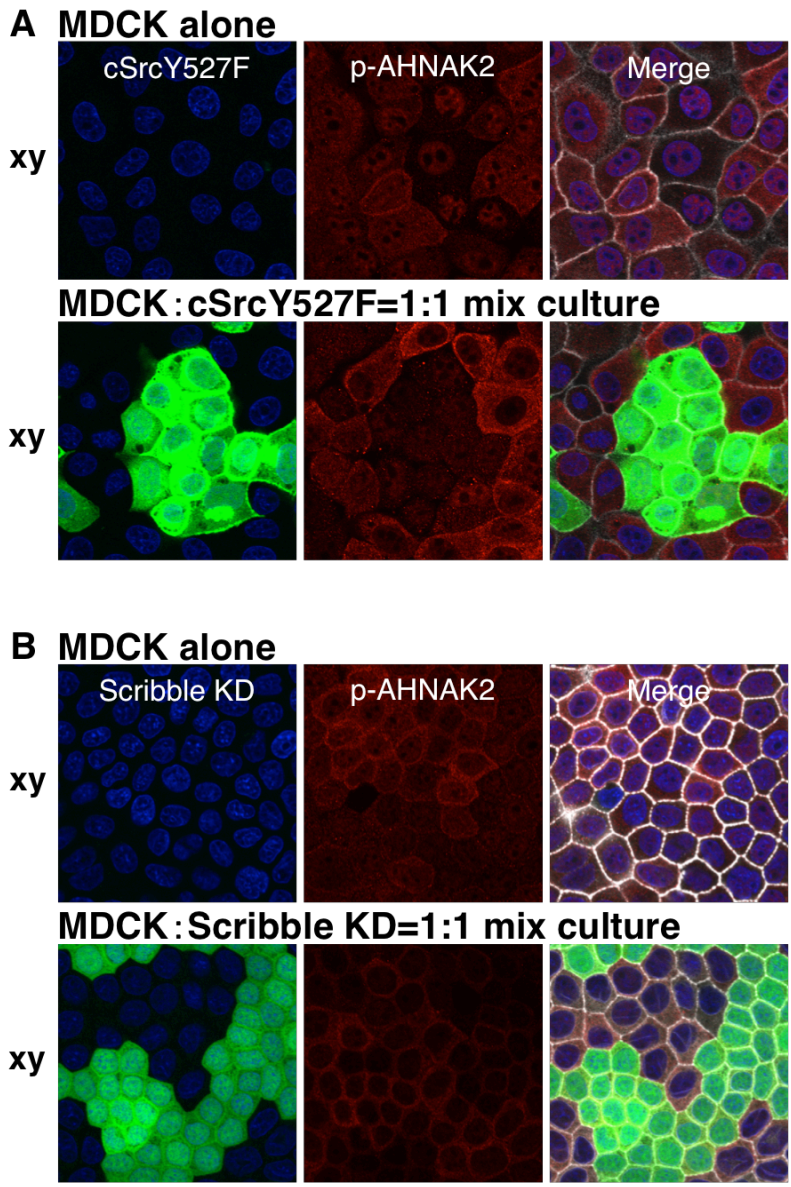

Fig. 3-4 The phosphorylation of AHNAK2 is also upregulated in normal cells mixed with Src-transformed cells, but not in normal cells mixed with Scribble-knockdown cells. (**A**) Immunofluorescence images of phosphorylated AHNAK2. Normal MDCK cells were mixed with MDCK-pTR cSrcY527F-GFP cells or cultured alone for 6 hours, and were stained with Hoechst 33342 (blue), anti-p-AHNAK2 antibody (red) and Alexa-Fluor-647-conjugated phalloidin (white). (**B**) Immunofluorescence images of phosphorylated AHNAK2. Normal MDCK cells were mixed with MDCK-pTR Scribble-shRNA cells or cultured alone for 36 hours, and were stained with Hoechst 33342 (blue), anti-p-AHNAK2 antibody (red) and Alexa-Fluor-647-conjugated phalloidin (white).

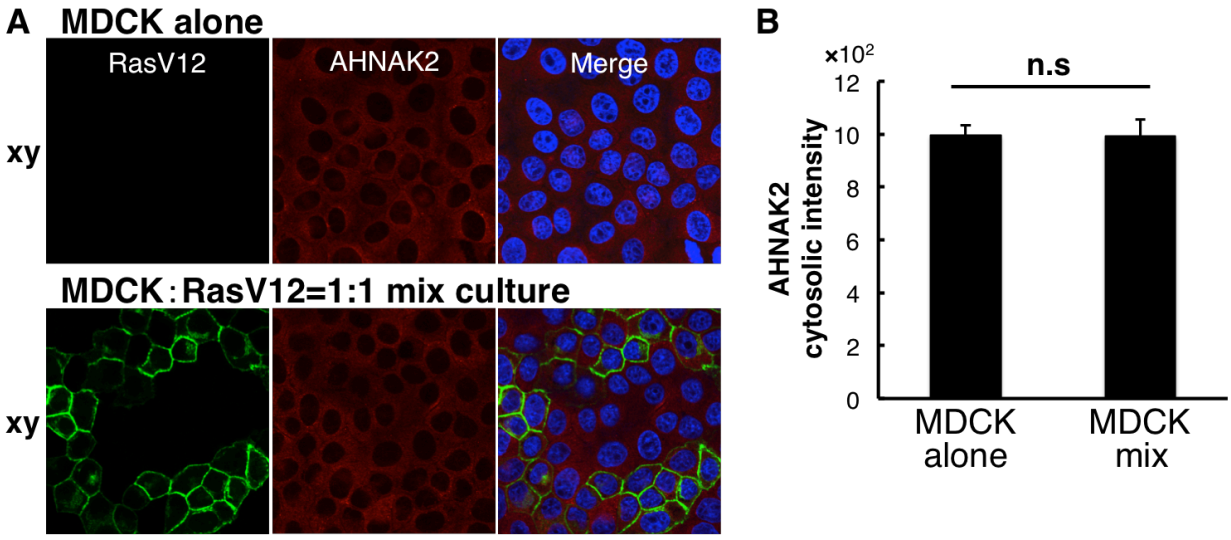

Fig. 3-5 The expression of AHNAK2 is not upregulated in normal cells mixed with RasV12-transformed cells. (**A**) Immunofluorescence images of AHNAK2. Normal MDCK cells were mixed with MDCK-pTR GFP-RasV12 cells or cultured alone for 6 hours and were stained with Hoechst 33342 (blue) and anti-AHNAK2 antibody (red). (**B**) Quantification of the fluorescence intensity of cytosolic AHNAK2. Data are mean ± s.e.m. unpaired two-tailed *t* -test; *n* = three independent experiments.

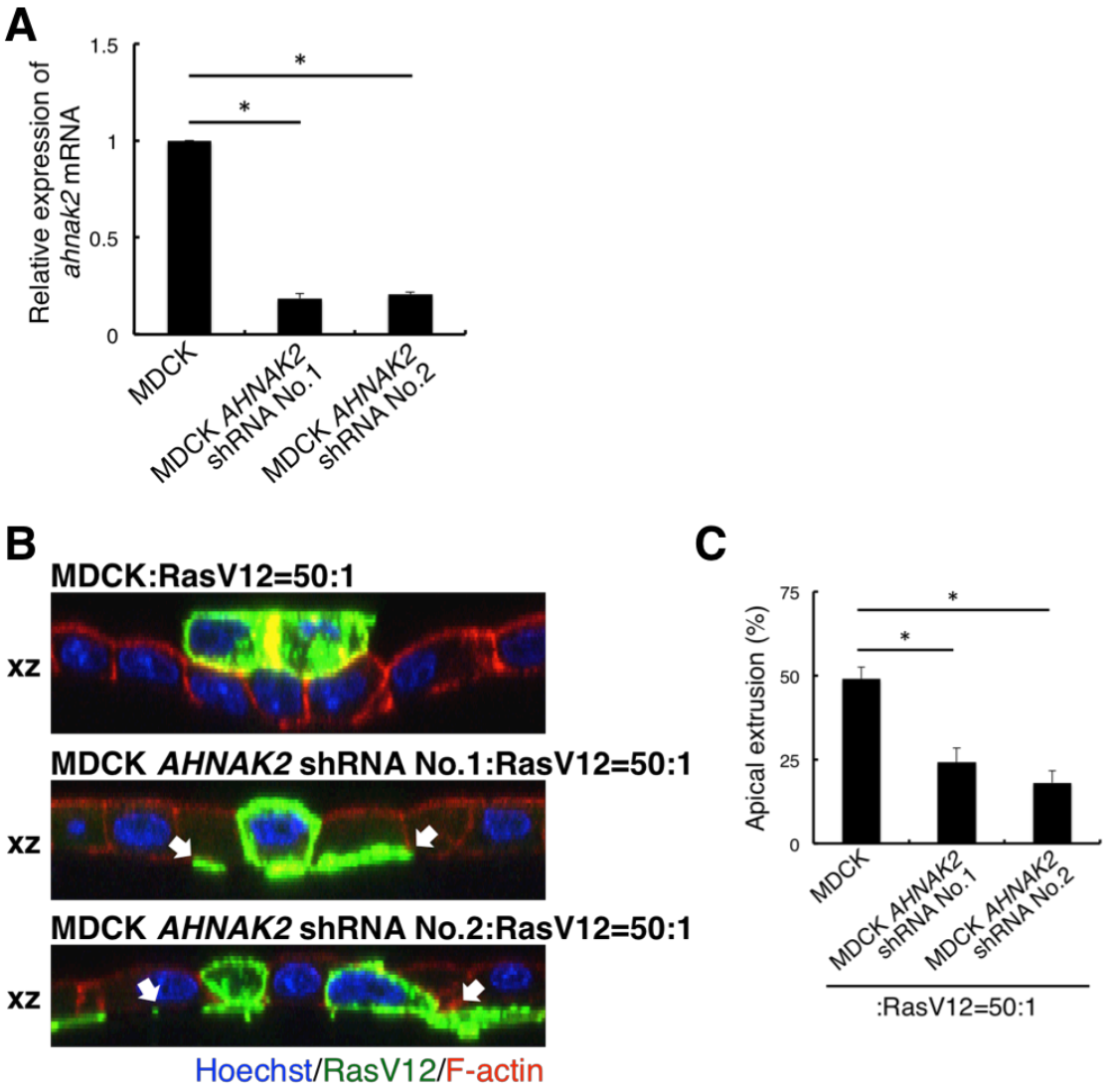

Fig. 3-6 Effect of AHANK2-knockdown on apical extrusion. (**A**) Establishment of MDCK cells expressing *AHNAK2* shRNA1 or *AHNAK2* shRNA2. Knockdown of *AHNAK2* was confirmed by qrtPCR. Data are mean ± s.e.m. **P* < 0.01, unpaired two-tailed *t* -test; *n* = three independent experiments. (**B**) Immunofluorescence images of *xz* sections of MDCK-pTR GFP-RasV12 cells surrounded by normal MDCK cells, MDCK *AHNAK2* shRNA1 or MDCK *AHNAK2* shRNA2. Arrowheads indicate the basal protrusion. (**C**) Quantification of the apical extrusion. Data are mean ± s.e.m. **P* < 0.05, unpaired two-tailed *t* -test; *n* = three independent experiments.

3.3.3. Phosphorylation of AHNAK2 is regulated by PKC in normal cells mixed with transformed cells

To reveal the molecular mechanism that causes phosphorylation of AHNAK2 in the mix culture, we examined the effect of various kinase inhibitors on AHNAK2 phosphorylation. We found that the PKA inhibitor KT5720 and the PKC inhibitor BIM-I suppressed the upregulation of AHNAK2 phosphorylation (Fig. 3-7). Immunofluorescence of phosphorylated-PKC-substrate or phosphorylated-PKA-substrate, which reflects the activity of PKC and PKA respectively, showed that the activity of PKC, but not the activity of PKA, was also upregulated in normal cells mixed with RasV12 cells (Fig. 3-8 and 9). In a previous study, we demonstrated that EPLIN accumulates in RasV12-transformed cells surrounded by normal cells and plays a positive role in the apical extrusion via activation of the downstream molecules PKA and myosin II. So the effect of the PKA inhibitor KT5720 on AHNAK2 phosphorylation might be caused by inhibition of PKA in RasV12 cells not in normal cells. These results suggest that phosphorylation of AHNAK2 is regulated by PKC activity in normal cells when they are mixed with RasV12 cells.

A

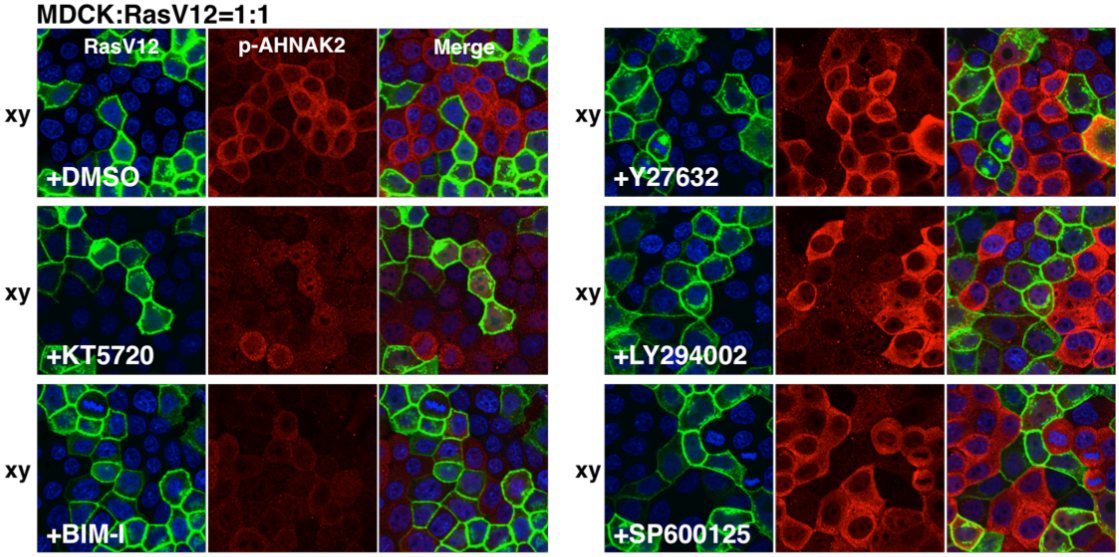

B

Inhibitor	Target	p-AHNAK2 upregulation
KT5720	PKA	↓
BIM-I	PKC	↓
Y27632	Rho kinase	No effect
LY294002	PI3K	No effect
SP600125	JNK	No effect

Fig. 3-7 Effect of various inhibitors on AHNAK2 phosphorylation. (**A**) Normal MDCK cells were co-cultured with MDCK-pTR GFP-RasV12 cells in the presence of various inhibitors for 6 hours and stained with anti-p-AHNAK2 (red). Each inhibitor inhibits the following molecule or cellular process; KT5720: PKA, BIM-I: PKC, Y27632: Rho kinase, LY294002: PI3K, SP600125: JNK. (**B**) Effect of various inhibitors on AHNAK2 phosphorylation.

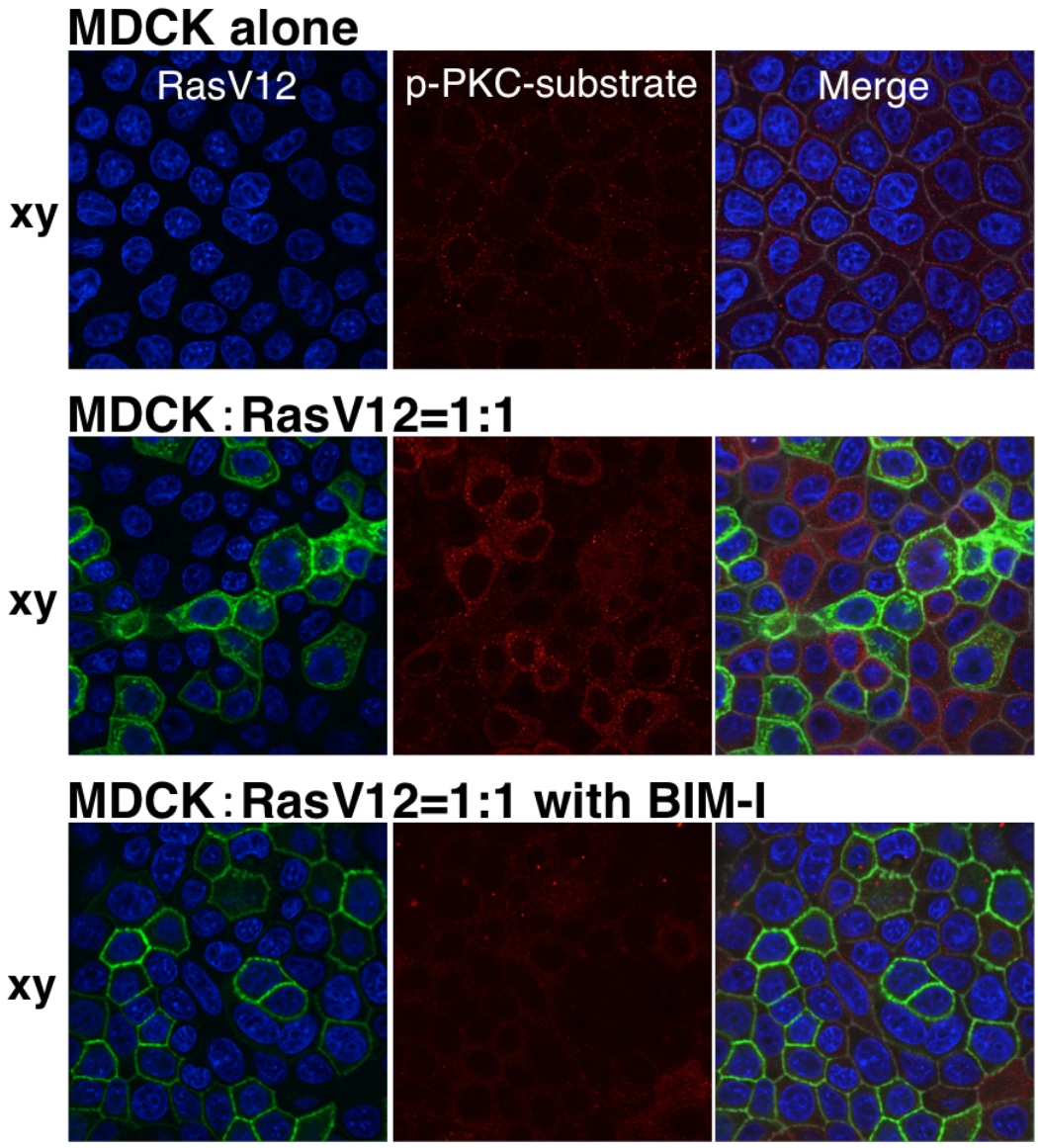

Fig. 3-8 PKC activity is upregulated in normal cells mixed with RasV12-transformed cells. Immunofluorescence images of phosphorylated PKC-substrate. Normal MDCK cells were cultured alone or mixed with MDCK-pTR GFP-RasV12 cells or with PKC inhibitor BIM-I for 6 hours and were stained with Hoechst 33342 (blue), anti-p-PKC-substrate antibody (red) and Alexa-Fluor-647-conjugated phalloidin (white).

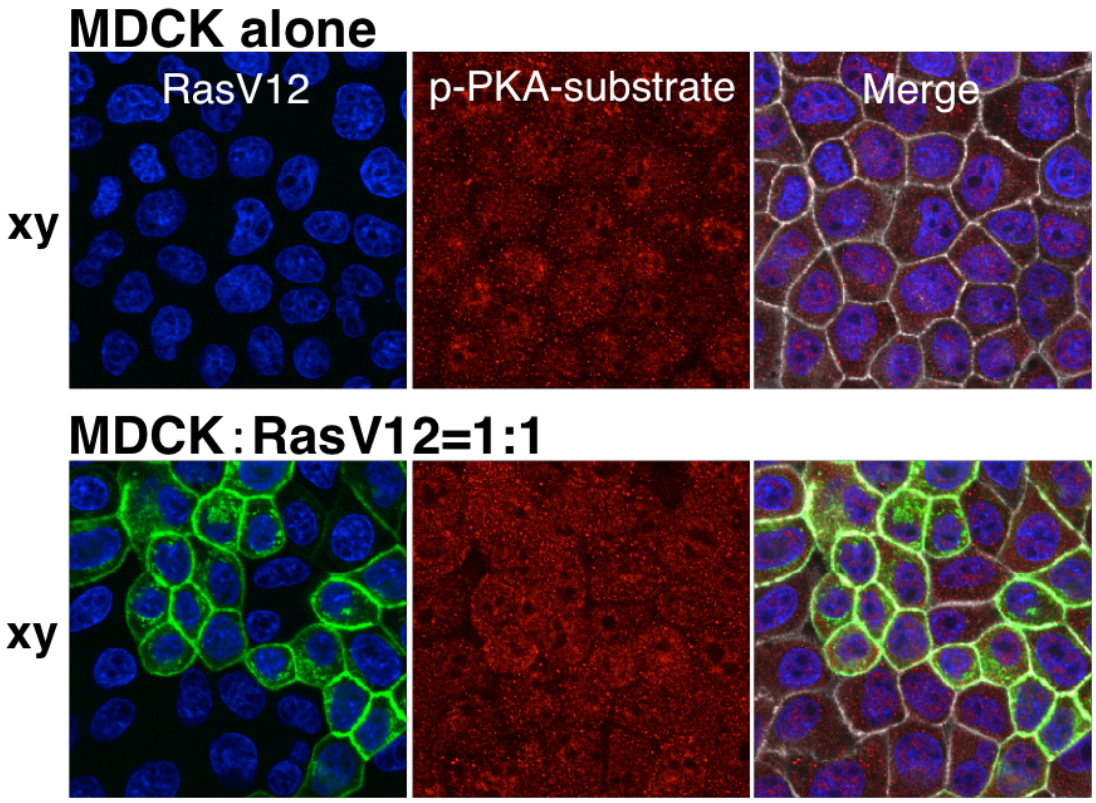

Fig. 3-9 PKA activity is not upregulated in normal cells mixed with RasV12-transformed cells. Immunofluorescence images of phosphorylated PKA-substrate. Normal MDCK cells were cultured alone or mixed with MDCK-pTR GFP-RasV12 cells for 6 hours and were stained with Hoechst 33342 (blue), anti-p-PKA-substrate antibody (red) and Alexa-Fluor-647-conjugated phalloidin (white).

3.3.4. Phosphorylation of AHNAK2 depends on mechano-sensitive calcium channel TRPC1 under mix culture- or stretched-condition

We further examined the molecular mechanism underlying phosphorylation of AHNAK2 in the mix culture. At first, we checked the involvement of PLC, which is known as one of the upstream molecule of PKC, in AHNAK2 phosphorylation. We found that the PLC inhibitor U73122 suppressed AHNAK2 phosphorylation in normal cells mixed with RasV12 cells (Fig.3-10), suggesting that PLC-PKC pathway regulates AHNAK2 phosphorylation. In addition, we tried to identify which type of PKC is involved in AHNAK2 phosphorylation. PKC family is composed of 3 subtypes; conventional PKC (cPKC) which requires diacylglycerol (DAG) and calcium, novel PKC (nPKC) which requires only DAG, atypical PKC (aPKC) which requires no second messenger binding.Using the cPKC specific inhibitor Go6976, we found that Go6976 suppressed the non-cell autonomous AHNAK2 phosphorylation (Fig. 3-11), suggesting that AHNAK2 is phosphorylated by cPKC which is known as calcium dependent PKC. So, next, we examined the involvement of calcium signaling in AHNAK2 phosphorylation. We first examined the effect of ionomycin, a membrane permeable calcium ionophore, on AHNAK2 phosphorylation. We found that AHNAK2 phosphorylation was upregulated by ionomycin treatment (Fig. 3-12), indicating that treatment with calcium is sufficient to cause AHNAK2 phosphorylation. In addition, to examine the intracellular calcium level in the mix culture condition, we performed timelapse observation using MDCK stably expressing GCaMP6S which is a GFP-based calcium sensor. We found that enhancement of GCaMP intensity was often

observed in normal cells mixed with RasV12 cells compared to alone culture (Fig. 3-13). These data suggesting that the non-cell-autonomous calcium uptake activates cPKC and it causes AHNAK2 phosphorylation in normal cells mixed with RasV12 cells. To examine the molecular mechanism of the enhancement of calcium uptake, we established GCaMP6S cells expressing TRPC1 shRNA (Fig. 3-14). TRPC1 is mechanosensitive (stretch-activated) calcium channel. To check the character of TRPC1 knockdown GCaMP6S cells, we performed cell stretching assay using stretch chamber. After stretch, control GCaMP cells showed the enhancement of intracellular calcium level. On the other hand, TRPC1 knockdown suppressed the enhancement of intracellular calcium level (Fig. 3-15). In this condition, we examined the effect of cell stretching on AHNAK2 phosphorylation. We found that AHNAK2 phosphorylation was upregulated by cell stretching (Fig. 3-16). In addition, TRPC1 knockdown suppressed AHNAK2 phosphorylation under stretch condition (Fig. 3-16), indicating that AHNAK2 could react to mechanical tension via calcium uptake, in other words, AHNAK2 could be a mechano-sensor protein. Moreover, TRPC1 knockdown also suppressed the upregulation of AHNAK2 phosphorylation in normal cells mixed with RasV12 cells (Fig. 3-17), indicating that mechanical tension is generated and causes AHNAK2 phosphorylation in the mix culture condition.

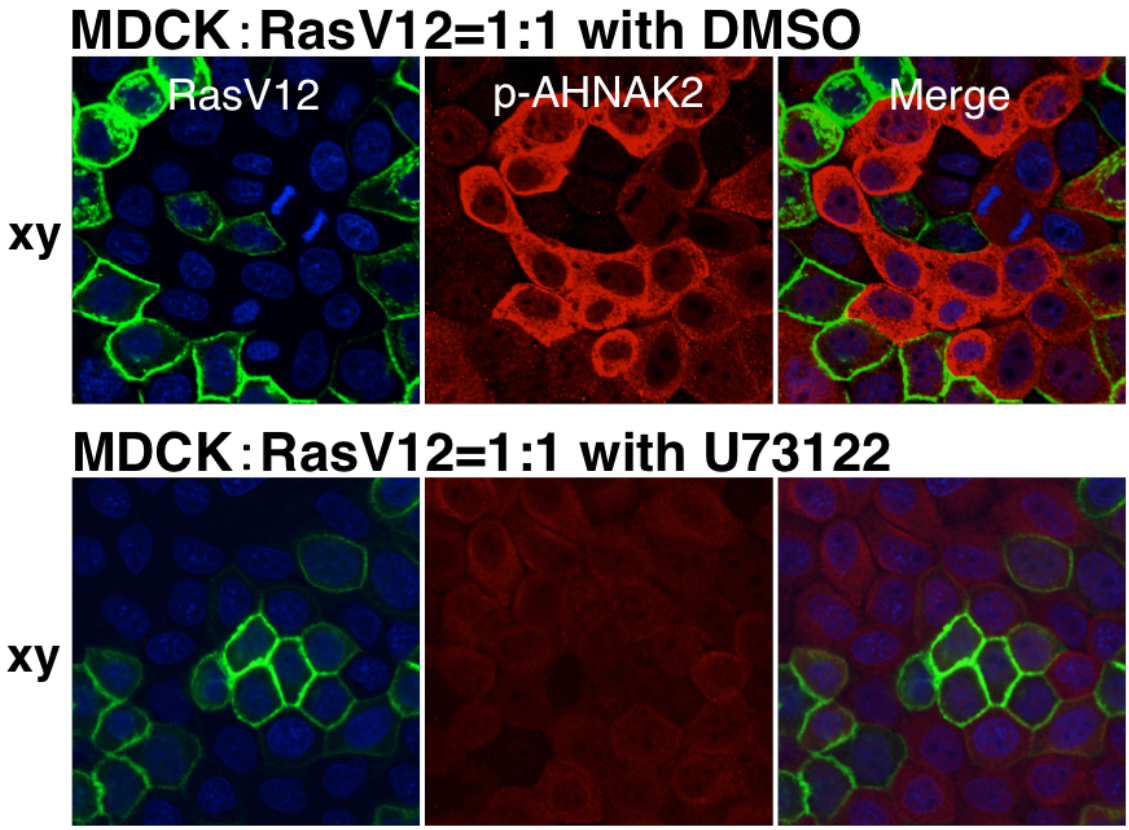

Fig. 3-10 Treatment with PLC inhibitor U73122 suppresses the upregulation of AHNAK2 phosphorylation. Immunofluorescence images of p-AHNAK2. Normal MDCK cells were mixed with MDCK-pTR GFP-RasV12 cells with DMSO or the PLC inhibitor U73122 for 6 hours and were stained with Hoechst 33342 (blue), anti-p-AHNAK2 antibody (red).

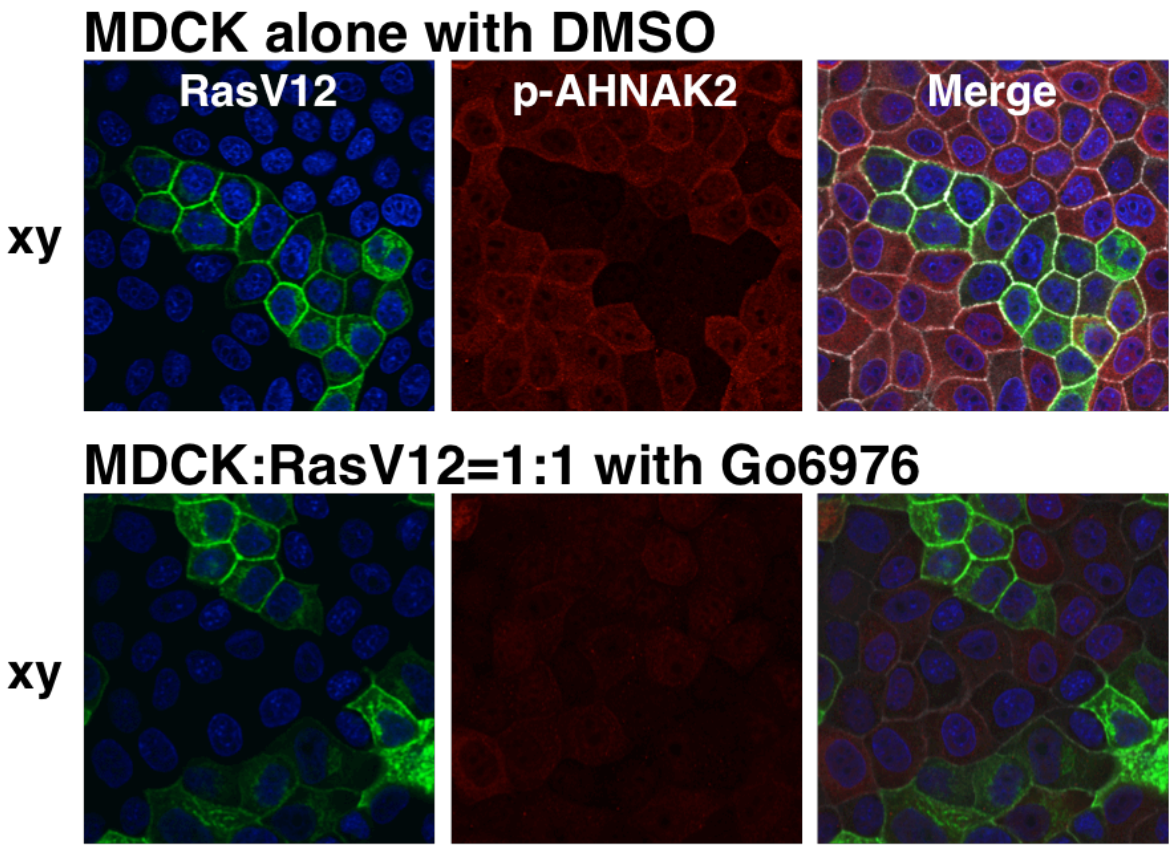

Fig. 3-11 Treatment with cPKC specific inhibitor Go6976 suppresses the upregulation of AHNAK2 phosphorylation. Immunofluorescence images of p-AHNAK2. Normal MDCK cells were mixed with MDCK-pTR GFP-RasV12 cells with DMSO or cPKC specific inhibitor Go6976 for 6 hours and were stained with Hoechst 33342 (blue), anti-p-AHNAK2 antibody (red) and Alexa-Fluor-647-conjugated phalloidin (white).

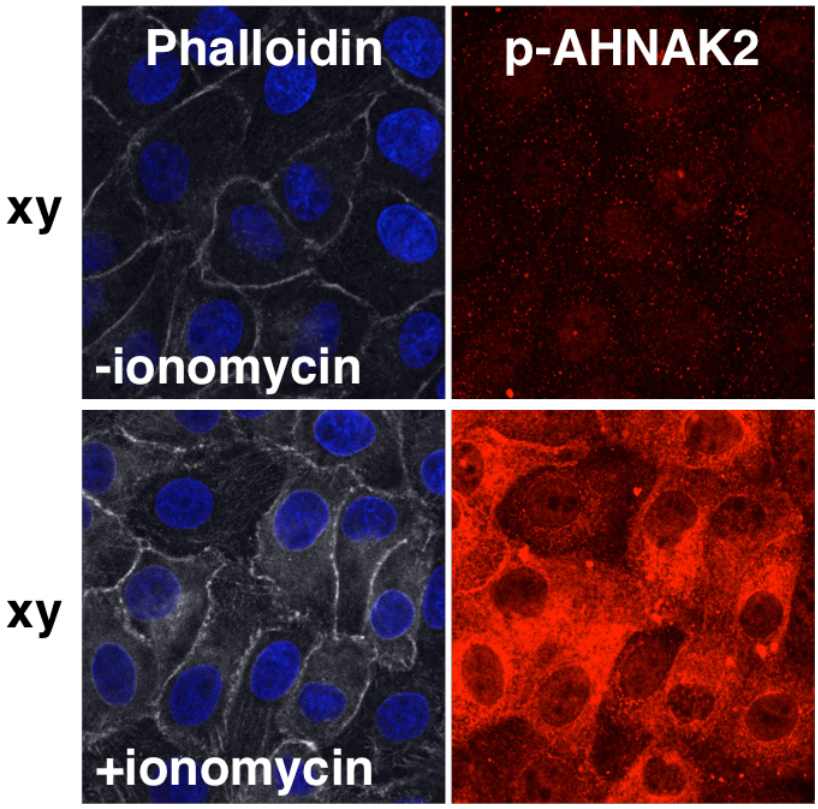

Fig. 3-12 The effect of calcium ionophore on AHNAK2 phosphorylation. Immunofluorescence images of p-AHNAK2. Normal MDCK cells were treated with DMSO or calcium ionophore ionomycin and were stained with Hoechst 33342 (blue), anti-p-AHNAK2 antibody (red) and Alexa-Fluor-647-conjugated phalloidin (white).

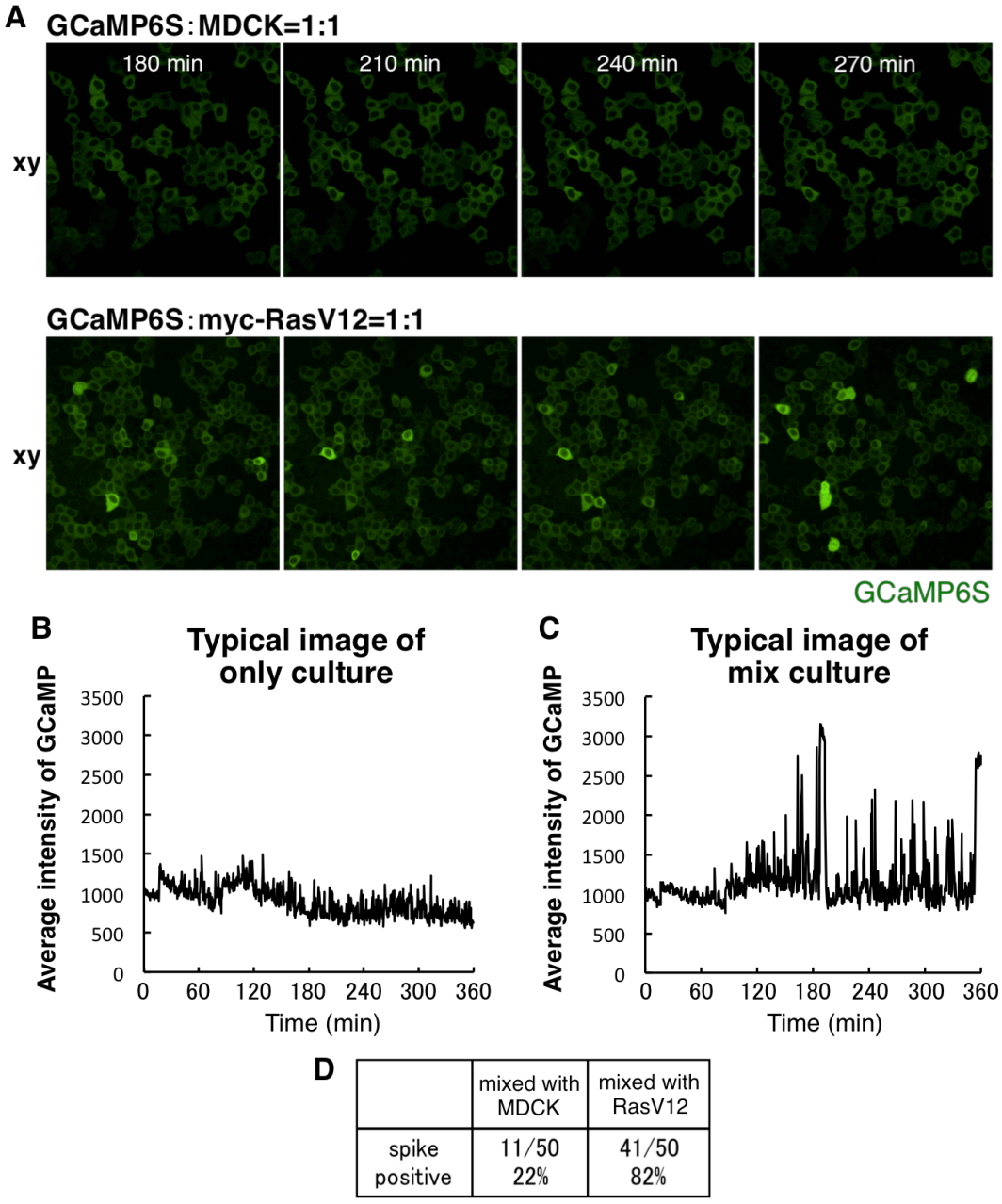

	mixed with MDCK	mixed with RasV12
spike positive	11/50 22%	41/50 82%

Fig. 3-13 Calcium spark is often observed in normal cells mixed with RasV12 cells. (**A**) MDCK GCaMP6S cells were mixed with normal MDCK cells or MDCK-pTRE3G myc-RasV12 cells. After treatment with doxycycline to induce RasV12 expression, we performed time-lapse observation for 8 hours. (interval time: 30 sec). (**B**) Typical quantification result of GCaMP intensity in the mixed with normal cells. (**C**) Typical quantification result of GCaMP intensity in the mixed with myc-RasV12 cells. (**D**) Quantification of the number of calcium spike positive cells in each condition from three independent experiments. Criteria of spike positive is more than 2-fold than starting point.

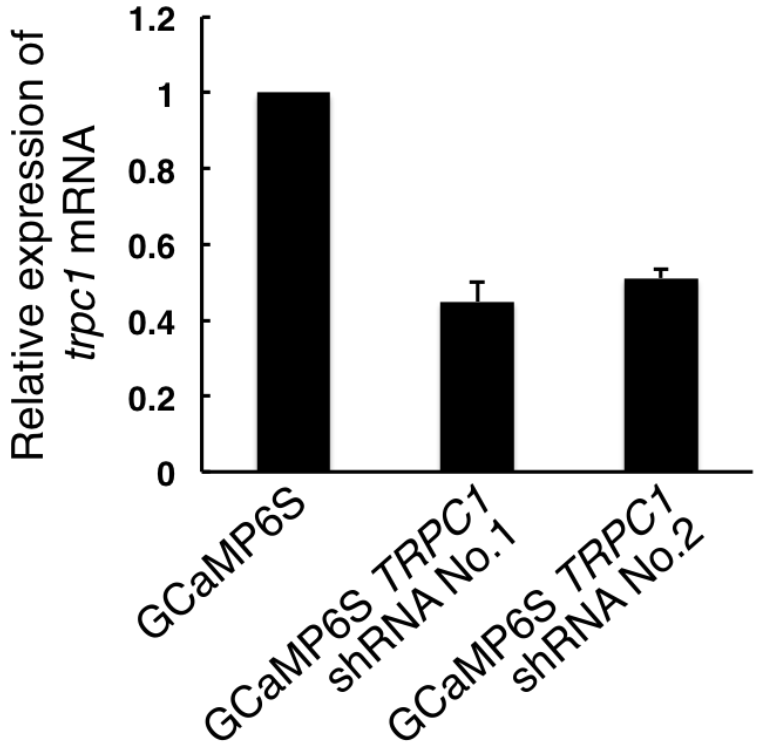

Fig. 3-14 Establishment of MDCK GCaMP6S cells expressing *TRPC1* shRNA1 or *AHNAK2* shRNA2. Knockdown of *TRPC1* was confirmed by qrtPCR. Data are mean ± s.e.m.; *n* = two independent experiments.

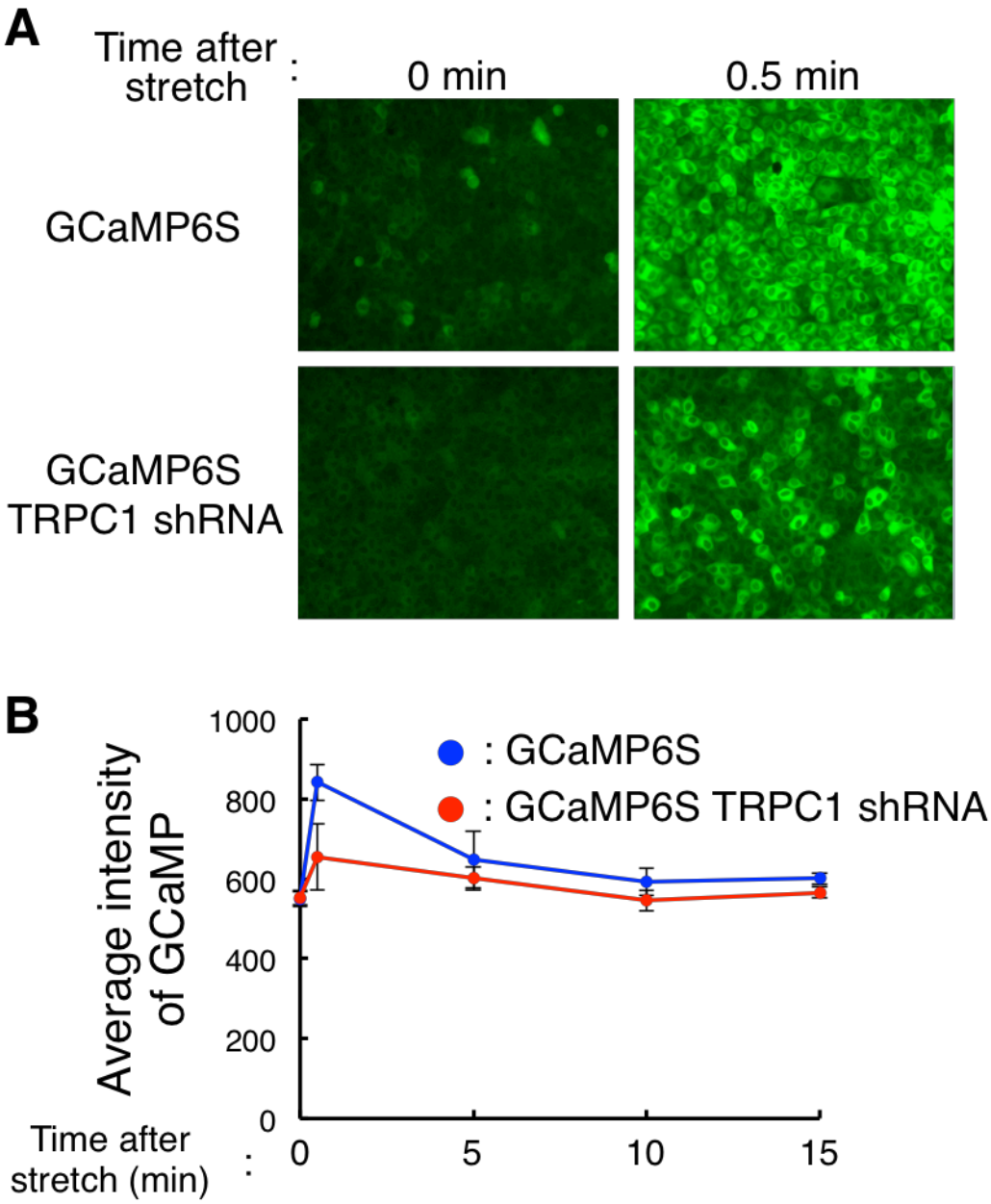

Fig. 3-15 Effect of *TRPC1 knockdown* on mechanical stretch-induced calcium uptake. (**A**) MDCK GCaMP6S cells or MDCK GCaMP6S TRPC1 shRNA cells were incubated on stretch chamber. After forming monolayer, cells were stretched by 10 % for 15 min. (**B**) Quantification of GCaMP intensity of GCaMP6S cells and GCaMP6S TRPC1 knockdown cells. The indicating time is minute after stretch. ; *n* = two independent experiments.

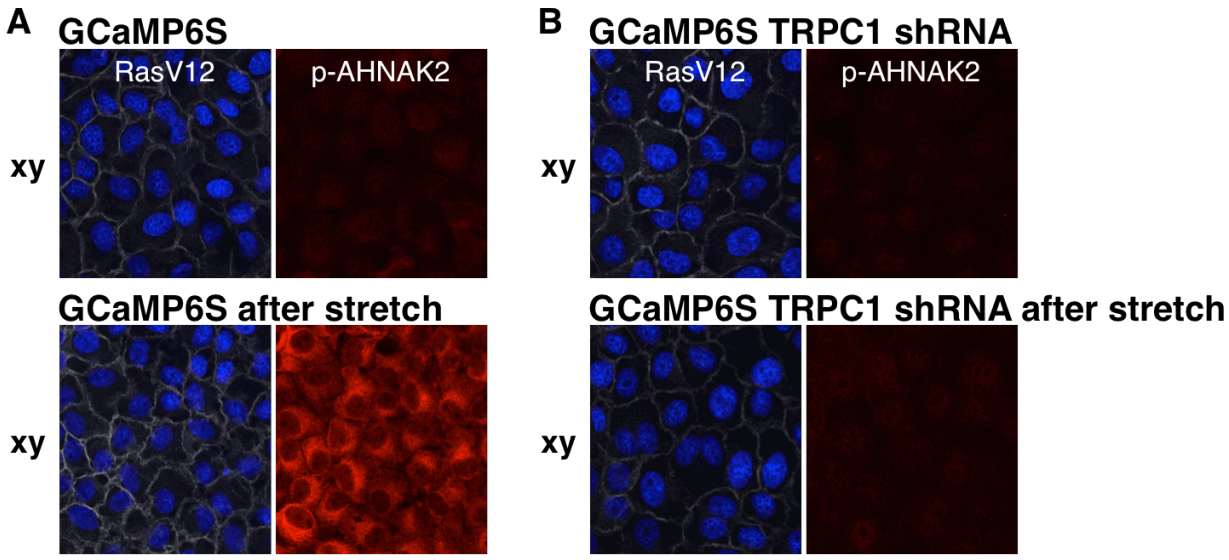

Fig. 3-16 Effect of *TRPC1 knockdown* on mechanical stretch-induced phosphorylation of AHNAK2. (**A**) MDCK GCaMP6S cells were stretched by 10 % for 10 min and stained with Hoechst 33342 (blue), anti-p-AHNAK2 antibody (red) and Alexa-Fluor-647-conjugated phalloidin (white). (**B**) MDCK GCaMP6S TRPC1 shRNA cells were stretched by 10 % for 10 min and stained with Hoechst 33342 (blue), anti-p-AHNAK2 antibody (red) and Alexa-Fluor-647-conjugated phalloidin (white).

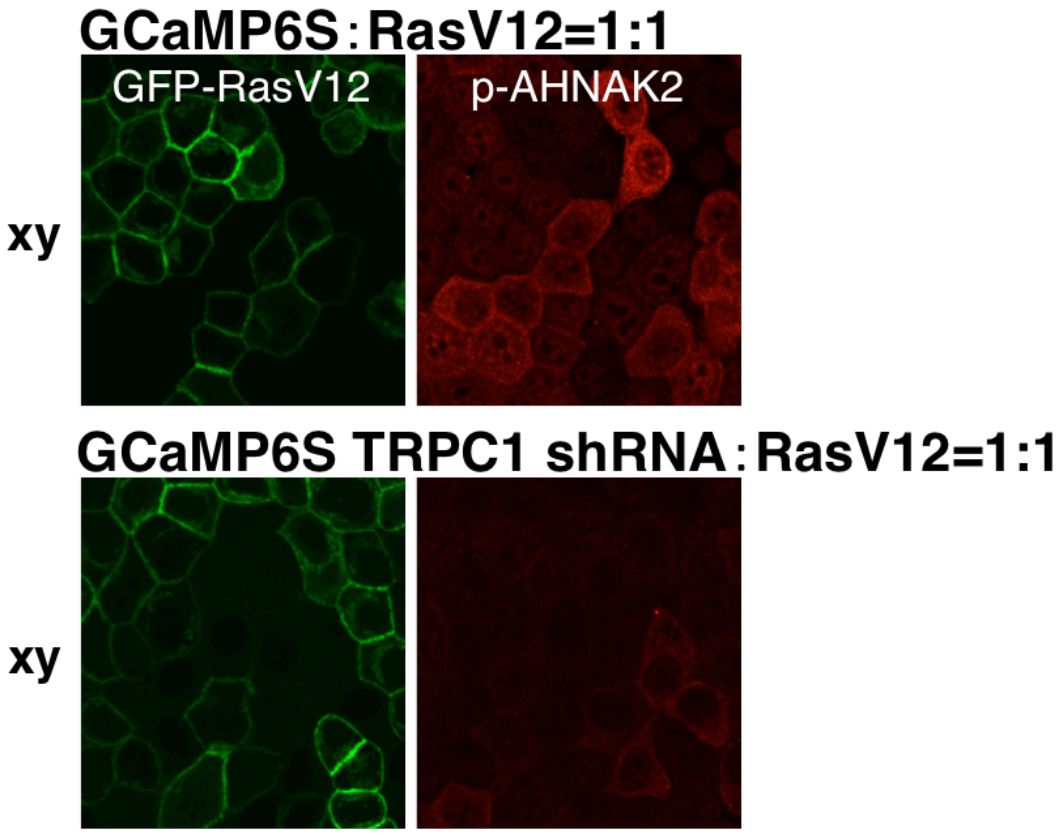

Fig. 3-17 Effect of *TRPC1 knockdown* on AHNAK2 phosphorylation in normal cells mixed with RasV12 cells. (**A**) MDCK GCaMP6S cells or MDCK GCaMP6S TRPC1 shRNA cells were mixed with MDCK-pTR GFP-RasV12 cells for 6 hours and stained with Hoechst 33342 (blue), anti-p-AHNAK2 antibody (red).

3.3.5. AHNAK2 is important for cellular movement in the mix culture condition

What is the functional significance of AHNAK2 phosphorylation in normal cells mixed with RasV12 cells? Epithelial cells maintain and restore epithelial homeostasis by inducing cell proliferation or cell motility when it is collapsed by such as tissue damage or imbalance. In addition, we found that actin stress fiber was increased in AHNAK2 knockdown cells compared to normal cells (Fig. 3-18), suggesting that AHNAK2 might be important for cell migration. To examine the involvement of AHNAK2 in cell migration, we performed wound healing assay using AHNAK2 knockdown cells. We found that cell migration was suppressed by AHNAK2 knockdown after wounding compared to control cells (Fig. 3-19), indicating that AHNAK2 is important for cell migration after wounding. Finally, we evaluated cell motility in the mix culture condition. We found that cell motility of normal cells was increased when they are mixed with RasV12 cells especially in the later time point (6.5~8.0 hours after RasV12 induction) (Fig. 3-20). These results suggest that AHNAK2 have an important role in cell motility and cell motility is increased in normal cells when they are mixed with RasV12-transformed cells.

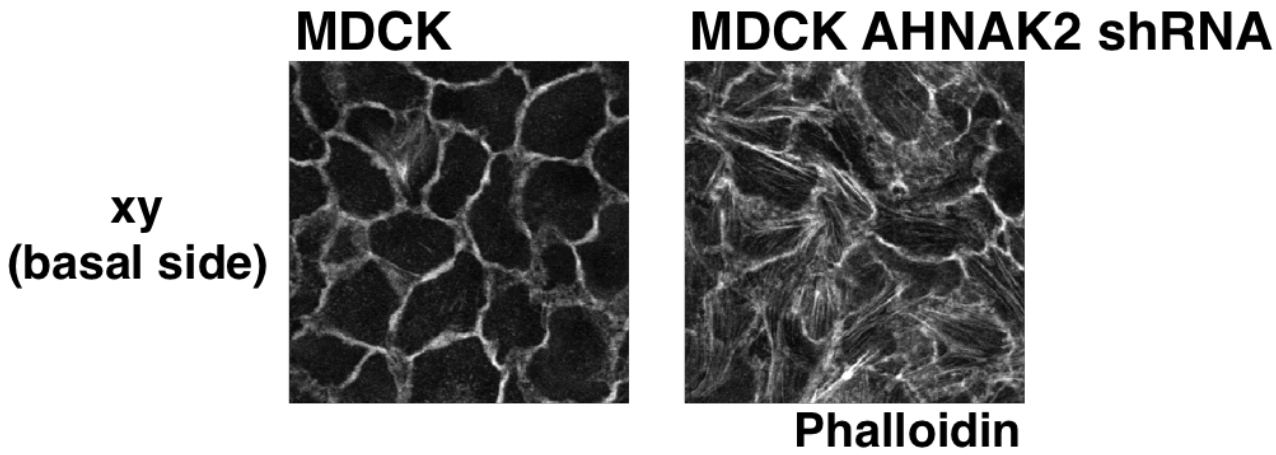

Fig. 3-18 Effect of *AHNAK2 knockdown* on F-actin structure. (**A**) MDCK cells or MDCK AHNAK2 shRNA cells were stained with Alexa-Fluor-647-conjugated phalloidin (white).

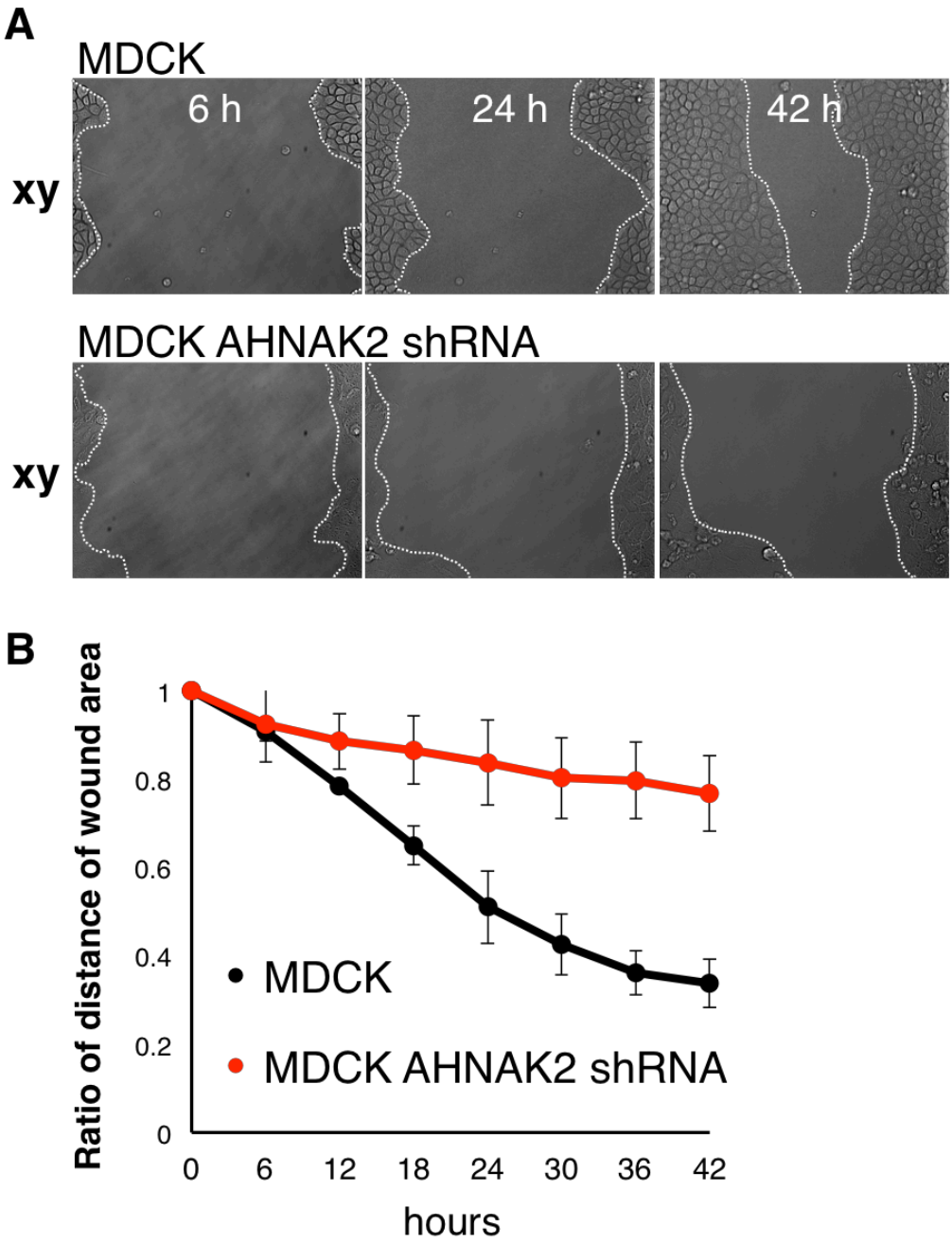

Fig. 3-19 AHNAK2 knockdown suppresses cell migration during wound healing. (**A**) Cropped images of time-lapse observation. MDCK cells or MDCK AHNAK2 shRNA cells were incubated. After forming monolayer, we scratched cell layer to generate wound and performed time-lapse observation for 42 hours. (**B**) Quantification of the distance of wound area in each time points after scratching. ; *n* = two independent experiments.

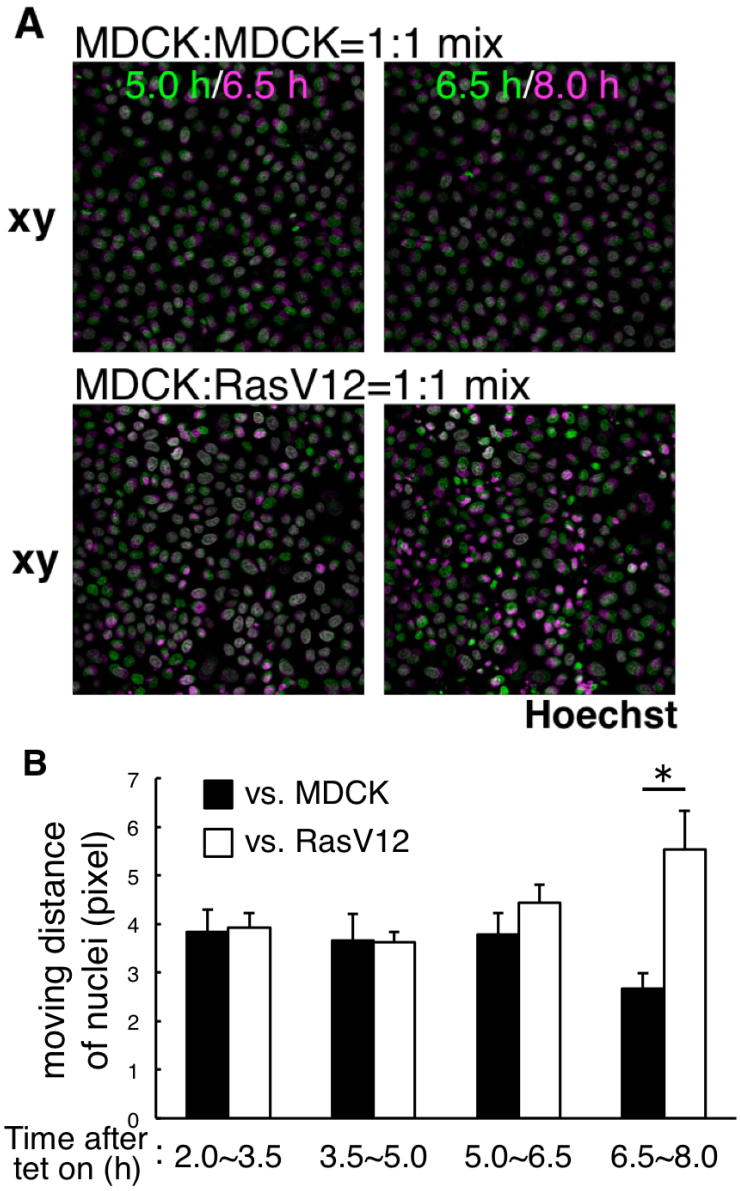

Fig. 3-20 Cell motility in normal MDCK cells is upregulated in the mix culture with RasV12 cells. (**A**) Merged images of nuclei in each indicating time (Left side; green: 5.0 hours, magenta: 6.5 hours after RasV12 induction, Right side; green: 6.5 hours, magenta: 8.0 hours after RasV12 induction). MDCK cells mixed with MDCK cells or RasV12 cells were incubated. After forming monolayer, we stained cells with Hoechst and treated with tetracycline and performed time-lapse observation for 8 hours. (**B**) Quantification of the moving distance of nuclei between indicating time. Data are mean ± s.e.m. unpaired two-tailed *t* -test; *n* = 50 cells pooled from three independent experiments.

3.4. Discussion

Based on the data obtained in this study, we show that AHNAK2 phosphorylation is upregulated in normal cells mixed with transformed cells. Importantly, AHNAK2 phosphorylation is not upregulated when normal cells are cultured alone, suggesting that the interaction between normal cells and transformed cells is important for AHNAK2 phosphorylation. Furthermore, AHNAK2 knockdown in surrounding normal cells suppressed apical extrusion of surrounded RasV12-transformed cells, indicating that AHNAK2 plays an important role in apical extrusion. The upregulation of AHNAK2 phosphorylation is regulated by calcium dependent PKC, and that is regulated by calcium influx via mechanosensitive calcium channel TRPC1 in normal cells. Indeed, AHNAK2 is phosphorylated after mechanical stretching, suggesting that AHNAK2 could sense mechanical tension which is generated by the heterogeneity of epithelial layer. In addition, AHNAK2 knockdown suppresses cell migration during wound healing, suggesting that AHNAK2 is important for cell migration after damage in epithelial layer.

These data indicate that in the heterogeneity in epithelial layer including cell competition, mechanical forces such as stretch or compaction are generated and it causes calcium influx via mechanosensitive calcium channel. After that, PKC-AHNAK2 pathway is upregulated and cause cell migration to restore epithelial homeostasis by removing transformed cells.

In future studies, it should be examined the significance of AHNAK2 phosphorylation in epithelial homeostasis and the forces which is generated in the mix culture of normal and transformed cells.

3.5. References

Hanahan, D. & Weinberg, R. A. The hallmarks of cancer. Cell 100, 57–70 (2000).

Fialkow, P. J. Clonal origin of human tumors. Biochim. Biophys. Acta. 458, 283–321 (1976).

Nowell, P. C. The clonal evolution of tumor cell populations. Science 194, 23–28 (1976).

Schoenenberger, C. A., Zuk, A., Kendall, D. & Matlin, K. S. Multilayering and loss of apical polarity in MDCK cells transformed with viral K-ras. J. Cell Biol. 112, 873–889 (1991).

Rosenblatt, J., Raff, M. C. & Cramer, L. P. An epithelial cell destined for apoptosis signals its neighbors to extrude it by an actin- and myosin-dependent mechanism. Curr. Biol. 11, 1847–1857 (2001).

Bos, J. L. Ras-like GTPases. Biochim. Biophys. Acta. 1333, M19–31 (1997).
Baena-Lopez, L. A., Pastor-Pareja, J. C. & Resino, J. Wg and Egfr signalling antagonise the development of the peripodial epithelium in Drosophila wing discs. Development 130, 6497–6506 (2003).

Rodriguez-Viciana, P. et al. Role of phosphoinositide 3-OH kinase in cell transformation and control of the actin cytoskeleton by Ras. Cell 89, 457–467 (1997).

Cantrell, D. A. Phosphoinositide 3-kinase signalling pathways. J. Cell Sci. 114, 1439– 1445 (2001).

Karnoub, A. E. & Weinberg, R. A. Ras oncogenes: split personalities. Nature Rev. Mol. Cell Biol. 9, 517–531 (2008).

Kimura, K. et al. Regulation of myosin phosphatase by Rho and Rho-associated kinase (Rho-kinase). Science 273, 245–248 (1996).
Jaffe, A. B. & Hall, A. Rho GTPases: biochemistry and biology. Annu. Rev. Cell Dev. Biol. 21, 247–269 (2005).

Vega, F. M. & Ridley, A. J. Rho GTPases in cancer cell biology. FEBS Lett. 582, 2093–2101 (2008).

Sahai, E., Olson, M. F. & Marshall, C. J. Cross-talk between Ras and Rho signalling pathways in transformation favours proliferation and increased motility. EMBO J. 20, 755–766 (2001).

de la Cova, C., Abril, M., Bellosta, P., Gallant, P. & Johnston, L. A. Drosophila Myc regulates organ size by inducing cell competition. Cell 117, 107–116 (2004).

Moreno, E. & Basler, K. dMyc transforms cells into super-competitors. Cell 117, 117– 129 (2004).

Vidal, M., Larson, D. E. & Cagan, R. L. Csk-deficient boundary cells are eliminated from normal Drosophila epithelia by exclusion, migration, and apoptosis. Dev. Cell 10, 33–44 (2006).

Brumby, A. M. & Richardson, H. E. scribble mutants cooperate with oncogenic Ras or Notch to cause neoplastic overgrowth in Drosophila. EMBO J. 22, 5769–5779 (2003).

Stoker, M. G., Shearer, M. & O'Neill, C. Growth inhibition of polyoma-transformed cells by contact with static normal fibroblasts. J. Cell Sci. 1, 297–310 (1966).

Bignami, M., Rosa, S., La Rocca, S. A., Falcone, G. & Tato, F. Differential influence of adjacent normal cells on the proliferation of mammalian cells transformed by the viral oncogenes myc, ras and src. Oncogene 2, 509–514 (1988).

Alexander, D. B. et al. Normal cells control the growth of neighboring transformed cells independent of gap junctional communication and SRC activity. Cancer Res. 64, 1347–1358 (2004).

Wells, C. M., Walmsley, M., Ooi, S., Tybulewicz, V. & Ridley, A. J. Rac1-deficient macrophages exhibit defects in cell spreading and membrane ruffling but not migration. J. Cell Sci. 117, 1259–1268 (2004).

Hogan, C. et al. Rap1 regulates the formation of E-cadherin-based cell-cell contacts. Mol. Cell. Biol. 24, 6690–6700 (2004).

Shtivelman, E., Cohen, F. E. & Bishop, J. M. (1992) Proc. Natl. Acad. Sci. USA 89, 5472–5476.

Hashimoto, T., Gamou, S., Shimizu, N., Kitajima, Y. & Nishikawa, T. (1995)

Exp. Cell. Res. 217, 258–266.

Hieda, Y., Tsukita, S. & Tsukita, S. (1989) J. Cell Biol. 109, 1511–1518.

Sekiya, F., Bae, Y. S., Jhon, D. Y., Hwang, S. C. & Rhee, S. G. (1999)J. Biol. Chem. 274, 13900–13907.

Haase, H., Podzuweit, T., Lutsch, G., Hohaus, A., Kostka, S., Lindschau, C., Kott, M., Kraft, R. & Morano, I. (1999) FASEB J. 13, 2161–2172.

Chapter 4:

CONCLUSION

4. Conclusion

In this study, we revealed the mechanisms of apical extrusion of transformed cells surrounded by normal cells.

In the first topic, we focused on the metabolic alteration during cell competition. We show that mitochondrial membrane potential is diminished in RasV12-transformed cells when they are surrounded by normal cells. In addition, glucose uptake is elevated, leading to higher lactate production. The mitochondrial dysfunction is driven by upregulation of PDK4, which positively regulates elimination of RasV12-transformed cells. Furthermore, EDAC from the surrounding normal cells, involving filamin, drives the Warburg-effect-like metabolic alteration. These data indicate that non-cell-autonomous metabolic modulation is a crucial regulator for cell competition.

In the second topic, we performed SILAC-based mass spectrometry analysis, and we identified AHNAK2 whose phosphorylation was upregulated in normal cells mixed with transformed cells compared to alone culture. AHNAK2 phosphorylation is regulated by calcium-PKC pathway, which is upregulated in normal cells in the mix culture condition. Furthermore, the upregulation of calcium uptake is caused by mechanosensitive calcium channel TRPC1. In addition, AHNAK2 is important for cell migration during wound healing. These data indicate that mechanical force which is generated by epithelial heterogeneity could regulates the homeostasis of epithelial layer via calcium-AHNAK2 pathway.

Collectively, to maintain the epithelial homeostasis including cell

competition, epithelial cells cause dynamic alteration such as metabolic changes or mechanical status and try to suppress heterogeneity. In other wards, this study could give a new insight that epithelial cells have ability to suppress heterogeneity not only in the initial stage of carcinogenesis, but also other phenomena such as tissue damage repairing.